NASA CR-54326
TRW 4175-6013-SU-000

SUMMARY REPORT

PROGRAM OF LARGE HIGH PERVEANCE IONIZER STUDIES

by

J. C. Beynon, S. G. Forbes, and P. W. Kidd

Prepared for:

NATIONAL AERONAUTICS AND SPACE ADMINISTRATION

15 September 1965

Contract No. NAS3-5906

Technical Management
NASA Lewis Research Center
Cleveland, Ohio
Spacecraft Technology Division

PHYSICAL ELECTRONICS LABORATORY
Physical Research Division
TRW Systems
One Space Park
Redondo Beach, California

CONTENTS

LIST OF ILLUSTRATIONS

1. INTRODUCTION

The program described herein is a study of large porous tungsten sources of cesium ions, in which primary interest centered on performance at the high current densities.

BACKGROUND

The work described in this report follows logically under approximately two years of previous work conducted under different sponsorship.[1] These earlier efforts resulted in the production of a modular source ion thrustor, which will be described briefly to put the present report in perspective.

The TRW thrustor has the following principal characteristics:

1) The emitter is a single block of porous tungsten of large enough area (3x5 cm) that peripheral heat losses are small compared with frontal radiation.

2) The acceleration distance is small — about 1 mm — so that high current densities can be obtained with only moderate accelerating voltages. The perveance of the module is 5×10^{-6} amps/volts$^{3/2}$.

3) The ion optics are cylindrical; the ion-focusing system can therefore be formed by machining parallel grooves in the porous tungsten.

4) The engine is a diode, avoiding the mechanical and electrical complications of a three-electrode accel-decel system.

5) The ion optics are relatively insensitive to details of accelerating-grid geometry, providing the emitter surface has the correct shape. Small irregularities or displacements of the parallel bars of the accelerating grid are removed.by sputtering if they project into the ion beam.

6) Neutralization is accomplished from a single, or at most a small number, of electron sources adjacent to the beam. (This is now standard practice with all electrostatic thrustors but was a subject of considerable discussion when this thrustor design was first proposed.)

7) The accelerator grids are replaceable by a simple mechanism that enables a used grid to be removed and a new one to be installed without breaking the vacuum. It is therefore feasible to operate the engine at a current density high enough to give excellent efficiency, even though the lifetime of a single grid may be much shorter than the total life required of the thrustor.

The philosophy behind this thrustor design, in brief, is that items (1) and (2) are essential for high efficiency, and that these make item (7) essential for long life. The achievement of these goals is made feasible by the simplicity of design afforded by items (3), (4), (5), and (6).

The thrustor, which is illustrated in Figure 1, was constructed and operated satisfactorily prior to the start of the present contract. The design (including the grid-change feature, which had been used repeatedly without mishap) had been proved sound and feasible. Life tests were conducted, and by the termination date of the previous contract 180 hours had been accumulated. Peak current densities up to 40 ma/cm^2 were drawn for limited periods.

AIMS OF THE PRESENT PROGRAM

When sponsorship of this work was assumed by the NASA Lewis Research Center, it was decided that effort should be concentrated upon the most sensitive, and probably the limiting, feature of this and other contact ion engines — namely, the performance of the ionizer itself. Of special interest in this regard are data obtained at high current densities, particularly in configurations

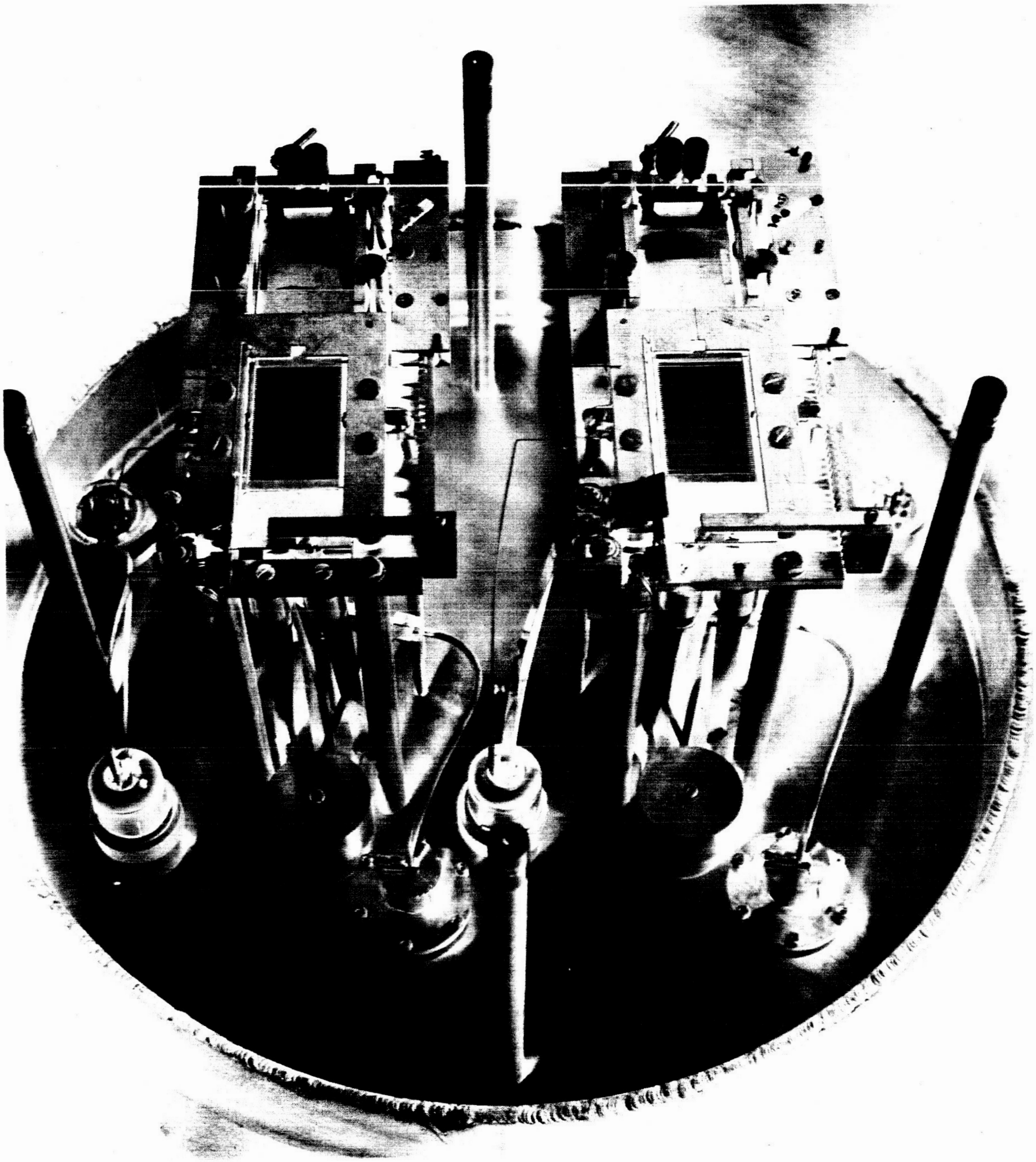

Figure 1. Dual-module engine.

practical for thrustors. The TRW thrustor design provides a very flexible and versatile means for emitter testing, and the contract therefore called for testing various samples of porous tungsten in the configuration of the replaceable grid thrustor. Emphasis has been placed both upon ionizer performance at high current densities and upon relating ionizer performance to physical properties such as density, pore size and uniformity, and transmissivity. Detailed studies of small samples of porous ionizer material were being concurrently tested under stringently controlled conditions under a separate contract (NAS3-5254), and it was decided to compare the measured performance of ionizer material under these testing conditions with performance in an actual engine structure.

The large thrustor emitters are 1.2x2.1 inches in size, with an emitting area of 15 cm^2 and a perveance of 5×10^{-6} $amps/volt^{3/2}$. Current densities up to 100 ma/cm^2 were anticipated. Tests on 1-cm^2 buttons implanted in the face of a 15-cm^2 solid tungsten slab were successfully operated up to 85 ma/cm^2, but the highest current density found to be usable with a full-size emitter was 50 ma/cm^2.

The original program was to include two samples each of four types of porous tungsten to be supplied by various sources to TRW through NASA. This plan was modified at the outset to include one sample each of eight types of material. In parallel with this program, 0.2-cm^2 sample buttons of the same material were to be tested under the separate contract for comparison with the large-ionizer data.

In the course of the experimental work it soon became apparent that the excellent characteristics obtained on the small buttons could not be duplicated in the large-ionizer tests. Successive improvement of two orders of magnitude in vacuum test conditions served only to aggravate the discrepancy.

During the latter portion of the program, effort was mainly directed toward a detailed examination of the causes of the poor behavior of the large ionizers. At the close of the contract period this problem was unsolved, despite a detailed re-examination of the fabrication, testing, and measurement procedures used. Data on the five ionizers that were thoroughly tested during this contract are presented in the following sections of this report. Many steps of the processes involved are described in considerable detail in order to document as completely as possible a problem that is not yet fully understood.

This work is continuing under Contract NAS3-7106.

2. EXPERIMENTAL PROCEDURES

FABRICATION PROCEDURE

The components comprising the 3x5 cm ionizers are shown in Figure 2. Starting from the lower right-hand corner, these are the following: the feed tube nut (stainless steel), the feed tube (rhenium), two indexing pins (tungsten), the back plate (tungsten), the ionizer base (tungsten), and the emitter (porous tungsten). The solid tungsten parts are formed by hot-machining from rods, plates, and billets. The emitter is either cold-machined, if the porous material is infiltrated, or hot-machined if it is not infiltrated. Cold-machining is considered preferable because of possible oxidation damage in hot-machining uninfiltrated material, although there is no direct evidence of this type of damage.

The first step in ionizer fabrication is to machine the plenum chamber. The interior surfaces are then electrolytically etched to remove burnished material and provide an open porous surface, and the front face is polished by standard metallurgical techniques to produce a suitable surface for subsequent pore evaluation. After polishing, the infiltrant is removed by vacuum evaporation at temperatures slowly increasing up to 1500°C. Measurements of pore count, pore size, density, and transmission characteristics are made prior to brazing, which is carried out in two steps: first, the back plate and feed tube are vacuum-brazed to the solid tungsten base to form an assembly that provides two parallel channels for the radiation heaters and also provides passage for the cesium flow from the rear of the assembly up to the ionizer plenum region; the second braze attaches the ionizer to the base (Figure 3). All brazes are made with pure rhodium foil or powder, which require brazing temperatures of about 2000°C for short periods. The brazing operation is followed by a recheck of the total transmission characteristics of the ionizer. (No significant changes have been encountered in such checks.) The emitter is also checked for uniformity of the through-put by bubble-testing with argon flow under freon. A typical bubble pattern is shown in Figure 4.

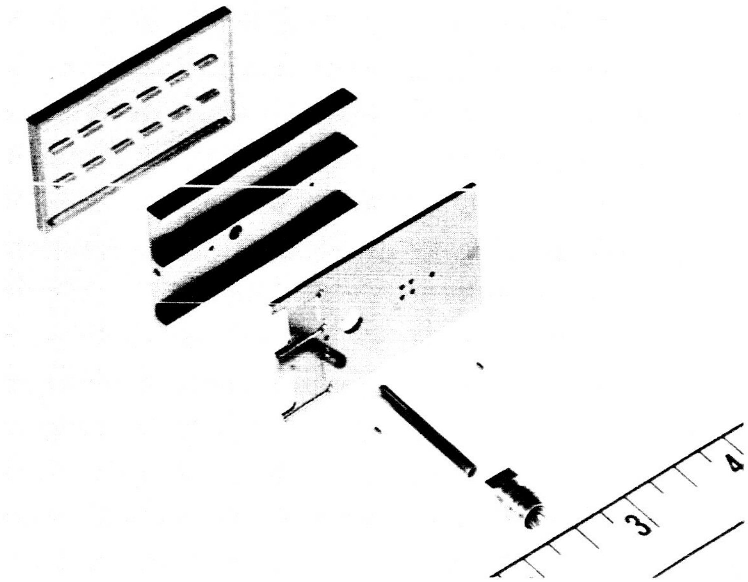

Figure 2. Exploded view of ionizer.

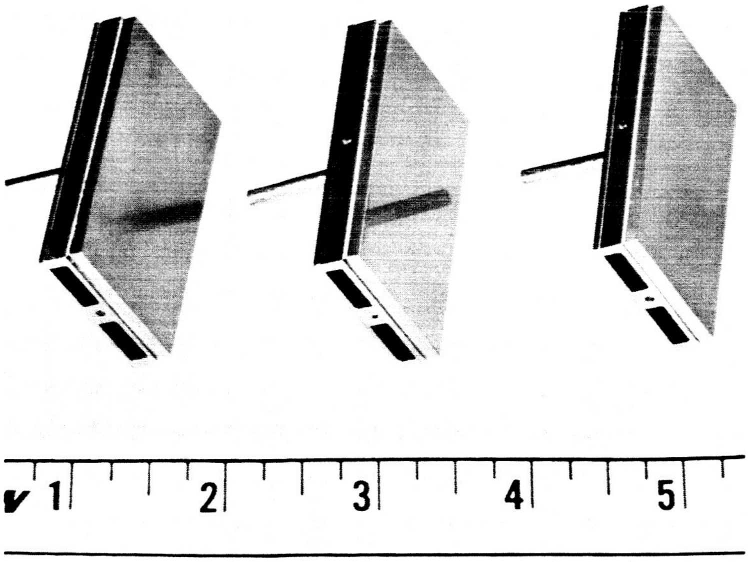

Figure 3. Brazed ionizer assemblies.

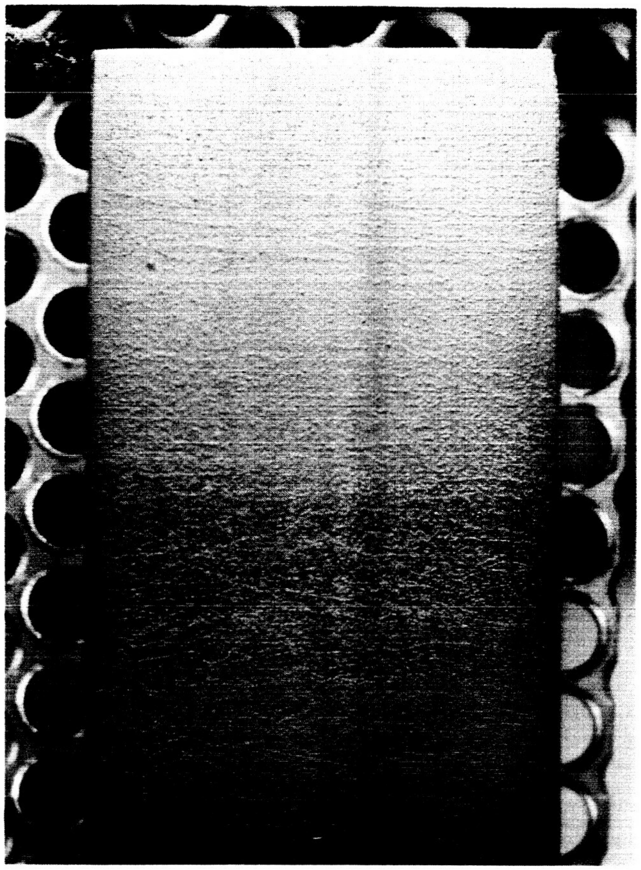

Figure 4. Typical bubble pattern obtained in testing uniformity of emitter.

The next operation is vapor deposition of solid tungsten on the sides and top of the porous ionizers. This solid deposit serves three important functions in the finished ionizer: (1) it seals the sides of the porous structure; (2) it provides a nonporous extension of the ion optical contour to reduce the electrode erosion at the edges of the ionizer; and (3) it provides nonporous flute ridges on the ionizer surface to reduce ionization from regions that could lead to direct ion impingement on the accelerator. These functions are extremely important in obtaining thrustor durability. Although the vapor-deposition process has been one of the troublesome development problems in this work, it appears to be by far the most satisfactory approach to integral ion optical control for an ionizer design to take advantage of the benefits of small accelerator dimensions.

Electrical discharge machining (EDM) is used to square the irregular vapor deposit on the sides of the ionizer and to produce the fluted, 1-mm-pitch ionizer surface. In this latter operation the depth of the fluting is controlled to leave about 0.1 mm of solid tungsten on the flute ridges, thereby forming the 53 integral focus electrodes on the finished ionizer. The final EDM operation is precision location of the four ionizer mounting holes with reference to the ionizer surface, which results in all ionizers being interchangeable and automatically aligned with the accelerating electrode structure. After this operation the ionizer is flushed with kerosene to remove the residue.

The feed tube nut is vacuum-brazed (with copper) to the rhenium feed tube, and the ionizer is then ready for assembly (see Figure 5). For thrustor operation, the ionizer is brought to operating temperature by two radiation heaters of the type shown in Figure 6. The heating element of each of these heaters is made of graphite, supported by rhenium pins, which are mounted with fused alumina in a rhenium plate. One pin is "grounded" to the plate, which attaches to the ionizer base in the machined slots provided for that purpose. The two heaters used in each ionizer thus form a "center-grounded" pair.

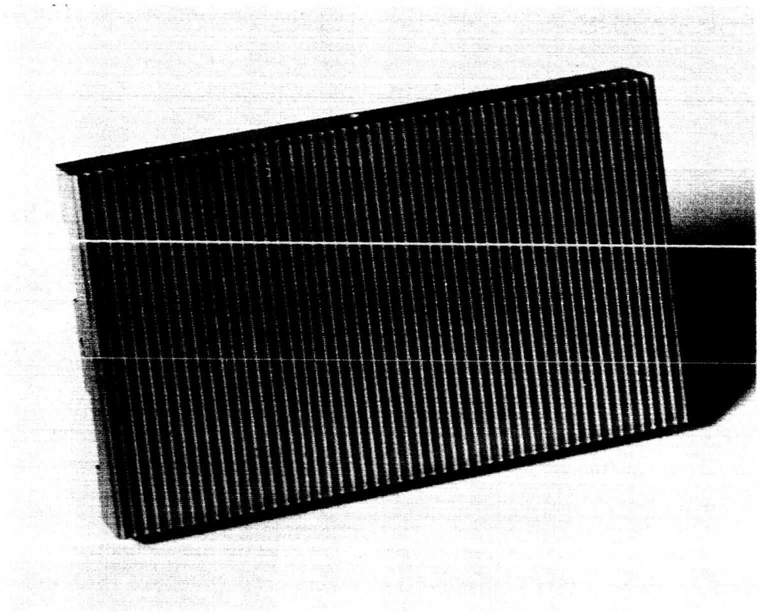

Figure 5. Completed ionizer assembly.

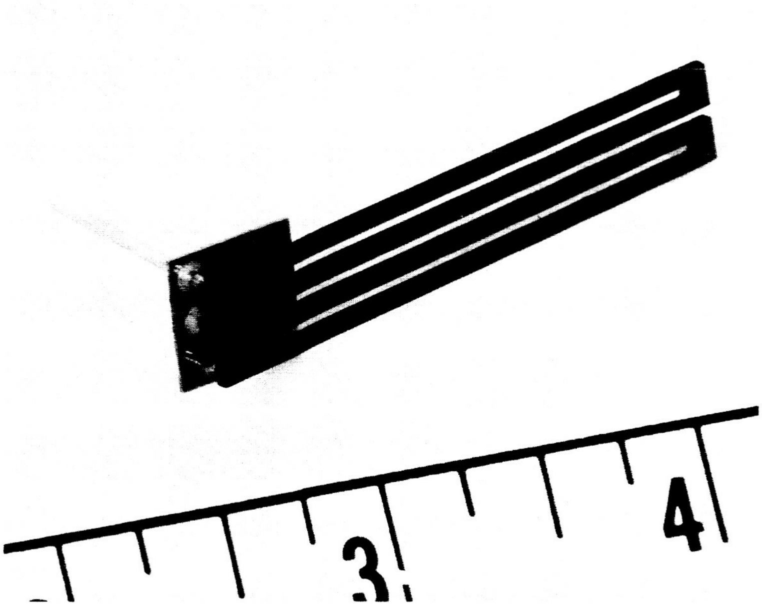

Figure 6. Graphite radiation heater.

PRE-RUN MEASUREMENTS

Each of the porous-tungsten ion emitter blanks were examined and characterized with respect to average bulk density, surface pore density and diameter, permeability (as indicated by measurement of the transmission coefficient), and emissivity.

Density

Density measurements were made on the as-machined emitter blanks, using a differential weighing technique that employed mercury as the displacement fluid.

Pore Count and Size

Data pertaining to surface pore density were obtained from metallographic studies by visually counting the number of pores observed on photomicrographs. Since actual pore shapes deviate from idealized circular pores, a standard was selected to provide a measure of the number of equivalent circular pores. The surface pore density data presented here were obtained using the rule that elongated pore shapes be counted as multiple pores equal to the number of average pore diameters represented by the elongation. This procedure leads to somewhat higher values of surface pore densities than would be obtained by other methods, but it is believed that these data are pertinent to emitter evaluation.

Average pore size was determined by measuring pores on a random basis, using photomicrographs at 1000-diameters magnification. In the case of elongated pores, the pore diameter was taken as the minor, or small dimension. Specimens were prepared by metallographic polishing of infiltrated porous material, followed by sublimation and evaporation of the infiltrate. This procedure was used for all samples except emitter G-5, which was not made of infiltrated material. The surface of G-5 was prepared by standard metallographic polishing followed by chemical etching to reveal the matrix and pore structure.

Transmission Coefficient and Uniformity of Transmissivity

The transmission coefficient of the porous-tungsten emitters is measured after they are machined to the desired shape but before the brazing operations are performed. The device used to measure transmission is shown photographically in Figure 7 and schematically in Figure 8. The emitter is placed over a pump-out hole in a soft rubber mat that defines the region under test. The chamber is first evacuated and then filled to about 50 torr with argon, following which the time required for the pressure to drop to 25 torr is determined.

In Figure 9 the relationship between the flow rate and the absolute pressure is shown for a typical piece of porous tungsten. At argon pressures above about 120 torr the flow mechanism is seen to be changing to a mode with a greater mass flow rate. However, in the region from 120 torr down to about 20 torr the flow is proportional to the absolute pressure, giving the observed exponential decay of pressure vs time. The range from 50 to 25 torr used in the emitter tests was selected to match the range of plenum pressures encountered during cesium operation. Although inert gas flow is not necessarily the same as cesium flow, this procedure is at least indicative of the variations in cesium flow that can be expected under ionizer operation. The transmission coefficient is defined as the ratio of the pumping speeds with and without the sample in place and is, of course, the inverse of the ratio of pump-down times. The pump-down time without the sample is much too short for stop-watch measurement, and the pumping speed is too high to ignore the impedance of lines; therefore the calculated speed of the hole is used to compute the time required with no sample.

A hole size of 1/2-inch diameter was selected as a good compromise between spatial resolution and accuracy of measurement. The effective area of the hole is greater than the geometric area because of the lateral diffusion of gas inside the porous structure.

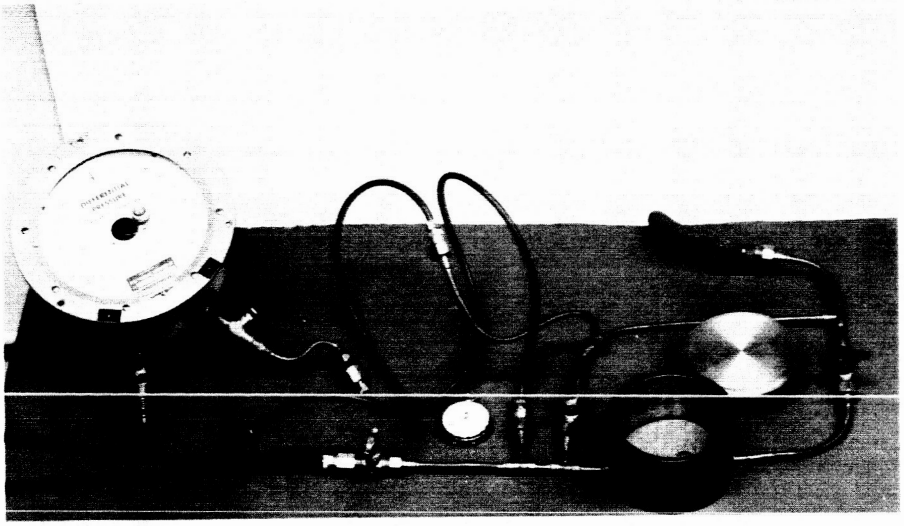

Figure 7a. Apparatus for measuring transmittivity.

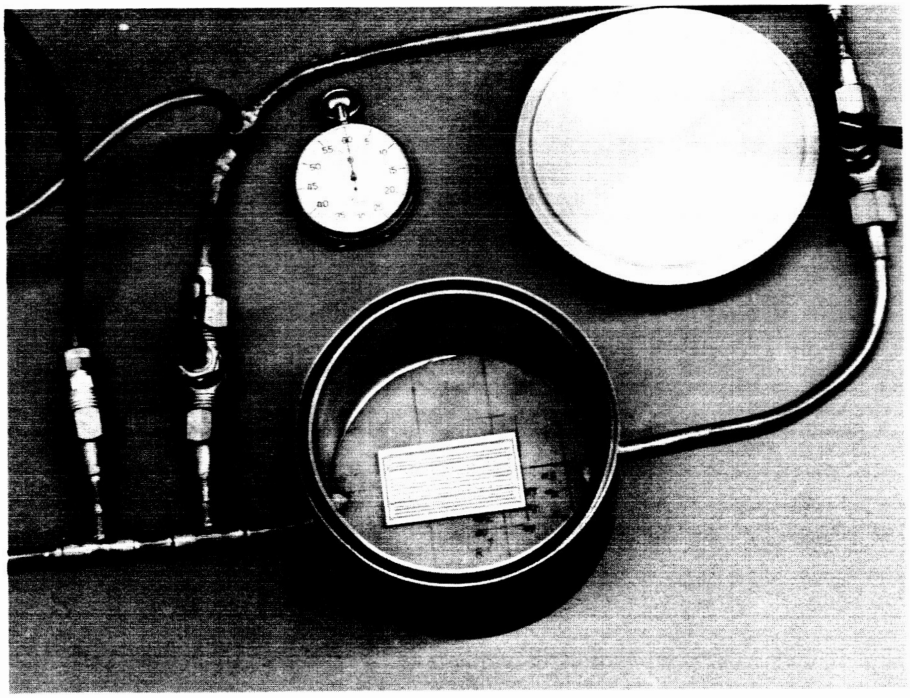

Figure 7b. Apparatus for measuring transmittivity.

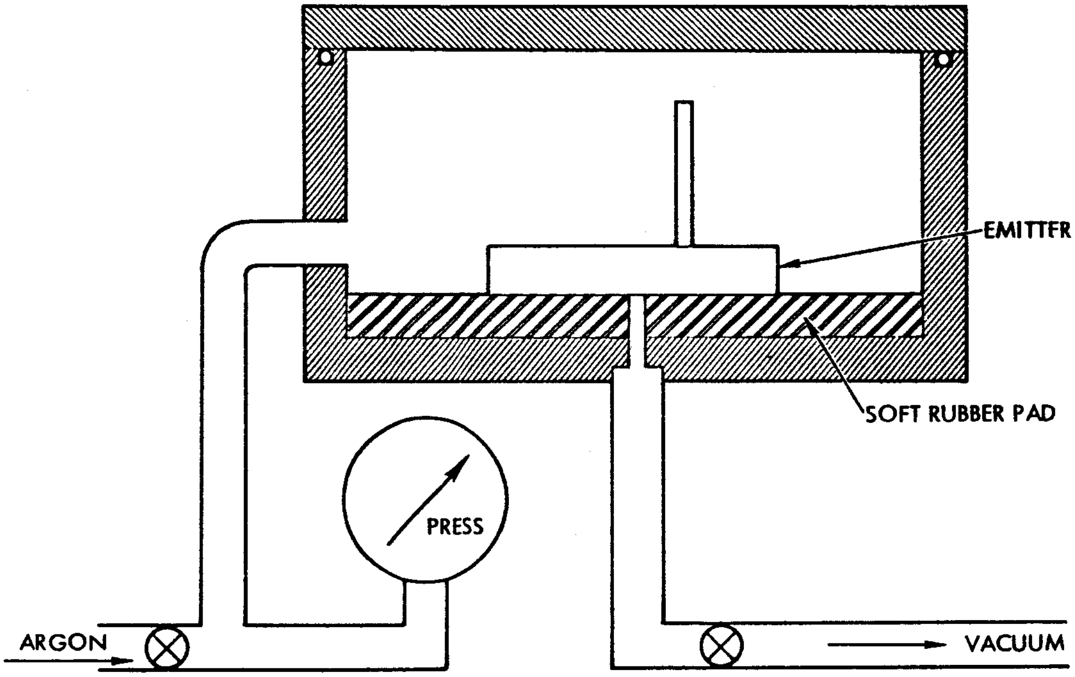

Figure 8. Schematic of equipment for measuring transmittivity.

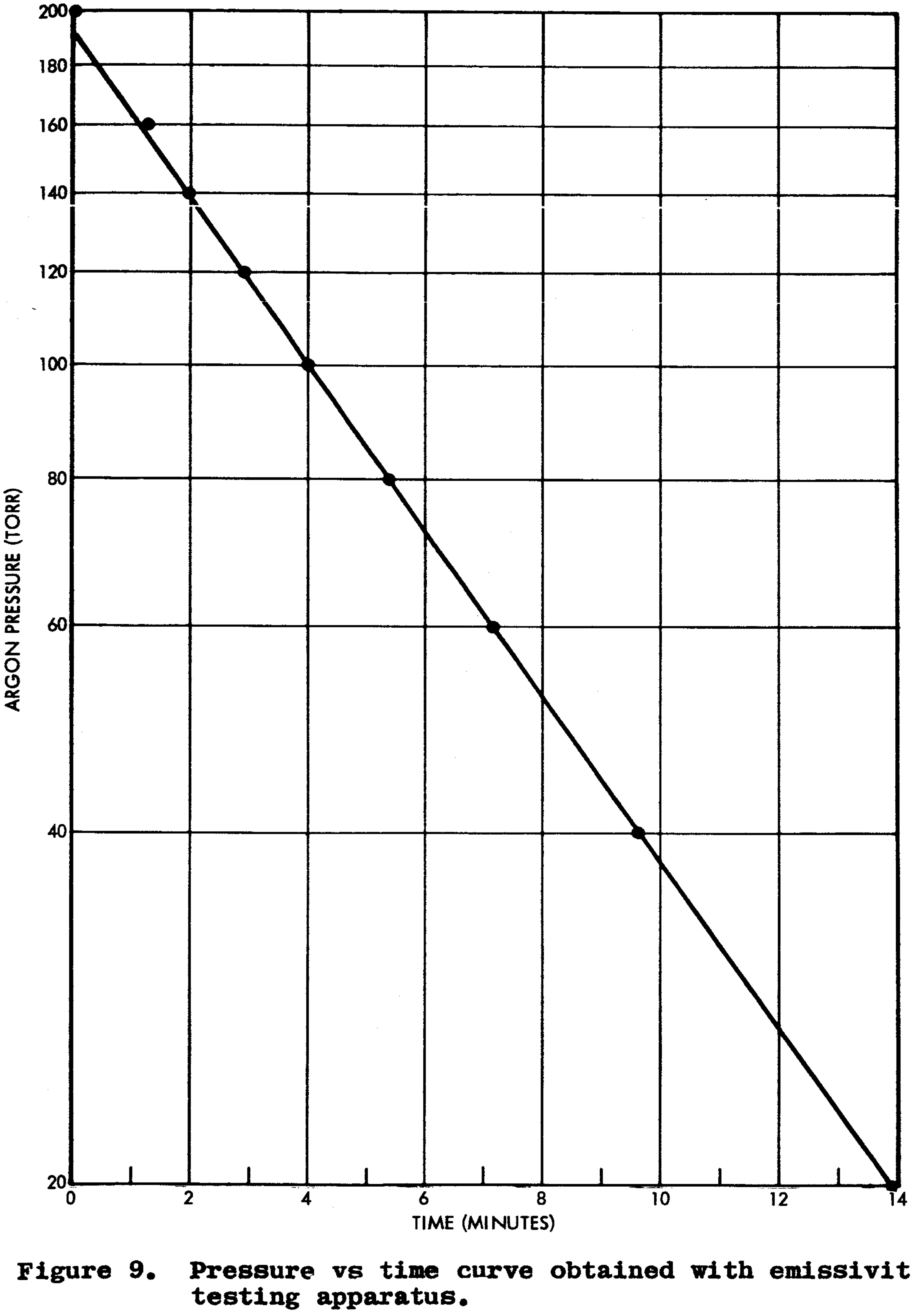

Figure 9. Pressure vs time curve obtained with emissivity testing apparatus.

As a first approximation to the necessary correction, the effective hole radius was assumed to be the geometric radius plus the thickness of the porous slab. The emitter is 0.065-inch thick, giving an effective radius of 0.315-inch and an equivalent area of 2 cm^2. The pumping speed of this "hole" for argon at $300^{\circ}K$ is 20 liters/second. The volume of the chamber is 0.46 liters, giving a calculated time of 1.6×10^{-2} second for a factor-of-two pressure drop. The measured pump-down time without sample is 2 seconds, and all Δt readings should be corrected for line impedance by subtracting this amount. The transmission is then

$$T_o = \frac{1.6 \times 10^{-2}}{\Delta t - 2}$$

For total transmission checks, the emitter is inverted and pumped from the plenum side. In this case the whole emitter area of about 16 cm^2 is available for pumping, giving a computed pump-down time of 2×10^{-3} sec. The transmission is then

$$T_t = \frac{2 \times 10^{-3}}{\Delta t - 2} \quad .$$

Emissivity

Emitter emissivity can be determined by measuring the power P_1 required with no grid in place to raise the emitter to a temperature T_1 and the power P_2 required with a polished molybdenum sheet placed over the emitter to raise it to the same temperature. The emissivity is then given by the following formula:

$$\epsilon_s = \left[P_1 - P_2 + 0.8\sigma T_1{}^4 + \epsilon_m A_m \sigma T_2{}^4\right] \Big/ A_s \sigma T_1{}^4 \qquad (1)$$

where A_m = area of the molybdenum sheet = 16.1 cm^2

T_2 = temperature of the molybdenum sheet when source is at T_1

ϵ_m = total emissivity of the molybdenum sheet at temperature T_2

A_s = total surface area of emitter = 19.3 cm^2.

The $0.8\sigma T_1^4$ term in Eq. (1) is an approximate correction for side leakage, which occurs because there is a finite spacing (0.025 inch) between the emitter and the molybdenum sheet, and for the reflection factor of the molybdenum sheet. (If the molybdenum were a perfect reflector, this leakage would be σT_1^4.) The emissivity of polished molybdenum, from published data, can be closely approximated by the relation

$$\epsilon_m = 0.0001 \, T_2 \quad .$$

The total area A_s is about 20% greater than the projected areas because of the shaping of the surface.

TEST FACILITIES

Vacuum Tank

At the beginning of the program the ionizers were tested in a vacuum facility consisting of two 18-inch-ID glass chimneys clamped end to end on a "T" section containing the pumping connection. The resulting ionizer-to-collector distance was about 1 meter. Two copper liners inside the chimneys protected the glass from thermal and ionic impingement and acted as a Faraday cage for measurement of the ion beam current. A 6-inch Kinney pumping station provided vacuua of about 10^{-5} torr or better with the ion beam turned on.

As the program progressed it became apparent that ionizer performance was not meeting expectations and that improvements in the vacuum conditions were needed. To reduce the backstreaming of pump oils, a new liquid-nitrogen cold trap for the 6-inch diffusion pump was designed and fabricated. With the cold trap, an operating pressure of 10^{-6} torr was obtained. While emitter tests showed fair behavior with regard to critical temperature and neutral fraction, the ionizer performance was still considerably short of that obtained by Cho and Shelton in their button tests.[2]

Since these vacuum conditions represented about the best that could be expected from the 6-inch pumping station, it was decided to provide a new engine test facility.

The new facility consists of a 4x8-foot stainless steel vacuum chamber, a LN_2 trap with a 10^{-4} transmission coefficient for back-streaming pump oil, and a 10-inch NRC diffusion pump. The ultimate vacuum attainable is about 7×10^{-8} torr. The tank is equipped with a quadrupole mass spectrometer for residual gas analysis and has a complete set of liners for ion beam collection. The ion beam strikes a 4-foot-diameter water-cooled collector at the end of the tank. This collector is made of 1/2-inch-thick copper. A water-cooled copper liner extends 4 feet toward the engine, and a refrigerated, 4-foot cylindrical liner is located next to the engine. The water-cooled surfaces operate at 20° to 30°C and the refrigerated surface at -10°C.

Residual Gas

During engine operation the operating pressure is usually 2 to 4×10^{-7} torr. The residual gases are predominantly mass 18 (H_2O) and mass 28 (CO), with a small 44 (CO_2) peak. Transient pressure increases caused by increasing the beam power or arcing are predominantly mass 1 (H). Higher mass peaks indicating hydrocarbons are sometimes seen during initial operation or following periods of operation without LN_2 in the trap. (Normal procedure is to maintain full LN_2 traps on a continuous basis, but lapses sometimes result from a faulty nitrogen controller or unexpected, high usage rates that exhaust the supply.)

Normal hydrocarbon levels appear to be two decades below the predominant gases. Mass 18 is invariably predominant during initial pump down, but eventually mass 28 remains as the predominant constituent.

These conditions represent a considerable improvement in vacuum cleanliness over that of earlier measurements; however, no improvement in ionizer performance was obtained. Neutral atom emission was in fact somewhat higher, indicating that oxygen or hydrocarbons may have been helpful in previous measurements. However, it was possible to obtain curves that were readily recognizable as oxygenated, "contaminated", and, in a few instances, "clean". In summary, the improvements in vacuum cleanliness did not solve the ionizer problem but served the useful function of revealing more clearly the existence of a distinct difference in behavior between buttons and large ionizers.

OPERATING MEASUREMENTS

Electrical

Electrical measurements are made with conventional current and volt meters that are installed in the control console as part of the normal instrumentation. These measurements include the following:

1) Emitter potential (0 to +4 kv)
2) Grid potential (0 to -500 volts)
3) Emitter current* (multirange 0 to 2 amp)
4) Grid current (multirange 0 to 2 amp)
5) Collector current (multirange 0 to 2 amp)
6) Heater power (0 to 700 watts)
7) Neutralizer current (multirange 0 to 2 amp)
8) Neutralizer power (0 to 300 watts)

The ion beam current is measured at the collector, which consists of the entire lining of the vacuum tank except for a small shield plate next to the engine. The sum of the collector current and grid current is compared to the emitter current to detect any stray ion or electron currents that might escape the

---

* Also referred to occasionally as "source current".

the metered paths and cause reading errors; as a double check the collector calorimeter power is also compared to electrical beam power. No reading discrepancies have been observed by these techniques in the configuration used for these experiments.

Current density is calculated by dividing the measured beam current by the 15-cm^2 projected emitter area. Under conditions of high neutral fraction, the current is corrected to the 100% ionization condition by using the neutral fraction indicated by the neutral cesium detectors. In general, the electrical measurements are straightforward, self consistent, and unlikely to contain errors greater than about 5%.

Emitter Temperature

Measurement of the ionizer temperature is important in evaluating emitter characteristics. This measurement is also one of the most difficult to make with accuracy. Two methods have been used in this program, optical pyrometry and thermocouple measurements.

The principal difficulties that have been encountered in using an optical pyrometer have arisen from the oblique viewing angle required, the porous, contoured, and visually rough surface being measured, and the completely obstructed view of the emitter surface when the accelerating grid is in place. Fortunately, the grid may be inserted and removed in vacua so that cross correlation between thermocouple and pyrometer measurements can be obtained with the grid removed. The surface presents no area of known spectral emissivity for viewing, hence it becomes necessary to make an assumption; empirically it has been found that an emissivity of 0.6 gives good correlation with the thermocouple measurements.

The thermocouples used are wires of Pt against Pt + 10% Rh, spot-welded individually to the back of the ionizer. Two pairs of wires are used to give a cross check on proper reading of the thermocouples. Various configurations have been used to increase mechanical reliability and reduce conduction loss errors. In the present configuration 0.015-inch wire is used for strength and the wires are carried for about 1 cm in insulating tubes parallel to the back of the emitter and inside the heat shields to minimize the thermal gradient at the junctions. Despite these precautions discrepancies of 20^o to 30^oK between thermocouples are frequently found. These differences are within the realm of possible temperature distributions resulting from uneven power generation in two ionizer heaters.

One of the difficulties with the use of Pt and Pt-Rh couples is that the W-Pt and W-Pt+Rh emf's are about a factor of three greater than the net output. Thus a small temperature difference between the attachment points for the thermocouple wires can lead to a large spurious output. In the past, differences of over 100^oK have been observed between two thermocouples and between thermocouples and the pyrometer. This problem is currently under fair control, but improvements in measuring techniques are certainly in order.

Neutral Fraction

The neutral cesium efflux from the ionizer is measured in the conventional manner by a hot tungsten ribbon located behind a collimator, the ion current from the ribbon being proportional to the neutral cesium efflux. The neutral detectors (two of which are used with the thrustor) are equipped with electrically actuated shutters that normally remain open but may be closed for obtaining background readings. The neutral detector body operates at a temperature above ambient by virtue of the 15 to 20 watts dissipated at the ribbon. The collimator consists of two apertures about 3 cm apart, between which is an ion deflector plate that removes any charged particles incident on the entrance aperture. The tungsten ribbon is operated from 10 to 100 volts positive with respect to the grounded case. The ion collector is operated at ground potential and therefore collects only a fraction of the ionized neutrals, this fraction being determined by electrode geometry and to a lesser extent by the potentials applied to the ribbon. Typical current saturation curves are shown in Figure 10. At low potentials the current follows a space-charge-limited $V^{3/2}$ curve, whereas above the knee of the saturation curve the current shows a small positive slope with increasing voltage. Normal operating practice is to set the voltage slightly above the knee of the saturation curve.

The sensitivity of the detector is constant from below 1 nano amp to over 5000 nano amp. In Figure 11 the detector response is plotted against the pressure applied to the cesium feed system. This pressure is equal to the cesium vapor pressure in the ionizer plenum chamber plus an additive term equal to the hydrostatic head of the liquid in the feed line. This hydrostatic head appears as a threshold pressure (about 70 torr) required to reach incipient cesium flow. It can be seen from the figure, in which the range shown corresponds to ion beam currents up to about 2 amp, or about 130 ma/cm^2, that the neutral detector output is proportional to the cesium pressure in the plenum chamber, and hence to the cesium flow rate. As an additional precaution the detector sensitivity is monitored periodically by comparing the beam-off neutral reading with the beam-on ion current reading. No significant changes of sensitivity have been observed.

The viewing area of the neutral detector is about 2 cm^2. To give better coverage of the ionizer, two units are used, each looking at a separate area. Crosstalk was tested with two 2.5-cm^2 buttons mounted in a common 15-cm^2 base and provided with independent feed systems. It was found that the response of each neutral detector to the button it was intended to measure was 100 times greater than its response to the neighboring button. This is in agreement with observations made on full-sized ionizers in which the neutral fractions from different portions of the area were observed to change independently.

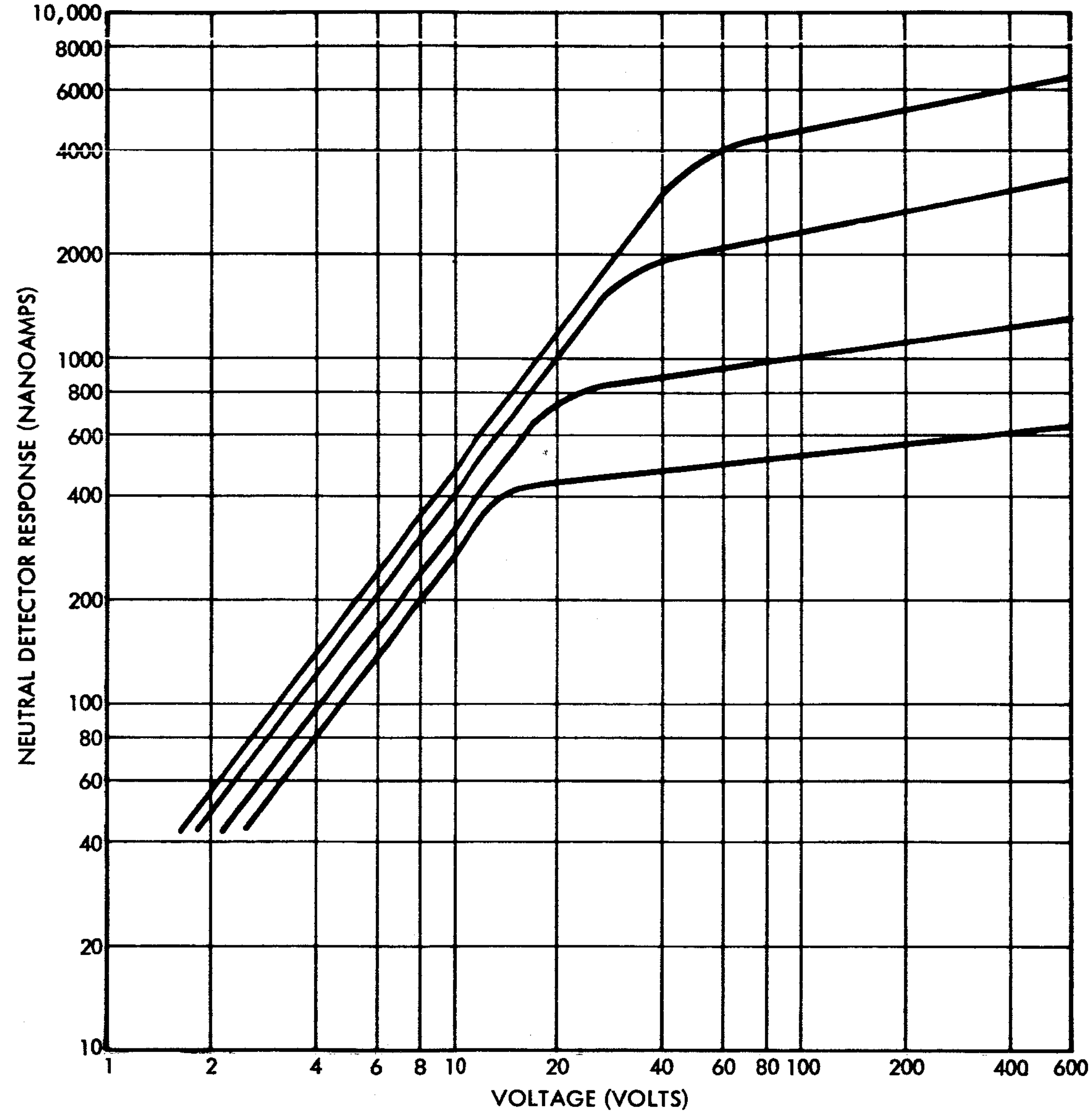

Figure 10. Neutral detector saturation characteristics at four flow levels.

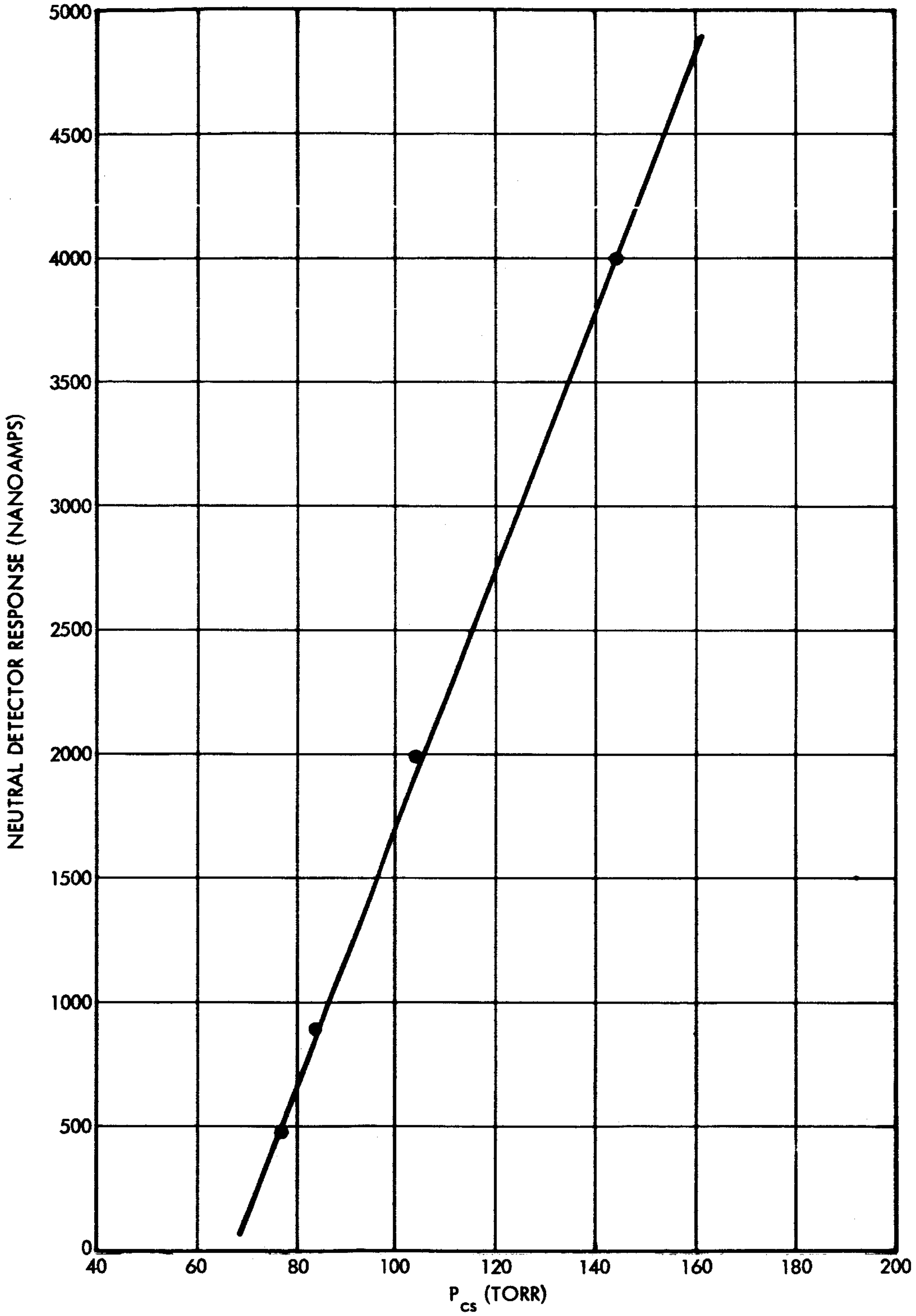

Figure 11. Neutral detector response versus cesium flow rate.

Neutral fraction measurements are made by comparing the neutral detector readings obtained with and without the accelerating voltage applied to the ionizer. The ratio of these two readings is taken to be the neutral fraction, α. Two possible sources of error in this technique are changes in angular distribution of neutral efflux resulting from the changed distribution of cesium near the pores and effects due to electrode scattering. The former problem falls outside the scope of this program, but the effects of grid scattering were part of the present investigation.

The reduction of neutral efflux by electrode backscattering has been discussed elsewhere.[3] An additional scattering effect has been observed in connection with the change in angular distribution of escaping neutrals introduced by the accelerator. The accelerator grid openings, which consist of channels 1/2-mm wide and 1-mm deep, act as fairly efficient collimators that concentrate the neutral efflux in the plane of the slot at the expense of efflux in the plane perpendicular to the slots. Calculations by H. Shelton had indicated that the increase of neutral efflux in the slot plane should be approximately 50%, and this was indeed found to be the case. The effect was determined by first measuring the beam-off neutral efflux at a constant feed rate without a grid and then remeasuring after inserting an accelerator grid.

There is no obvious reason to expect this effect to introduce an error in the neutral fraction measurements, since the geometry for neutral scattering is the same for the beam-on and beam-off measurements. The calculated amount of backscattering, taking into consideration the slot type geometry of the openings between the grid bars, indicate that 0.7 of the original neutrals are reflected back to the ionizer. The experiment to determine the grid backscattering factor G consisted of a series of neutral fraction measurements using grid bars of decreasing cross section. From these data it was planned to extrapolate to zero cross section to obtain the true neutral fraction. This approach proved unsuccessful. Most probably the changes in perveance with grid size, and the changes in ion optics and its effect of space charge at the surface of the ionizer made the experiment invalid by affecting the neutral fraction in a manner that was not related to grid scattering. It is important to note that this result is related to the relative orientation between the grid bars and the neutral detectors. If the neutral detector viewing axis were perpendicular to the plane of the slots, an enhanced grid-scattering effect would be expected. All neutral fraction data listed in this report are uncorrected for grid backscattering.

The ion beam current can be used to obtain an independent check on the neutral efflux by noting that the ion current decreases as the neutral fraction increases. The limitations on this approach are that the neutral fraction must be relatively large in order to get a measurable ion current decrease and that factors other than the neutral fraction, such as the emitter temperature, may influence the ion beam current. With these limitations in mind, the decrease in ion beam current was compared with the indicated neutral fraction, both as a function of emitter temperature and of applied accelerator voltage. In the latter case the voltage was allowed to fall below the saturation value so that the space charge limitation produced an increase in neutral efflux. In all cases the neutral detector measurements agreed with the change in ion current to within a factor of two. The largest disagreements occurred with large emitters, in which cases it is possible that the differences between the overall emitter behavior as seen from the ion beam and the local behavior as seen by the neutral detector may have been real.

It is concluded that the neutral detectors function properly to give readings that are proportional to the incident neutral efflux and that these readings are representative of the behavior of the ionizer. The exact relationship between the neutral fraction and the measured neutral efflux is moot, but in any event the uncertainty does not exceed a factor of two. This level of uncertainty is acceptable, since relatively minor changes in ionizer surface conditions produce effects that are larger than those associated with the measurement.

Beam Profile

A part of the program was concerned with the correlation between ionizer physical properties and ion beam density. Physical properties, such as transmissivity, pore count, and pore size, were determined in the previously described measurements at nine positions on the ionizer. During operation the ion beam was scanned to determine local current density for comparison with the pre-run measurements.

Two types of beam scanner — a calorimeter type and a Faraday cup — were tried. In principle, the calorimeter is relatively free from measurement ambiguities and can be made to have adequate sensitivity and fast response, and it is also capable of making measurements in high-intensity ion beams; however, in practice, maintenance of stable thermocouple calibrations introduced considerable errors in reproducibility.

Part of the problem with the calorimeter measurements arose from the substantial loss of probe material by ion sputtering and the consequent change in temperature distribution within the probe. Because of this source of difficulty, the Faraday cup proved to be much more practical, since its response can be made insensitive to large losses of electrode material. Suppression of secondary electrons and provision for adequate heat removal proved to be relatively straightforward.

The Faraday cup probe consists of a rectangular copper tube (wave guide) 5 mm x 8 mm x 13 cm long, containing a 0.02-cm^2 hole through which the ion beam sample passes. The current entering this aperture is measured on a collector electrode, which can be biased to suppress secondary electron emission. The collector is thermally clamped to the outer tube, which is in turn water-cooled. The probe arm swings on a 5-inch radius to provide scanning along the long axis of the emitter. Successive displacements of the pivot point provide a curved raster scan of the whole emitter fall, as shown in Figure 12. The plane of the scan is approximately 1 cm downstream from the accelerator grid. The width of the emitter

(2.08-inches) is indicated on each beam profile plot. The feed tube side of the emitter is indicated by a plus sign (+), the opposite side by a minus sign (-).

The chart recordings of the emitter profiles indicate the probe has a high resolution and shows much of the fine structure due to focussing of the beam through the grid openings. There are 53 grid bars and 52 openings in the grid. Each opening is 22 mils wide. Therefore, in some of the beam profiles it will be necessary to note that some of the sudden variations in beam density are due to this grid focussing.

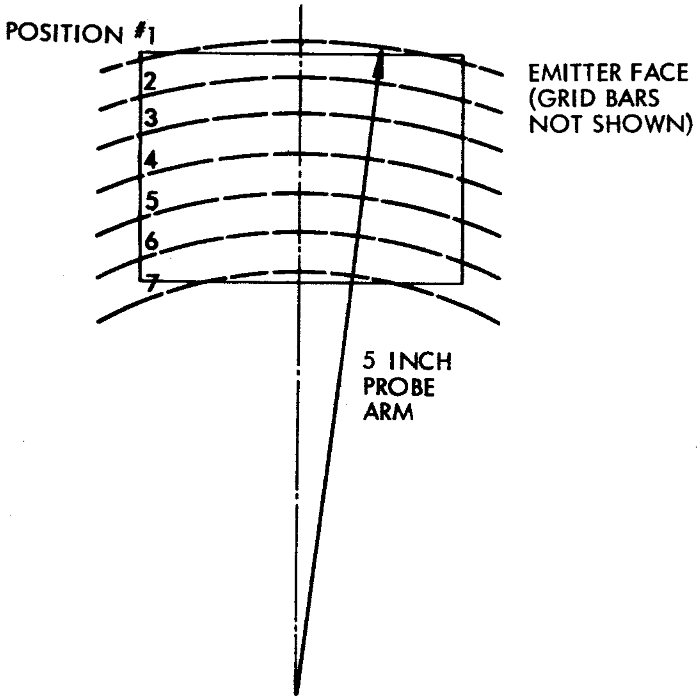

Figure 12. Diagram of beam probe paths down face of emitter.

3. EXPERIMENTAL RESULTS

This section presents the data obtained in tests of the five emitters that were studied in detail. The performance characteristics and descriptive data for these emitters (and Emitter G-2b) are summarized in Table 1. In the discussion that follows, the results for each emitter are grouped together and comparative data obtained by A. Cho in pellet tests are presented for the several materials.[2]

Since the period covered by this contract ended at a time when maximum effort was being devoted to isolation of suspected contaminants and other possible sources of inconsistent results, the discussion of over-all conclusions that follows is necessarily incomplete.

EMITTER G-1

Processing

Emitter G-1 was fabricated from porous material supplied by E.O.S. and designated as W.O. 5441, Bar No. 1, NASA. Three blanks plus two scrap pieces were cut from the piece supplied. Blank No. 2 came from the center of the slab and was the one used for the emitter.

Pore Data

The results of pore and transmission measurements are shown in Figure 13, where the values given in parentheses are ratios relative to the mean. The reproducibility of repeated transmission measurements was well within 1%. These repetitions involved two separate scans of the surface and thus the results include errors due to repositioning, etc. It will be noted that the average transmission obtained from the hole measurements agrees with the total transmission measurement within about 11%, which is considered good agreement in view of the approximate correction applied to the hole radius.

Table I. Summary of emitter characteristics.

EMITTER	ρ (gm/cm^3)	PORE COUNT (10^6/cm^2)	PORE SIZE (μ)	TRANS-MISSIVITY, MEASURED	TRANS-MISSIVITY, TOTAL	POWDER SIZE (μ)	SUPPLIER & CONTRACT	MATERIAL IDENTIFI-CATION
G-1	79.0	5.1	1.5	6.1×10^{-5}	5.4×10^{-5}	1-10	E.O.S. NAS3-5756	W.O. 5441 Bar No. 1
G-2b	83.3	10.7	1.2	1.9×10^{-5}	1.6×10^{-5}	2.8	Hughes NAS3-4110	2.8μ 150-S
G-3	---	4.6	1.5	6.6×10^{-5}	6.7×10^{-5}	1-10	E.O.S. NAS3-5253	W.A. 5141 Bar No. 5
G-4	79.4	4.4	1.4	6×10^{-5}	5.8×10^{-5}	---	E.O.S. NAS3-5253	Bar No. 2
G-5	79.4	5.5	1.6	2×10^{-4}	1.2×10^{-4}	2-5	TRW AF33(657) -11726	SW-10 Powder Lot
F-8	---	---	---	---	---	5	Spectramat AF33(657) -10788	5μ Powder

FEED TUBE END

1 Pore Count $4.5 \times 10^6/\text{cm}^2$ (0.88) Pore Size 1.3μ Transmission 6.02×10^{-5} (0.99) Relative J	4 Pore Count $5.3 \times 10^6/\text{cm}^2$ (1.04) Pore Size 1.5μ Transmission 6.2×10^{-5} (1.02) Relative J	7 Pore Count $5.0 \times 10^6/\text{cm}^2$ (0.98) Pore Size 1.4μ Transmission 6.5×10^{-5} (1.07) Relative J
2 Pore Count $5.1 \times 10^6/\text{cm}^2$ (1.00) Pore Size 1.6μ Transmission 5.6×10^{-5} (0.93) Relative J	5 Pore Count $5.4 \times 10^6/\text{cm}^2$ (1.06) Pore Size 1.4μ Transmission 5.5×10^{-5} (0.91) Relative J	8 Pore Count $5.5 \times 10^6/\text{cm}^2$ (1.08) Pore Size 1.3μ Transmission 6.6×10^{-5} (1.09) Relative J
3 Pore Count $5.2 \times 10^6/\text{cm}^2$ (1.02) Pore Size 1.4μ Transmission 6.5×10^{-5} (1.07) Relative J	6 Pore Count $5.2 \times 10^6/\text{cm}^2$ (1.02) Pore Size 1.5μ Transmission 5.5×10^{-5} (0.90) Relative J	9 Pore Count $4.6 \times 10^6/\text{cm}^2$ (0.90) Pore Size 1.4μ Transmission 6.0×10^{-5} (0.99) Relative J

Density 79.0% Theo.

Emitter - Top View

Mean Pore Count - $5.1 \times 10^6/\text{cm}^2$

Mean Transmission 6.1×10^{-5}; Total Transmission 5.4×10^{-5}

Material E.O.S. 1-10μ S.P.W.

Lot **W.O. 5441 Bar No. 1 NASA**

Sample **No. 2 (Emitter G-1)**

Figure 13. Pore-count and transmissivity data on Emitter G-1.

Two features of the data are apparent. First, the transmissivity measured in this manner shows good uniformity, the extremes being only about ±10% from the mean. Second, the transmissivity data follow the trend shown by the pore count data. High pore count areas show high transmissivity and, conversely, low pore count areas show lower transmissivity. The correlation is about as good as can be expected in view of the disparity between the areas included in the evaluation of pore data and the area used in transmission measurements.

When the transmission of emitter G-1 was rechecked after Elox contouring, the total transmission had increased to 1.3×10^{-4}. There is no apparent reason for this increase over the previous measurement. The earlier measurement was 5.4×10^{-5} with a thickness of 0.165 cm for a total of 8.9×10^{-6} cm transmissivity. The Elox process removes about 0.045 cm, which gives a calculated new transmissivity-thickness product of 1.56×10^{-5} cm. Elox machining is quite effective in opening up the porous surface, but it seems unlikely that this could account for a factor of two change.

Emissivity

The emissivity of the emitter when first installed was found to be 0.28 at 1577°K. Values of P_1, P_2, and T_2 measured on 20 October 1964 were 355 watts, 240 watts, and 1368°K, respectively (see Eq. 1, Page 16).

After operation to 45 ma/cm^2, during which time a partial vacuum leak occurred, the final emissivity was 0.38 at 1560°K, calculated from measurements of P_1, P_2, and T_2 as 396 watts, 216 watts, and 1350°, respectively (measured on 28 October 1964).

The emissivity of clean tungsten at 1560°K is 0.2.

Bubble Tests

The completed emitter was immersed in freon and bubble-tested with argon gas at various pressures. A reproducible bubble pattern was obtained, as shown in Figure 4. The fine tracery shown in this photo could be obtained repeatedly in spite of rather bizarre hysteresis effects produced by varying the sequence of wetting and pressure application. The significance of the lines of bubbles is unknown. They do not seem to follow any visible surface defects and may represent real differences in porosity, but this is by no means certain.

Test Data

The emitter was at operating temperature ($1300^{\circ}K$ to $1700^{\circ}K$) for a total of 64 hours. For approximately 34 hours of this time the ion engine was in operation (i.e., the accelerating voltage and cesium feed were on).

Figure 14 shows a plot of the neutral fraction α* as a function of emitter temperature at constant current density. Figure 15 shows α as a function of J, and Figure 16 shows α as a function of the accelerating voltage applied between the emitter and grid for various current densities. In addition, Figures 14 and 15 have data taken by A. Cho[2] for an Eloxed tungsten pellet of the same material as emitter G-1 (manufactured by E.O.S. with a 1-10μ particle size) for comparison.

Figures 17 and 18 show the grid drain current as a function of the accelerating voltage and the emitter temperature, respectively, for various ion current densities. Figures 19 and 20 show beam current versus accelerating voltage and emitter temperature, respectively, for various source currents.

Two neutral detectors were used in the experiment, each looking at the same area of the emitter. The data shown in Figure 20 indicate that emitter G-1 has no sharply defined critical temperature over the range of current densities measured. The data in Figure 15

---

* Both sets of data in Figure 14 are uncorrected. The data of Cho should be divided by 2 to get the true neutral fraction.[4] The data for the TRW ion engine should be multiplied by 3 to get the true neutral fraction (the backscattering coefficient is calculated to be 0.7 $\alpha \approx \alpha'/1-G$ where α = true neutral fraction, α' = uncorrected neutral fraction, G = backscattering coefficient).

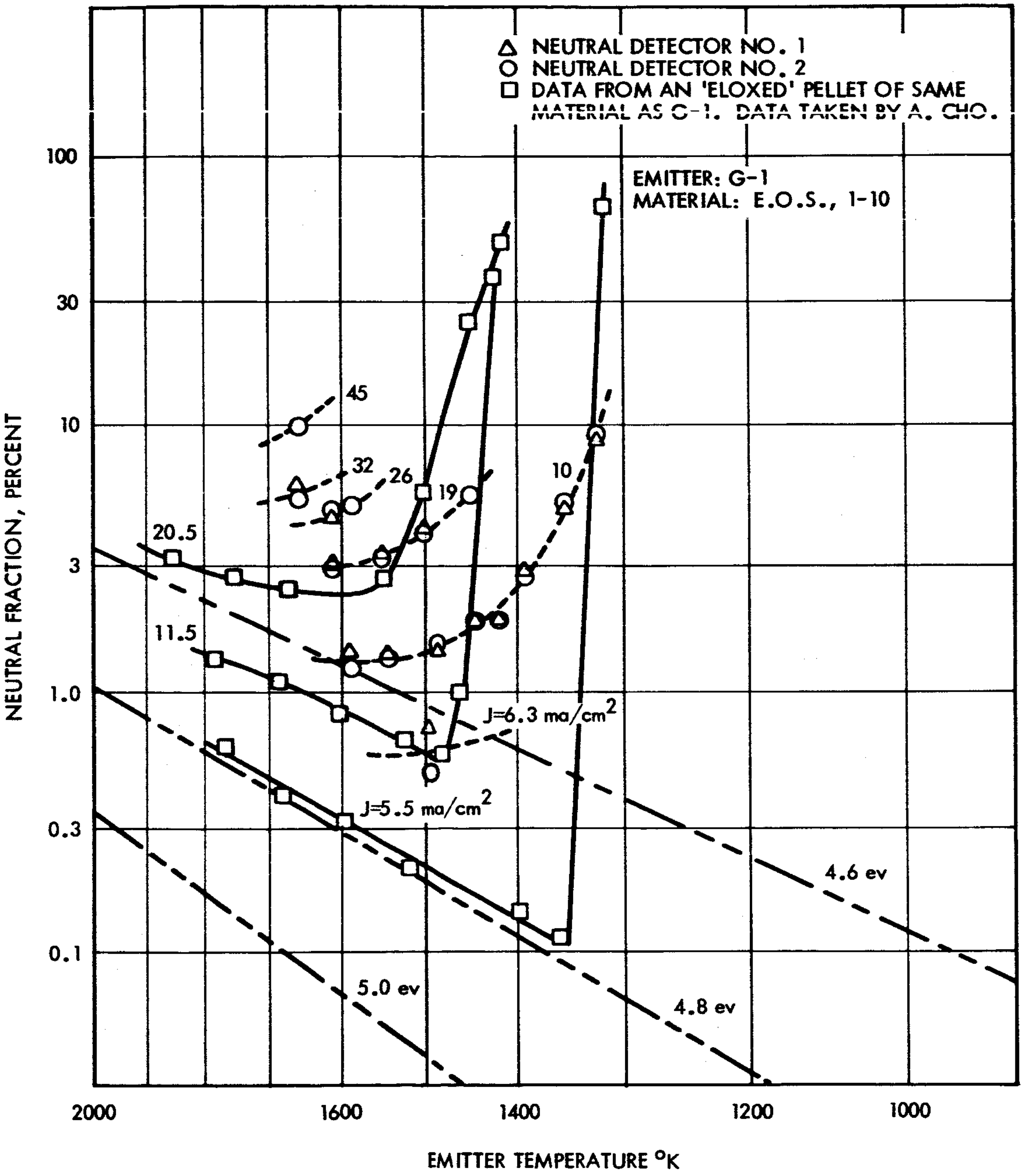

Figure 14. Cesium neutral fraction versus emitter temperature (G-1).

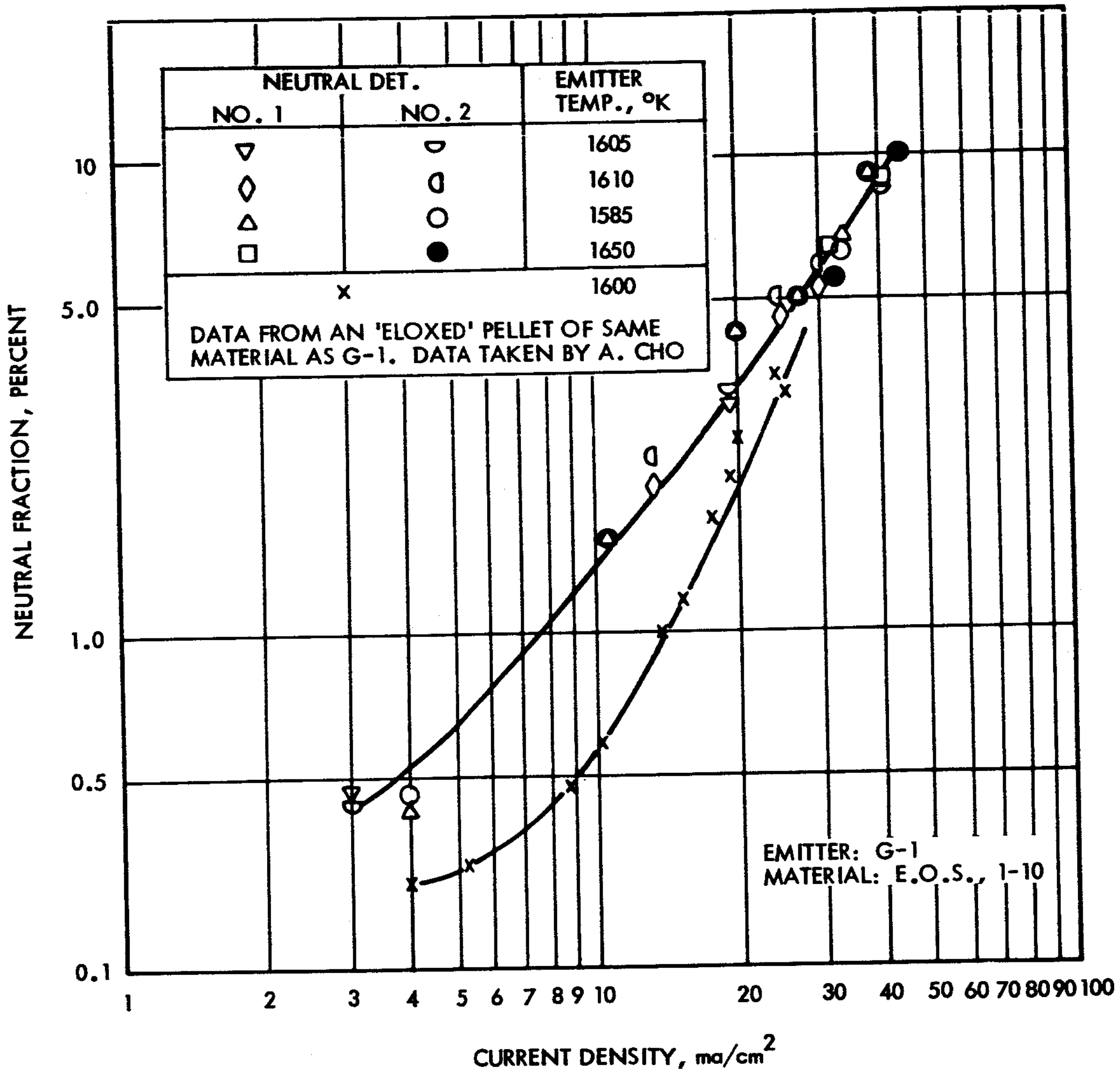

Figure 15. Cesium neutral fraction versus ion current density (G-1).

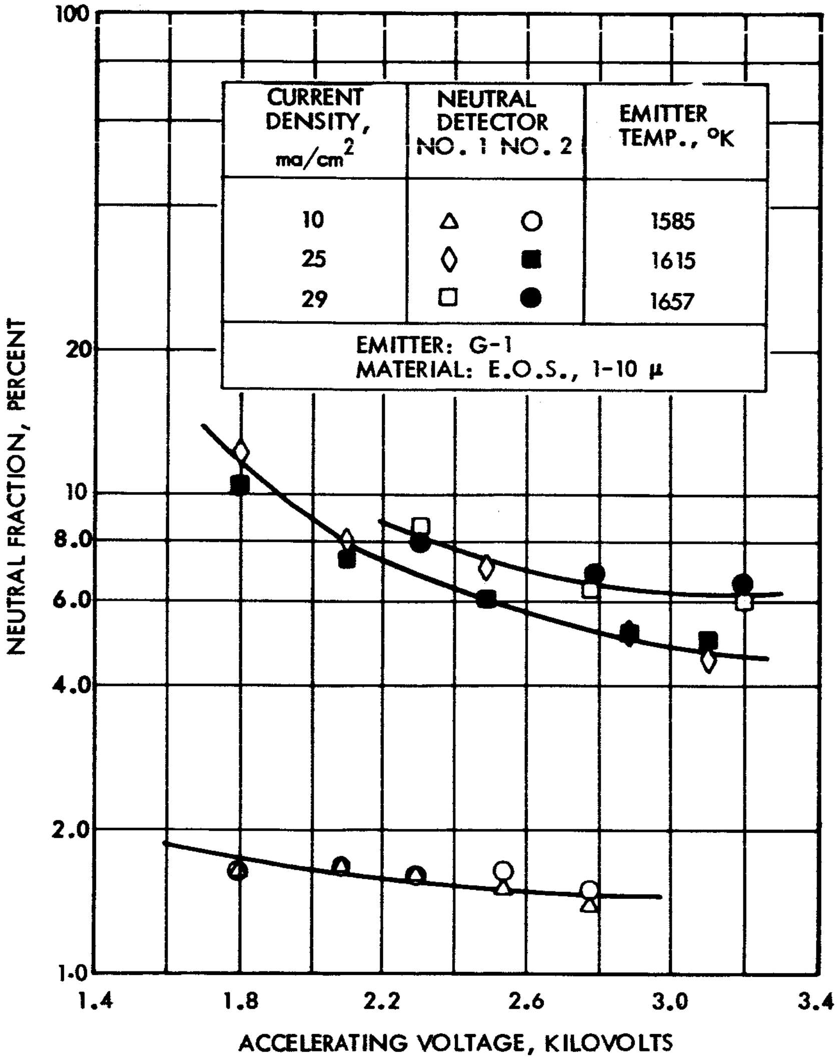

Figure 16. Cesium neutral fraction versus accelerating voltage (G-1).

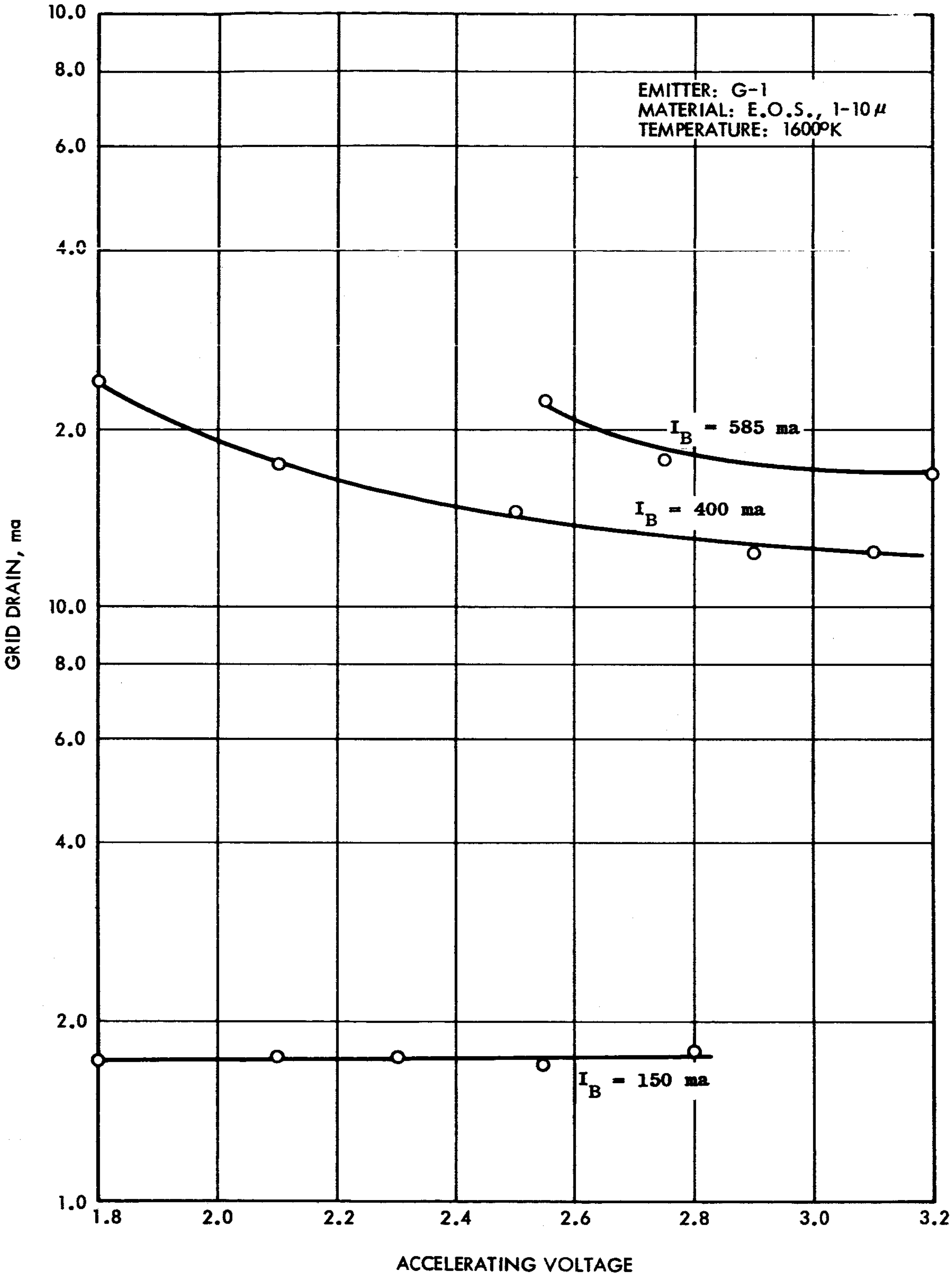

Figure 17. Grid drain current versus accelerating voltage (G-1).

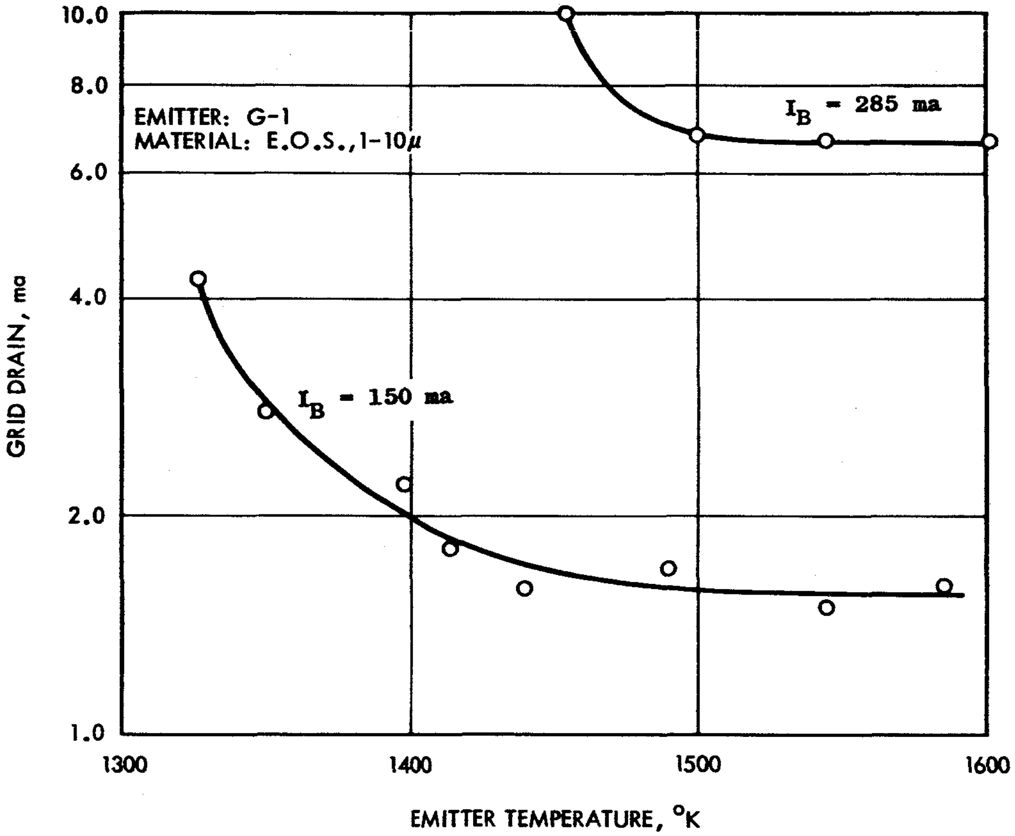

Figure 18. Grid drain current versus emitter temperature (G-1).

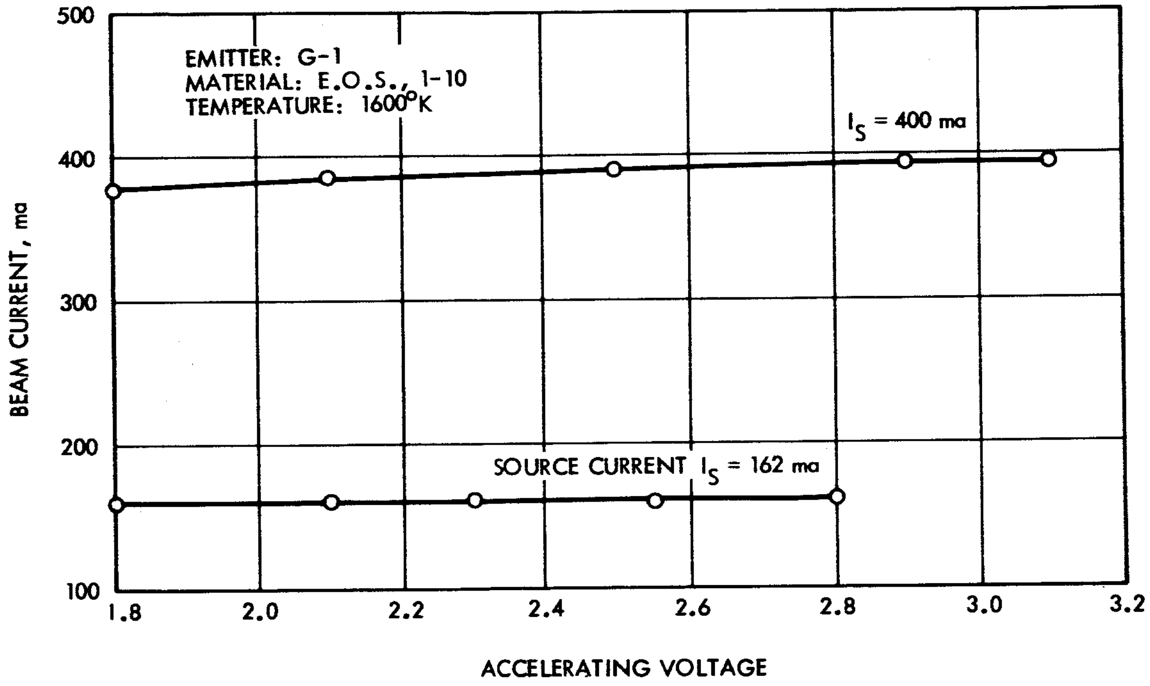

Figure 19. Beam current versus accelerating voltage (G-1).

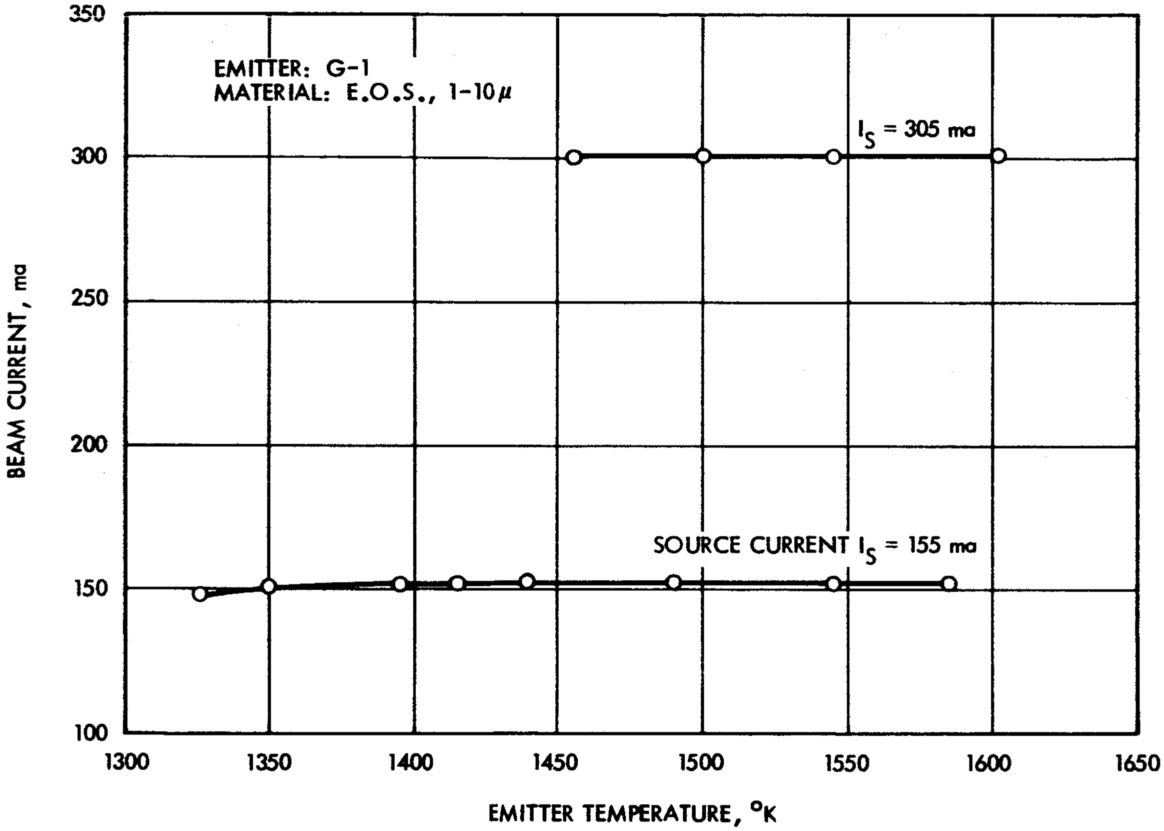

Figure 20. Beam current versus emitter temperature (G-1).

indicate that the α-versus-J relation is independent of temperature over the range of temperatures measured (1605°K to 1650°K) but that the neutral fraction of emitter G-1 was higher than that of the Eloxed emitter used by A. Cho by a factor that varies from 1.4 to 2.3.

Further Tests with Emitter G-1

Electropolish

After the first series of tests with emitter G-1, during which the emissivity increased from 0.28 to 0.38 after operation to 45 ma/cm^2 in a relatively poor vacuum environment, the emitter was electropolished by the Merel Co., Gardena, California, using a TRW fixture to shape the field. Nothing is known of the electropolish solution employed by this company except that only inorganic, water-soluble chemicals are used and that it is claimed that this solution will not attack tungsten without the application of an electric field.

After electropolishing, the appearance of the emitter indicated only superficial surface polishing and the opening up of several pit-holes along one side. In spite of this poor appearance, G-1 was re-installed in the ion engine so that emissivity, work function, beam profile, and grid reflection factor of the neutral fraction could be measured.

Emissivity

Emissivity measured 0.29 after electropolishing and remained virtually unchanged after the emitter was operated as an ion engine to 46 ma/cm^2.

Work Function

Work function measurements were made with the emitter held at 10 to 100 volts negative with respect to ground and with the accelerator grid and collector grounded. The measured electron current (with negligible cesium feed) for emitter temperatures in the range 1600° to 1800°K was used to compute the work function (see Figure 21).

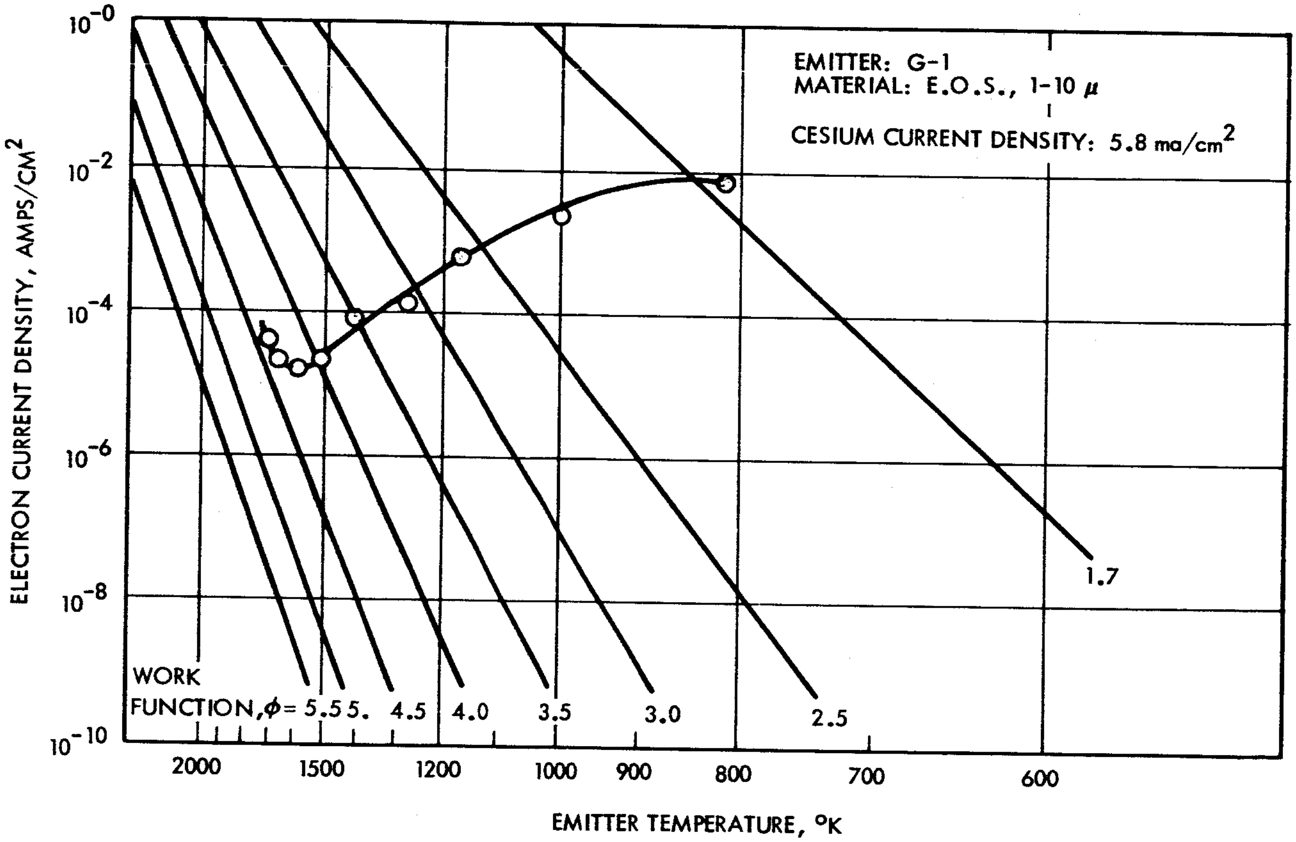

Figure 21. Electron current S curve (G-1).

At the beginning of the tests a work function of 4.5 ev was measured. At the conclusion of the test this had increased to 4.65 ev.

Neutral Fraction

The performance of this emitter as an ion engine had been drastically changed. Neutral fractions were somewhat less than Cho's "clean tungsten" data for E.O.S.'s 1-10μ pellets, and critical temperatures were also lowered. Typical measurements were 0.33% neutrals at 1650°K, 1% neutrals at 1535°K, and criticality at 1490°K with a current density of 30 ma/cm^2. In another measurement with an emitter temperature of 1700°K, the neutral fraction remained below 1% until the current density exceeded 45 ma/cm^2, at which point criticality was indicated.*

EMITTER G-3

Processing

This emitter was manufactured from E.O.S. 1-10μ powder, designated W.A. 5141 Bar No. 5.

The tests of emitter G-3 showed that under certain conditions an emitter can be contaminated with molybdenum. The ionizer baffle and other molybdenum parts of the engine (i.e., heat shields) that are at high temperatures become coated with MoO_3 if there is oxygen present in the system. MoO_3 has a high vapor pressure (1.15μ at 850°K) and spreads through the system. Sputtering may also cause contamination from the molybdenum grid clips. If the emitter is run at high temperatures for extended periods with neutral cesium present – introduced, say, by a poisoned emitter – ions formed on the ionizer baffle will be accelerated and strike the grid clips.

G-3 was run for several hours in an air leak and later in O_2 at pressures as high as 2×10^{-5} mm Hg. During this period the engine was probably contaminated by MoO_3 transport of molybdenum.

---

* Uncorrected neutral fraction. See footnote on Page 34.

Inspection of the grids indicated that extensive sputtering of the molybdenum grid clips had also occurred, particularly on those grids used later in the test run. (These grids were run for long periods during which the emitters had to be at high temperatures because of high critical temperatures and neutral fractions were quite high, i.e., 3 to 5%). Sputtering damage to grids is illustrated in Figures 22 and 23.

Pore Data and Transmissivity

Pore data and the transmissivity of emitter G-3 are shown in Figure 24.

Beam Profile (G-3)

Figure 25 shows the beam profile for positions 2, 4 and 6 (see Figure 12). The profile shows that the beam density in the center portion of the emitter varies by approximately 1/5 the average beam density. The average unbiased beam current was 0.265 ma. The current should have been 0.20 ma. The difference of approximately 0.06 ma was due to secondary emission from the probe. Much of the fine structure in these profiles is due to the beam being focussed between the grids, but the grosser variation that encompasses several grid openings are the result of variation in throughput. (There are 53 grid bars and 52 openings in the grid. Each opening is 22 mils wide.)

Emissivity

The total emissivity when the emitter was first installed was 0.302 at 1565^{o}K. During the test run the emissivity remained fairly constant, with a slight decrease toward the end of the run.

Work Function

After the air leak was stopped, the work function was measured from electrons thermionically emitted from the emitter and collected on a tungsten collector grid. The work function was 4.6 ev, see Figure 26.

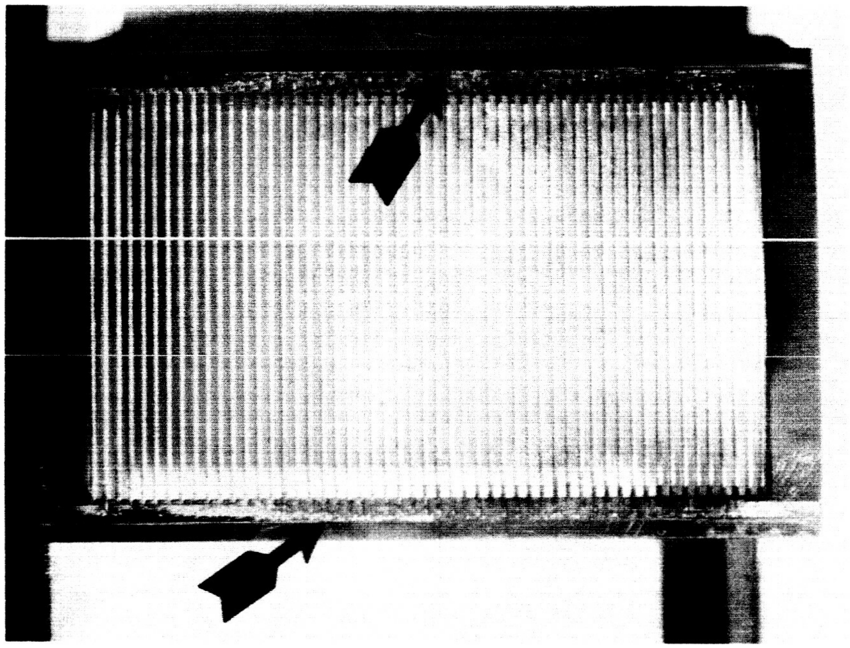

Figure 22. Grid showing molybdenum clips (arrows) completely sputtered through to the graphite grid frame.

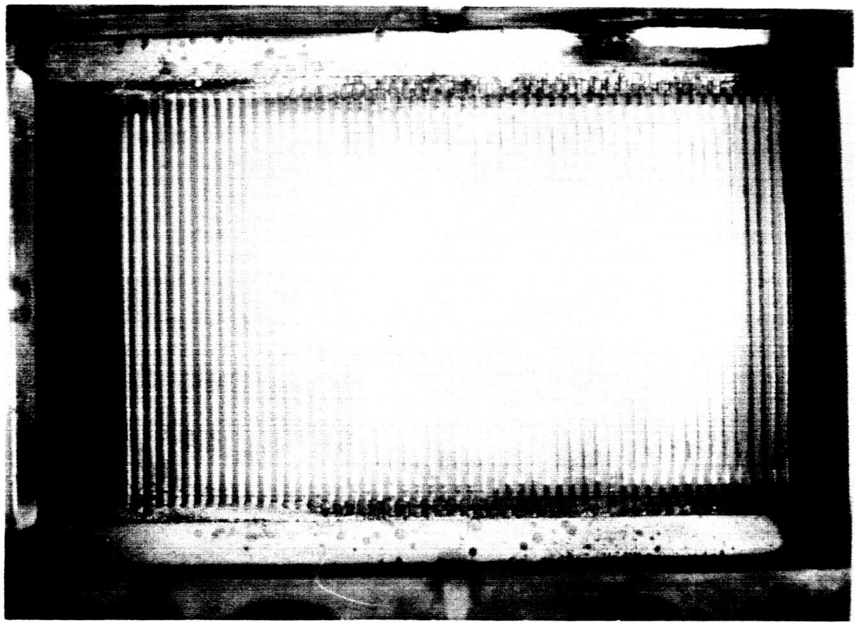

Figure 23. Partially sputtered grid.

FEED TUBE END

1 Pore Count $3.9 \times 10^6/\text{cm}^2$ (0.85) Pore Size 1.6μ Transmission 6.7×10^{-5} (1.01) Relative J	4 Pore Count $4.6 \times 10^6/\text{cm}^2$ (1.00) Pore Size 1.7μ Transmission 6.9×10^{-5} (1.04) Relative J	7 Pore Count $4.5 \times 10^6/\text{cm}^2$ (0.98) Pore Size 1.4μ Transmission 6.3×10^{-5} (0.95) Relative J
2 Pore Count $4.5 \times 10^6/\text{cm}^2$ (0.98) Pore Size 1.5μ Transmission 6.5×10^{-5} (0.98) Relative J	5 Pore Count $4.2 \times 10^6/\text{cm}^2$ (0.91) Pore Size 1.5μ Transmission 7.6×10^{-5} (1.15) Relative J	8 Pore Count $5.0 \times 10^6/\text{cm}^2$ (1.09) Pore Size 1.5μ Transmission 6.3×10^{-5} (0.95) Relative J
3 Pore Count $4.8 \times 10^6/\text{cm}^2$ (1.04) Pore Size 1.5μ Transmission 6.1×10^{-5} (0.92) Relative J	6 Pore Count $4.4 \times 10^6/\text{cm}^2$ (0.96) Pore Size 1.4μ Transmission 7.2×10^{-5} (1.09) Relative J	9 Pore Count $5.4 \times 10^6/\text{cm}^2$ (1.17) Pore Size 1.5μ Transmission 6.0×10^{-5} (0.91) Relative J

Density

Emitter - Top View

Mean Pore Count - $4.6 \times 10^6/\text{cm}^2$
Mean Transmission - 6.6×10^{-6}
Total Transmission - 6.7×10^{-5}

Material **E.O.S. 1-10μ**
Lot
Sample **Emitter (G-3)**

Figure 24. Pore-count and transmissivity data on Emitter G-3.

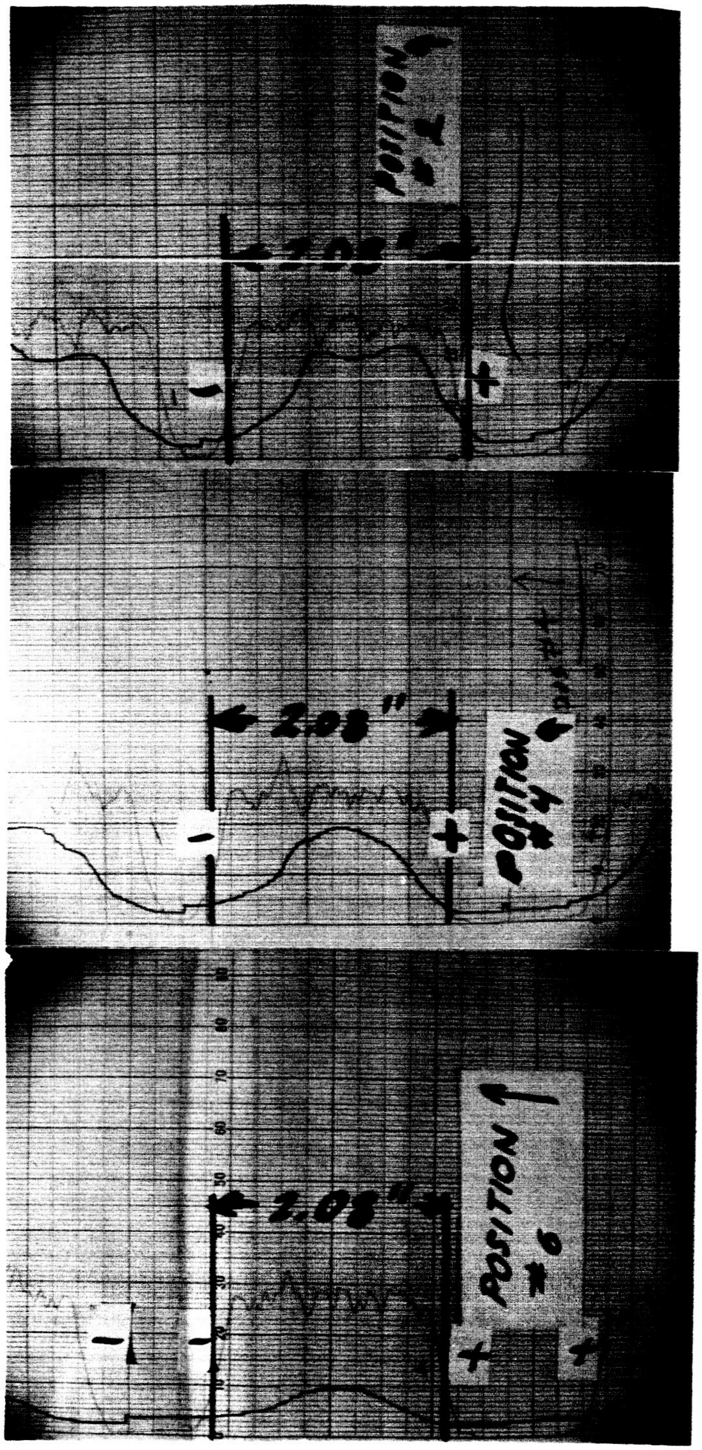

Figure 25. Photographs of the chart recording for positions 2, 4, and 6 (G-3). The upper trace (lighter of the two) shows the beam current. (Dark trace is a record of neutrals as probe swings across the beam.)

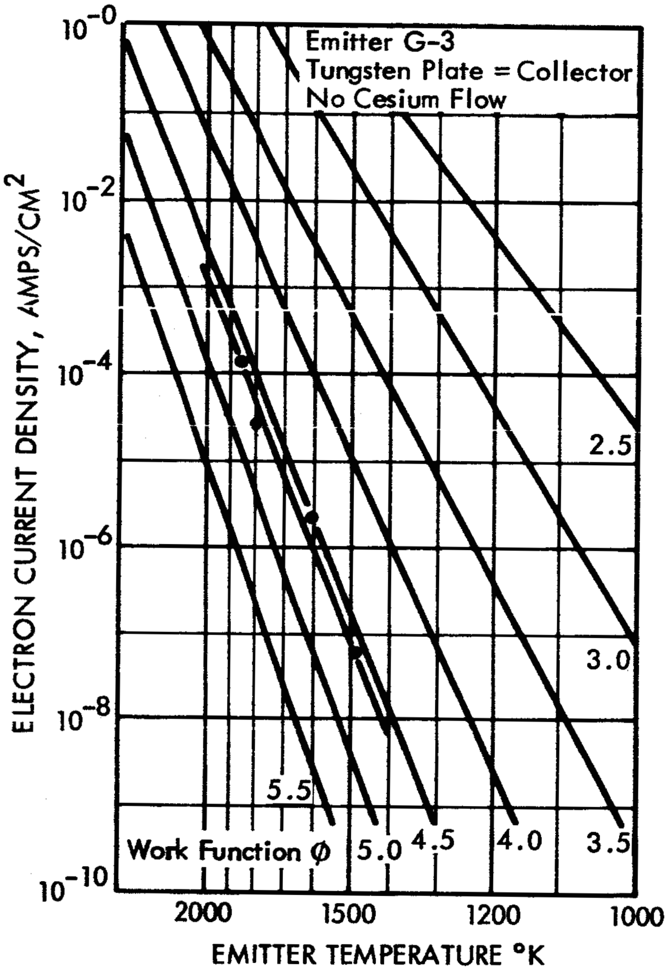

Figure 26. Work function data (G-3).

Test Data

The neutral fractions were generally quite high (3% or greater at 10 ma/cm^2) and the critical temperatures were poorly defined. When O_2 was present, the critical temperature was lower, the neutral fraction was less, and the critical temperature was more sharply defined. Figure 27 shows typical curves of neutrals versus temperature for 10 and 20 ma/cm^2, together with data taken at 10 ma/cm^2 by A. Cho[2] from an emitter made of the same material as G-3. Figure 28 compares the neutral fraction versus temperature for G-3 when there was an air leak with data taken by A. Cho when O_2 was present.*

*Uncorrected neutral data. See footnote on Page 34.

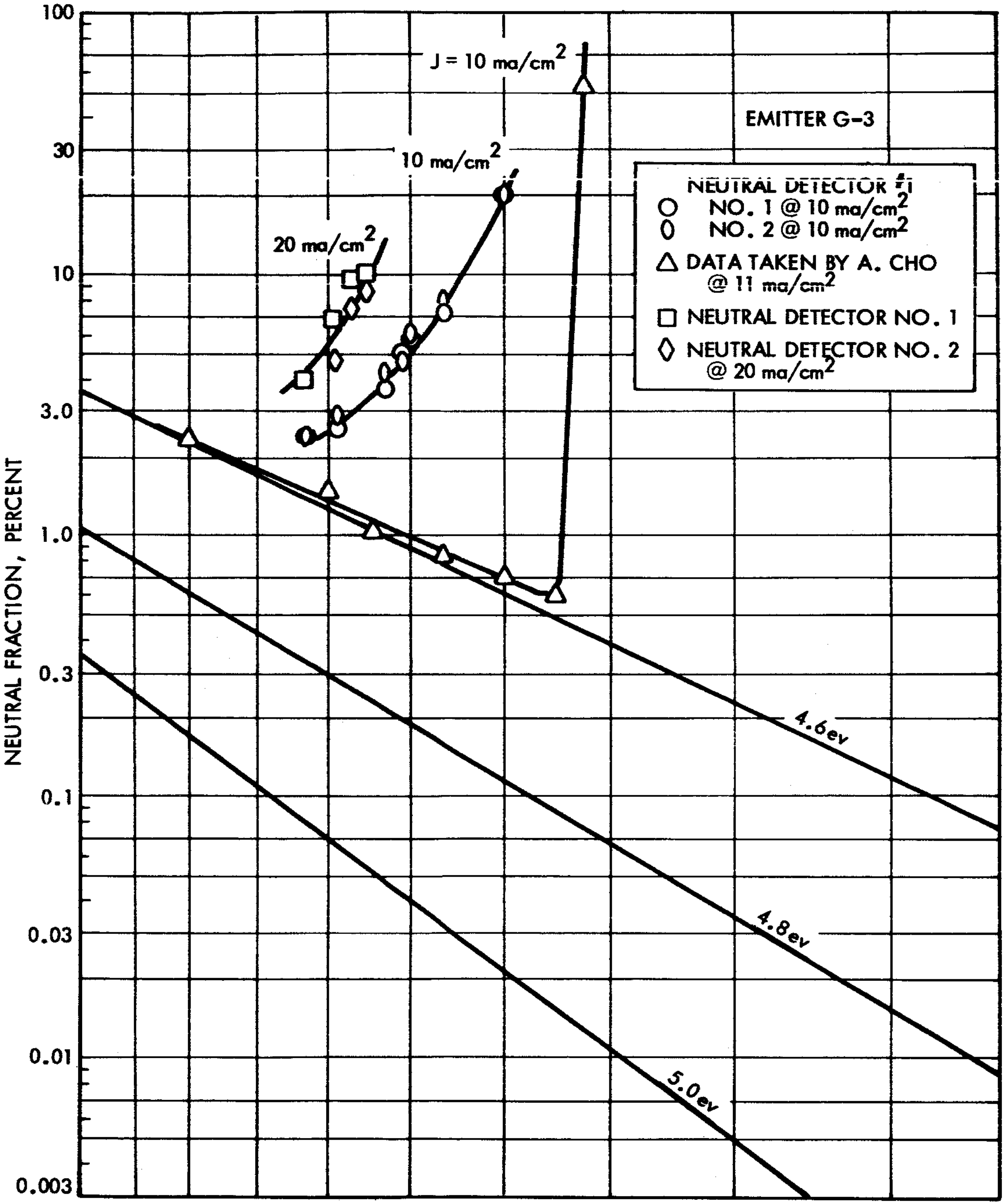

Figure 27. Neutral fraction versus temperature (G-3).

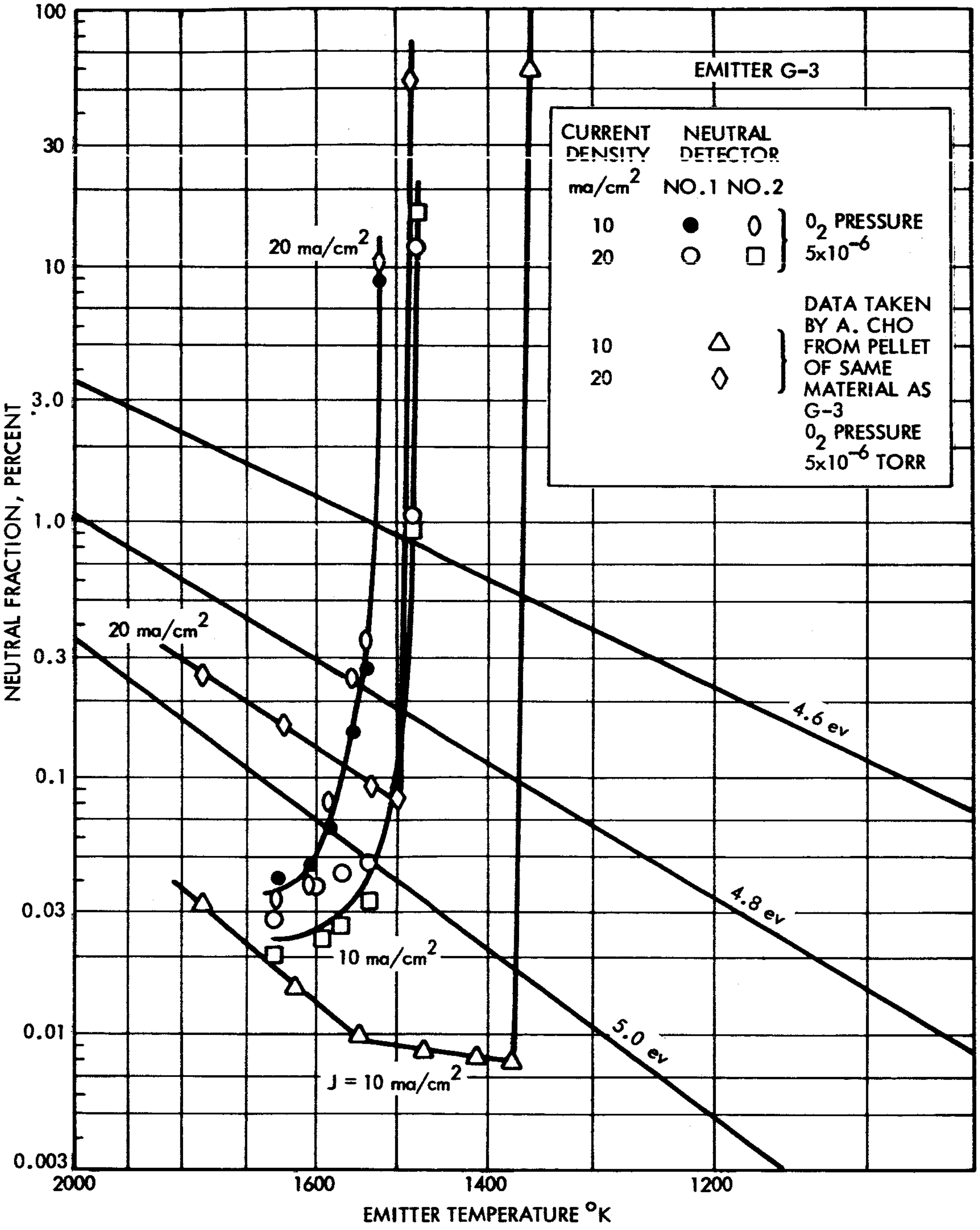

Figure 28. Neutral fraction versus temperature with O_2 present (G-3).

Figure 29 shows the neutral fraction versus accelerating voltage for G-3 at various current densities. Figures 30 through 33 show the following characteristics of G-3: Figure 30, grid drain versus temperature; Figure 31, beam current versus accelerating voltage; Figure 32, beam current versus emitter temperature; and Figure 33, grid drain versus accelerating voltage.

EMITTER G-4

Processing

G-4 was constructed from E.O.S. material (NAS3-5253, Bar No. 2).

Pore Data and Transmissivity

Pore data and the transmissivity of G-4 are shown in Figure 34.

Emissivity

The total emissivity of G-4 after eloxing but prior to sputtering was 0.29.

Work Function

The work function measurements for G-4 (prior to sputtering) indicated a low work function 4.3 ev.. See Figure 35.

Test Data

Performance characteristics for emitter G-4 are shown in Figures 36 through 41. Figure 42 shows data taken by A. Cho for an Eloxed emitter button of the G-4 type.*

Beam Profile

Figure 43 shows the beam profile for position 6 (see Figure 12) at 10 ma/cm^2 for G-4. The profile indicates a very regular beam density across the face of the emitter. The average probe current for G-4 was 0.2 ma.

---

* Uncorrected neutral fraction. See footnote on Page 34.

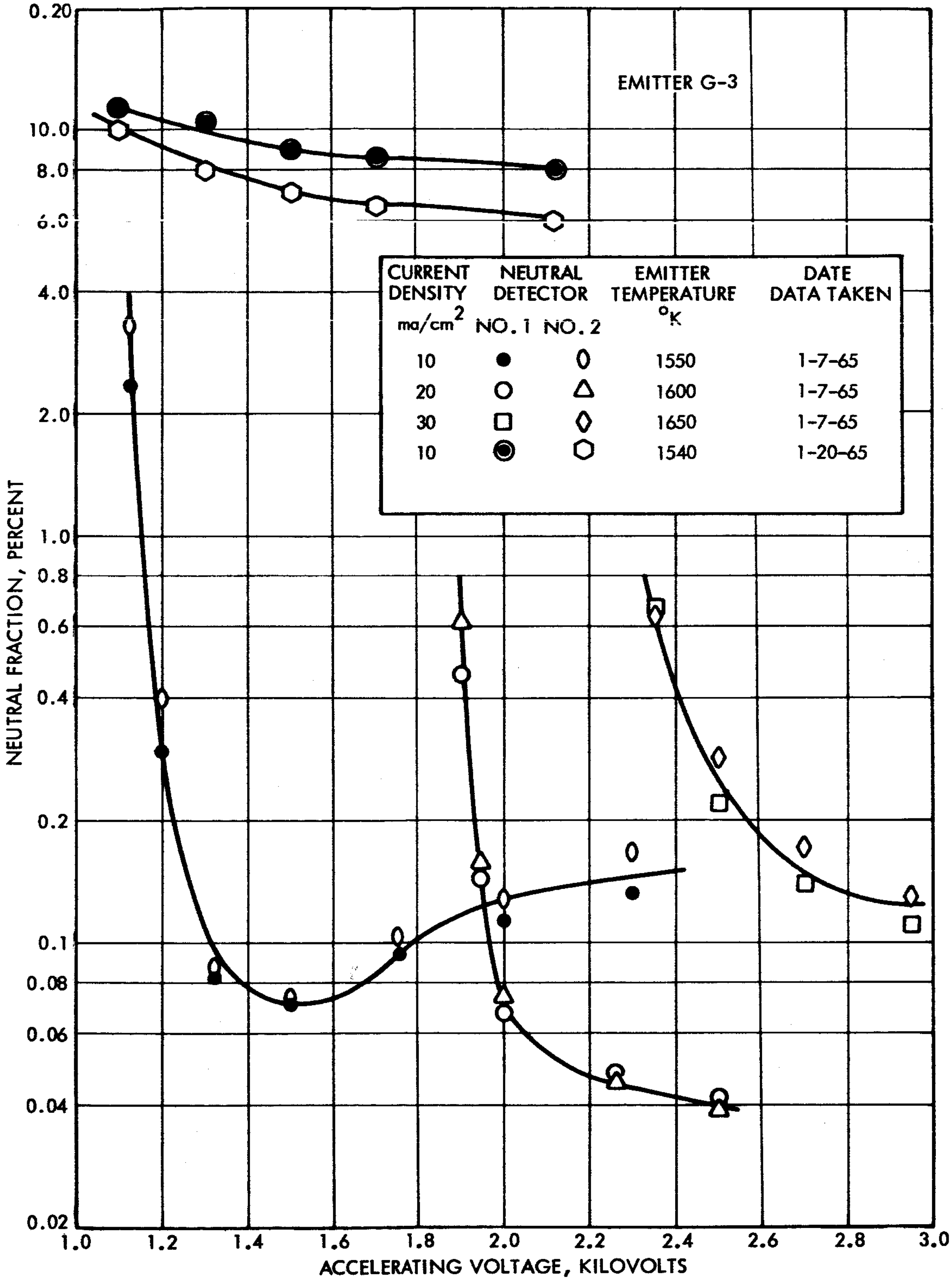

Figure 29. Neutral fraction versus accelerating voltage (G-3).

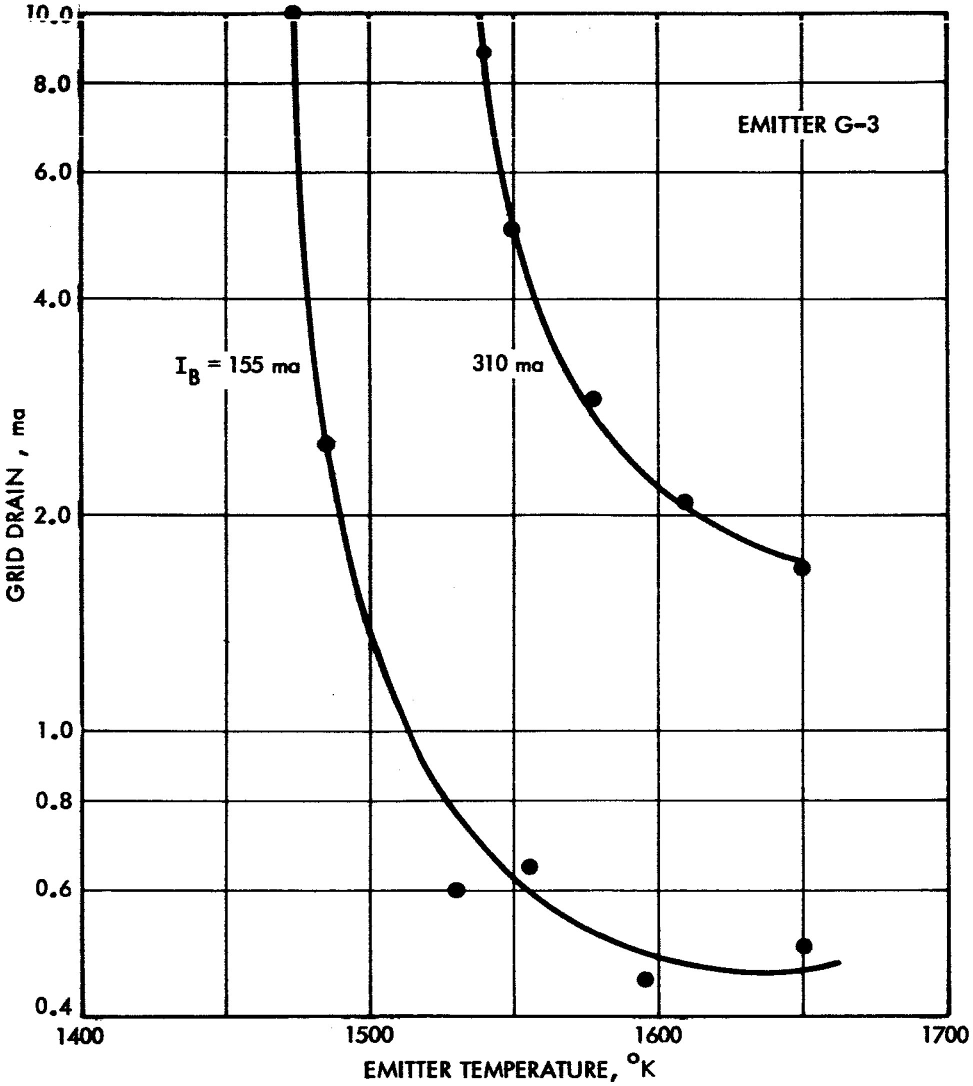

Figure 30. Grid drain versus temperature (G-3).

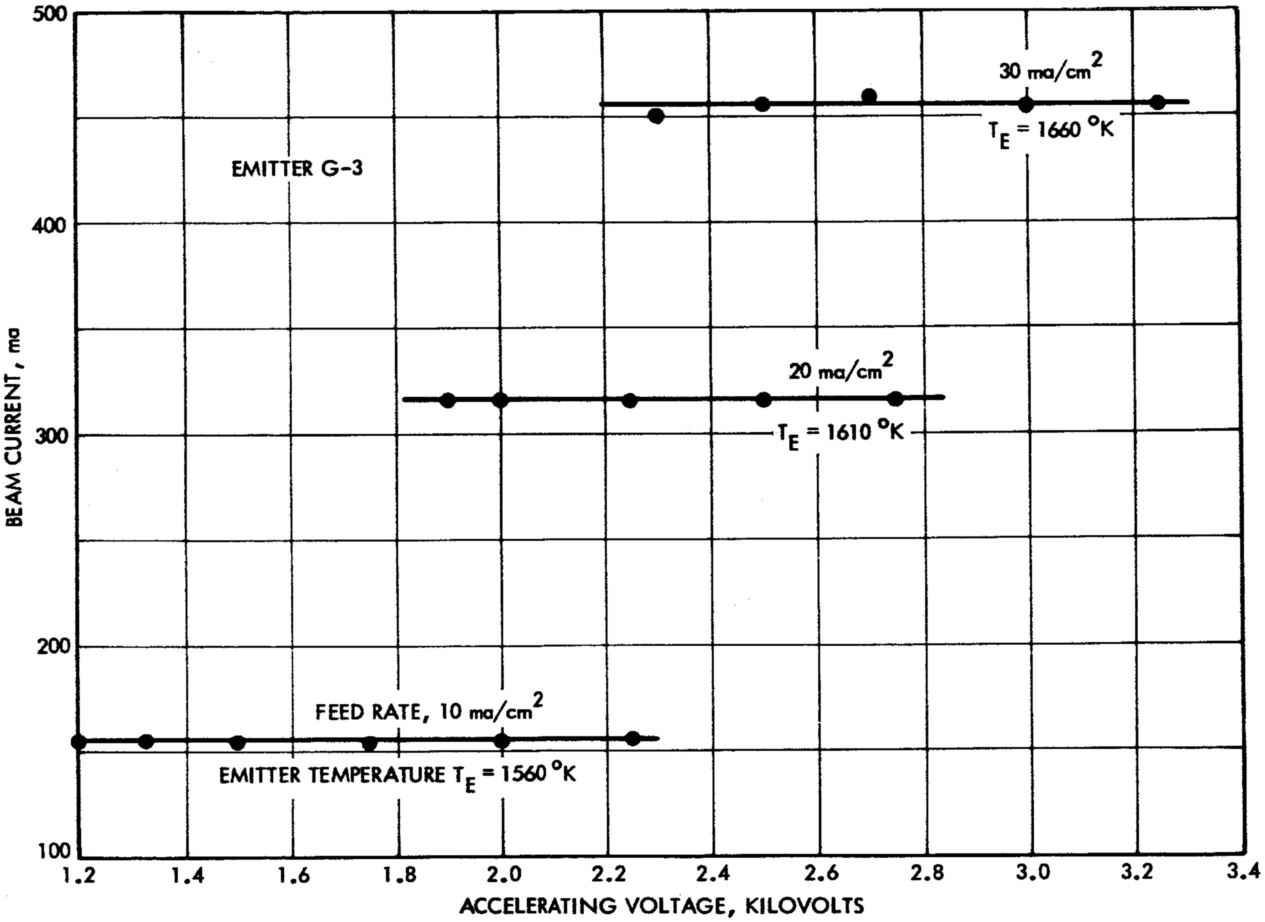

Figure 31. Beam current versus accelerating voltage (G-3).

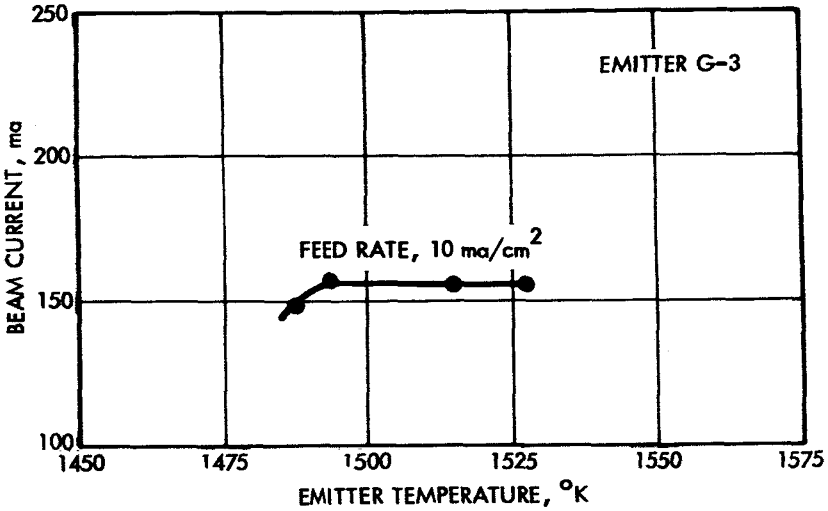

Figure 32. Beam current versus accelerating voltage (G-3).

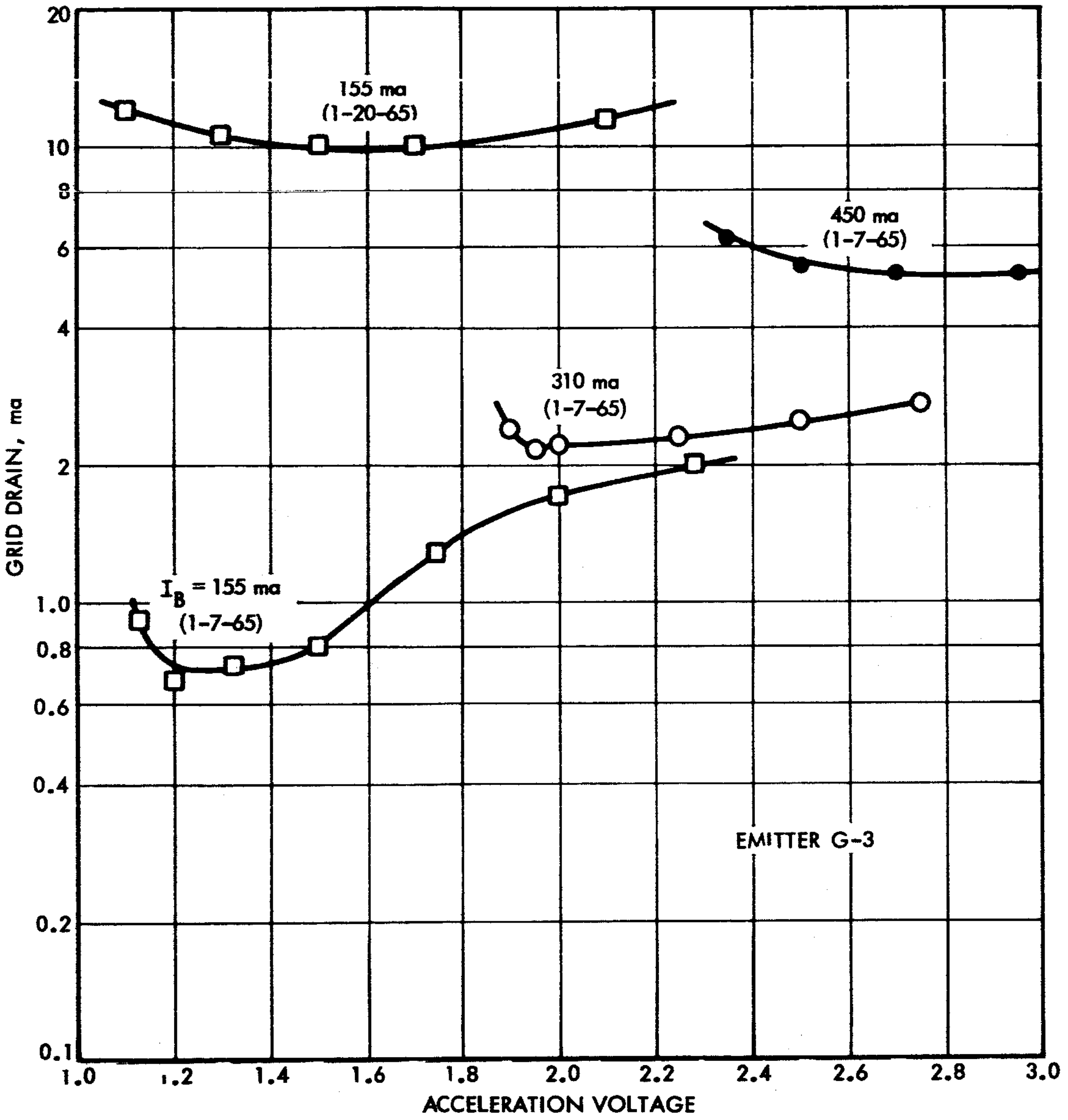

Figure 33. Grid drain versus accelerating voltage (G-3).

FEED TUBE END

1 Pore Count $4.5 \times 10^6/cm^2$ (1.02) Pore Size Transmission 6.0×10^{-5} (0.99) Relative J	4 Pore Count $5.2 \times 10^6/cm^2$ (1.18) Pore Size Transmission 6.0×10^{-5} (1.00) Relative J	7 Pore Count $4.3 \times 10^6/cm^2$ (0.98) Pore Size Transmission 6.1×10^{-5} (1.02) Relative J
2 Pore Count $4.8 \times 10^6/cm^2$ (1.12) Pore Size Transmission 6.3×10^{-5} (1.06) Relative J	5 Pore Count $4.1 \times 10^6/cm^2$ (0.95) Pore Size Transmission 6.2×10^{-5} (1.03) Relative J	8 Pore Count $4.4 \times 10^6/cm^2$ (1.0) Pore Size Transmission 5.9×10^{-5} (0.99) Relative J
3 Pore Count $4.6 \times 10^6/cm^2$ (1.05) Pore Size Transmission 5.9×10^{-5} (0.98) Relative J	6 Pore Count $3.5 \times 10^6/cm^2$ (0.80) Pore Size Transmission 6.0×10^{-5} (1.01) Relative J	9 Pore Count $4.3 \times 10^6/cm^2$ (0.98) Pore Size Transmission 5.5×10^{-5} (0.92) Relative J

Density 79.37%

Mean Pore Count - $4.4 \times 10^6/cm^2$

Mean Transmission - 6×10^{-5}

Total Transmission - 5.75×10^{-5}

Emitter - Top View

Material E.O.S.

Lot W.A. 5141 Bar No. 2

Sample (Emitter G-4)

Figure 34. Pore-count and emissivity data on Emitter G-4.

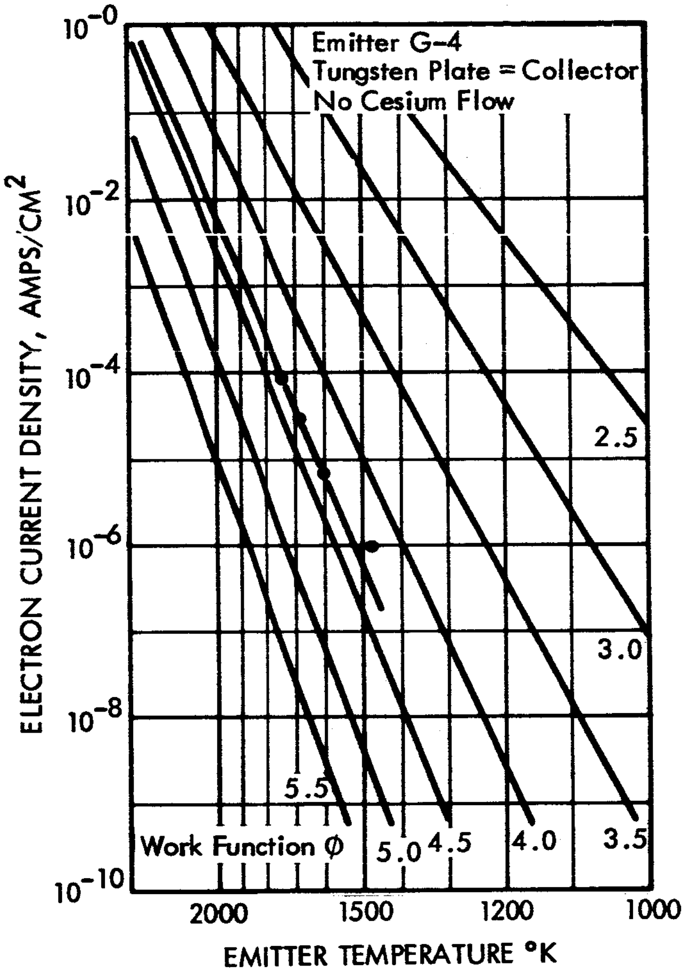

Figure 35. Work function Emitter G-4.

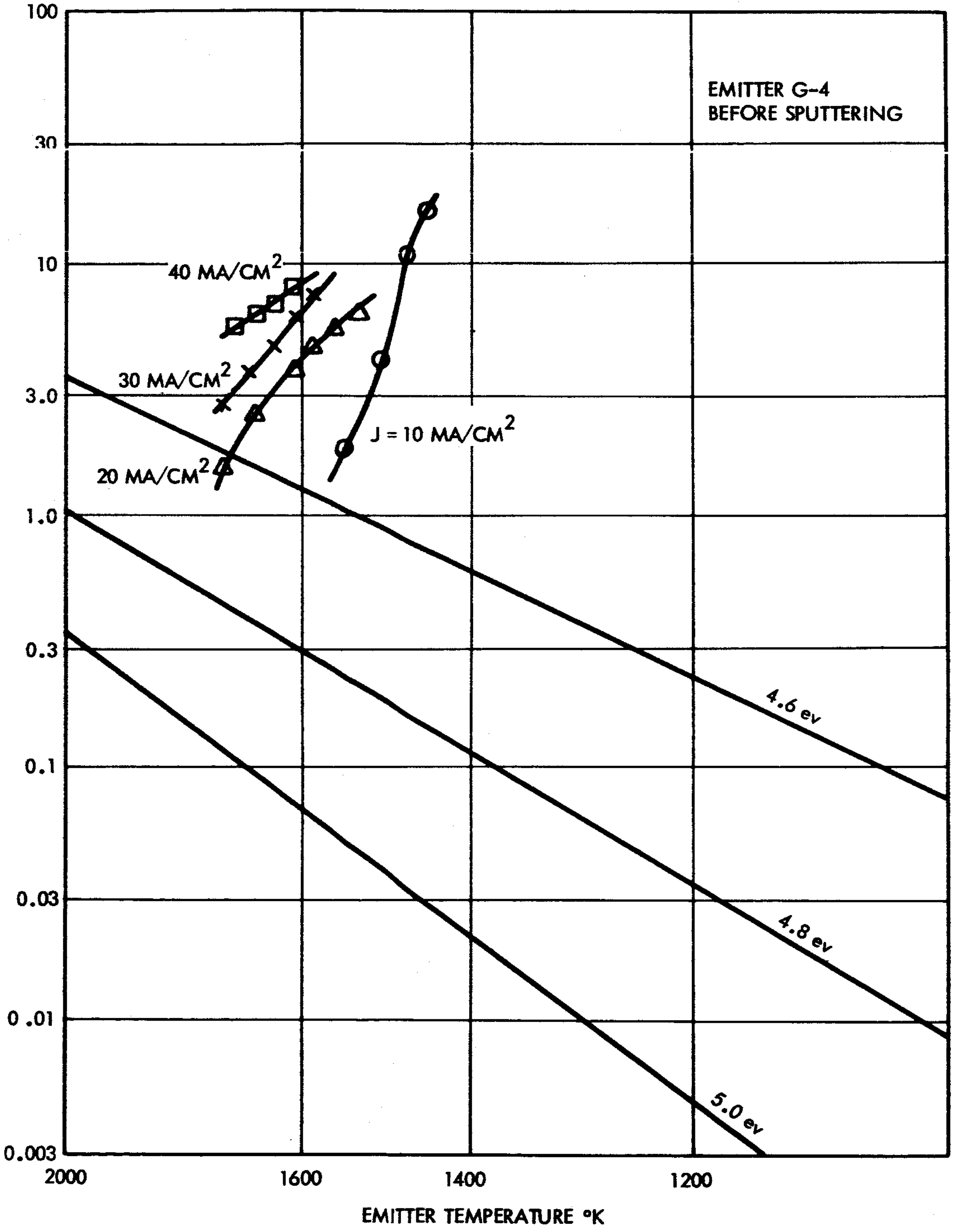

Figure 36. Neutral fraction versus temperature (G-4).

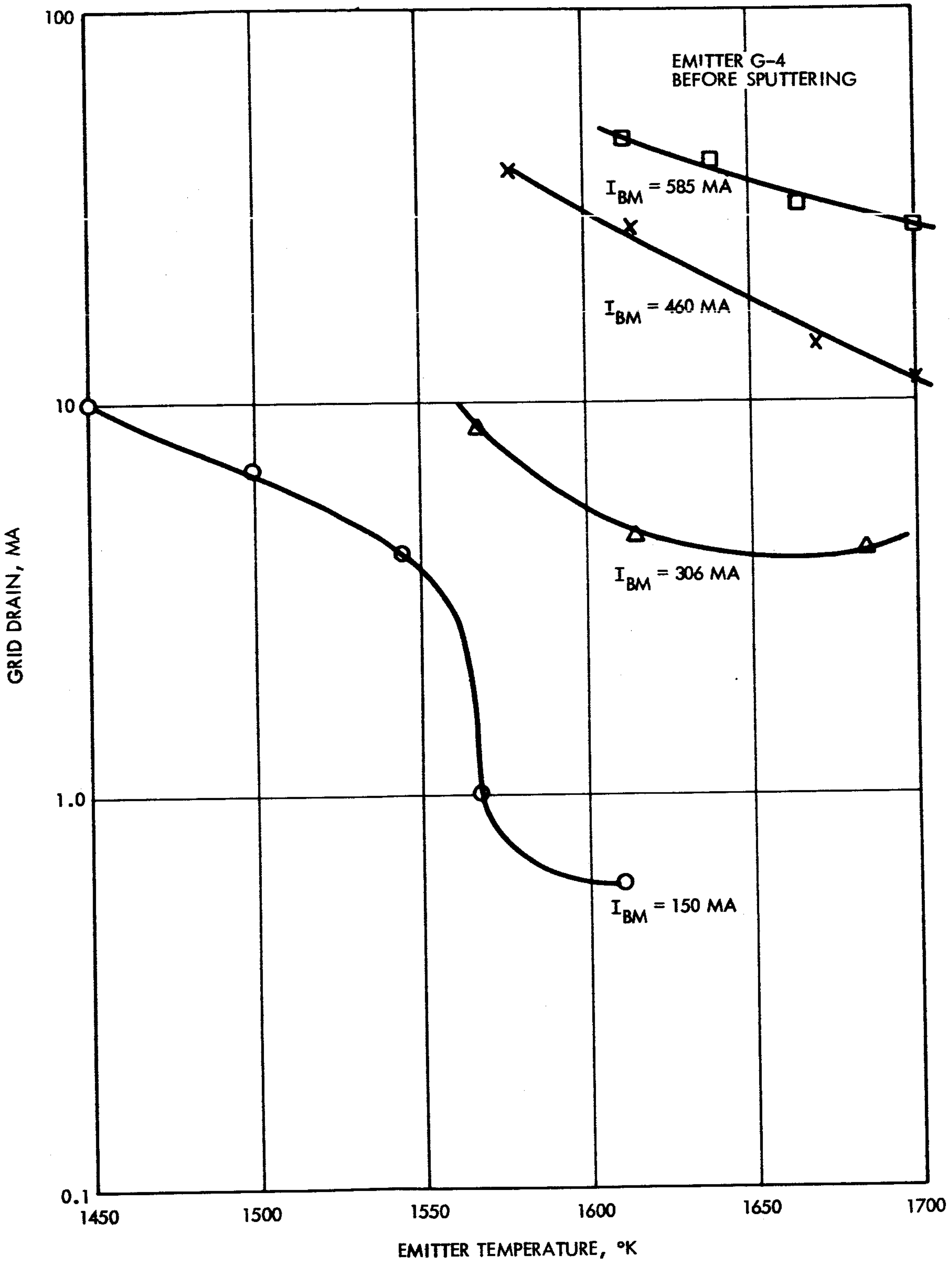

Figure 37. Grid drain versus temitter temperature (G-4).

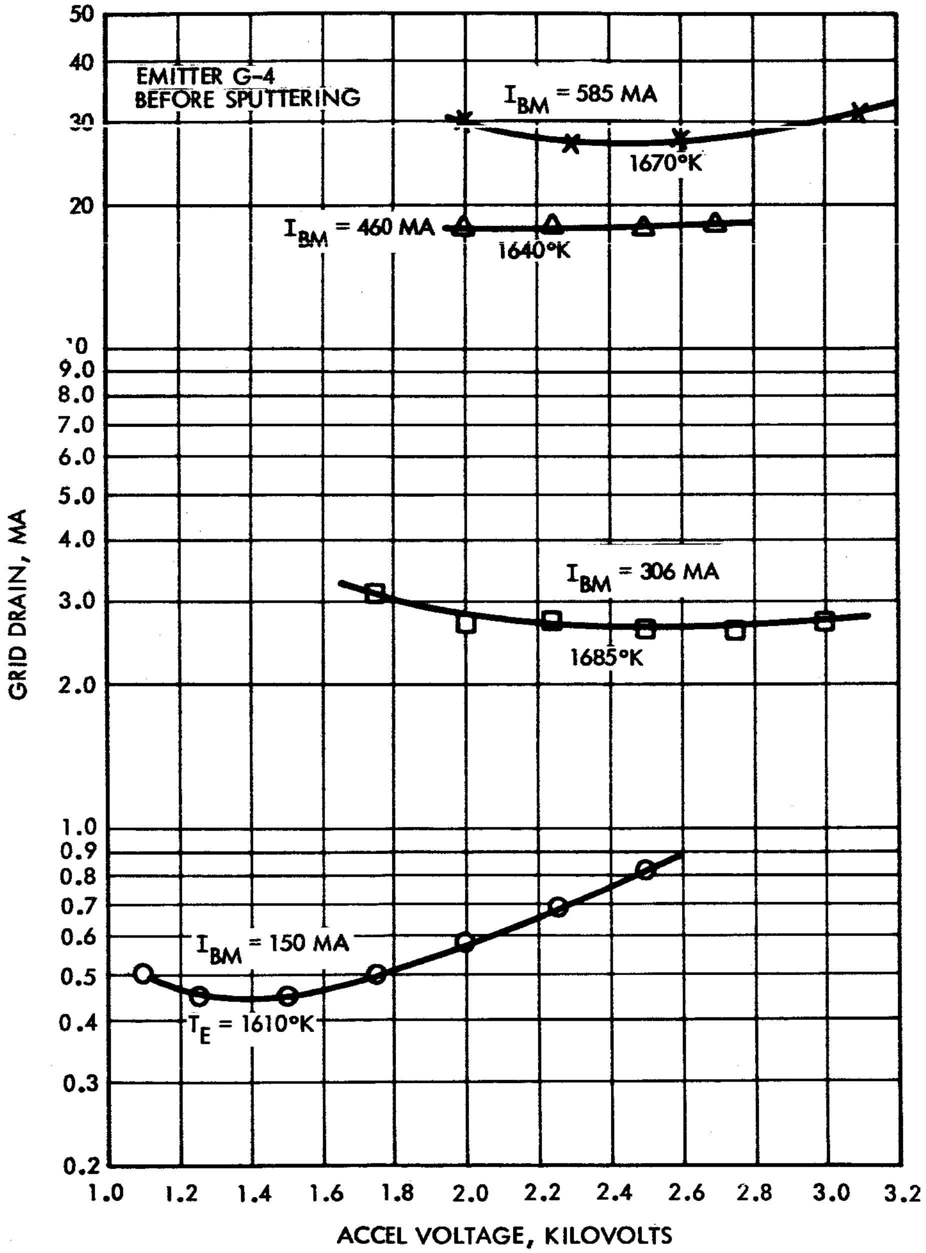

Figure 38. Grid drain versus accelerating voltage (G-4).

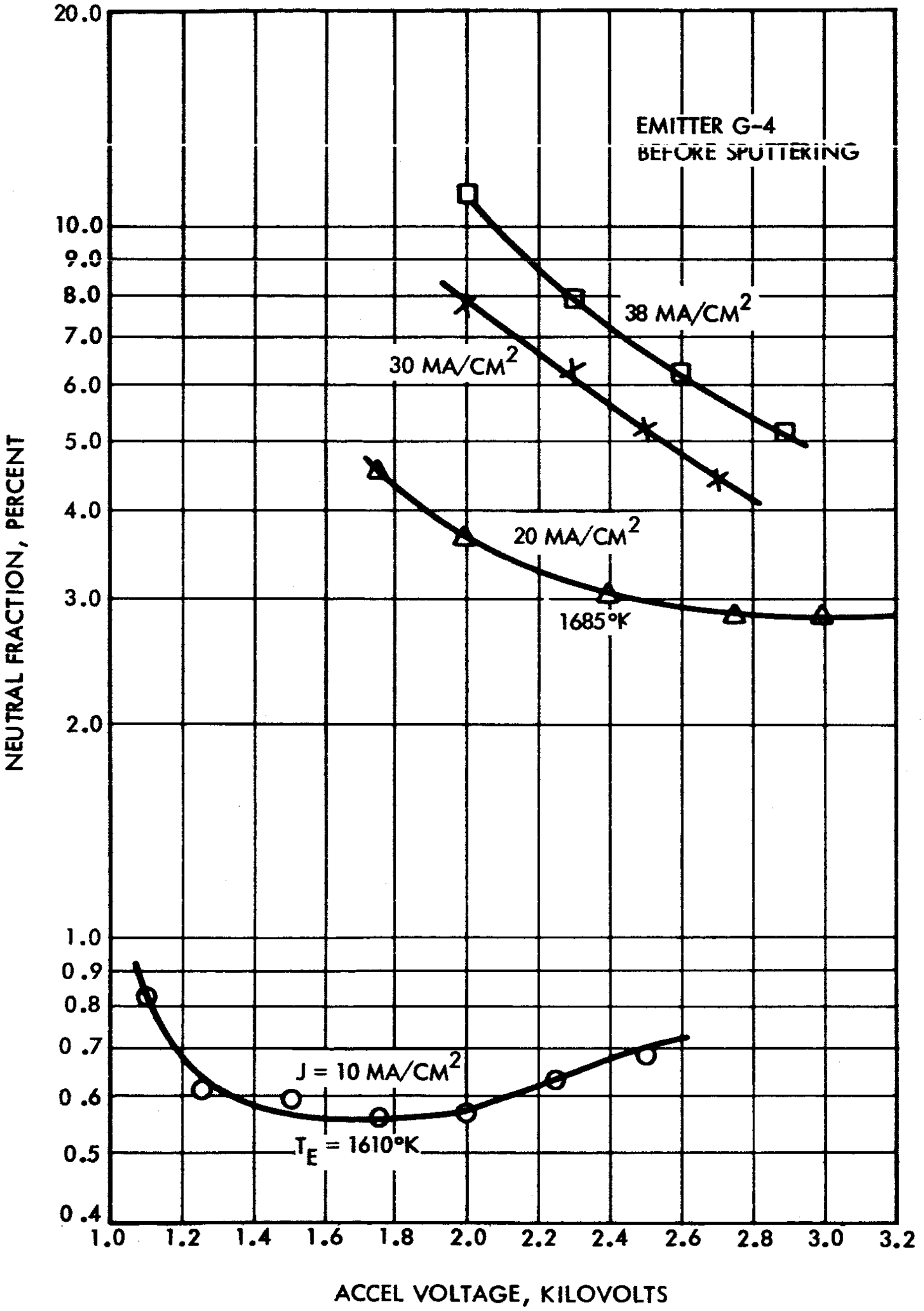

Figure 39. Neutral fraction versus accelerating voltage (G-4).

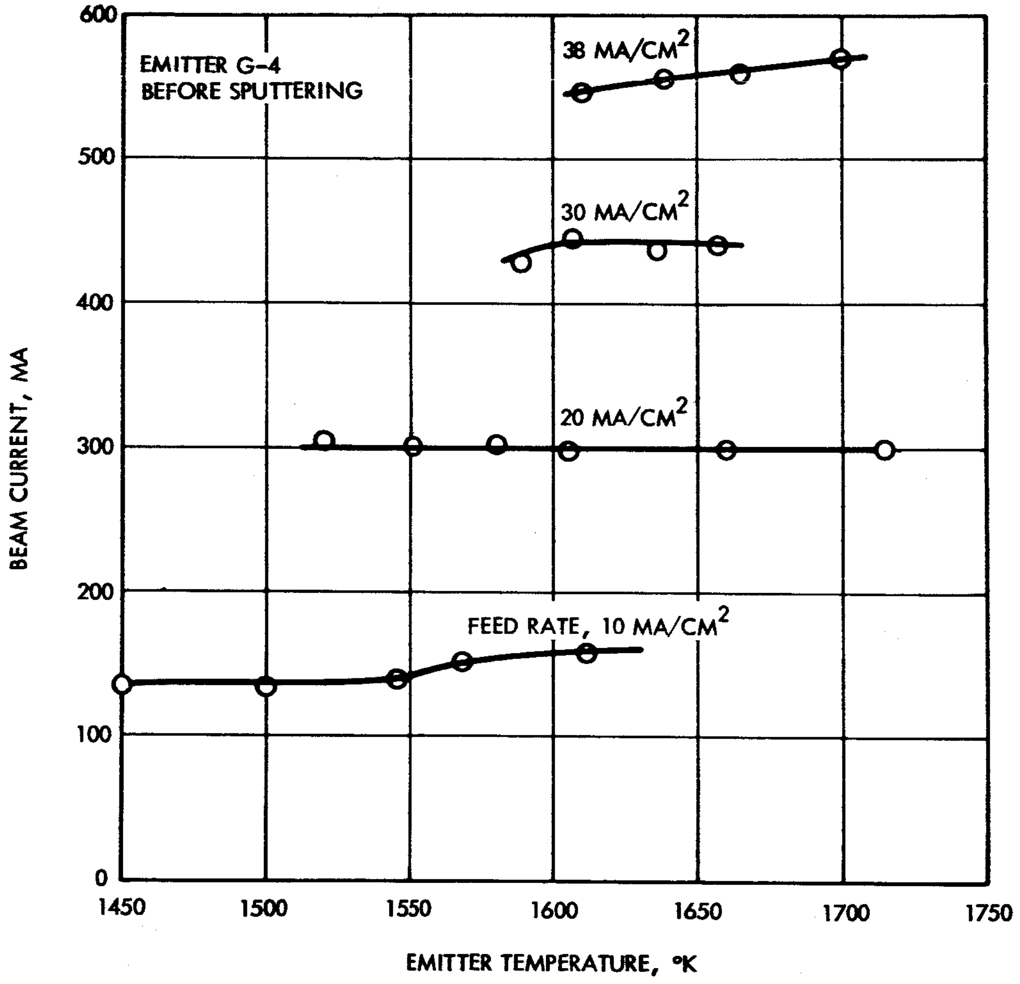

Figure 40. Beam current versus emitter temperature (G-4).

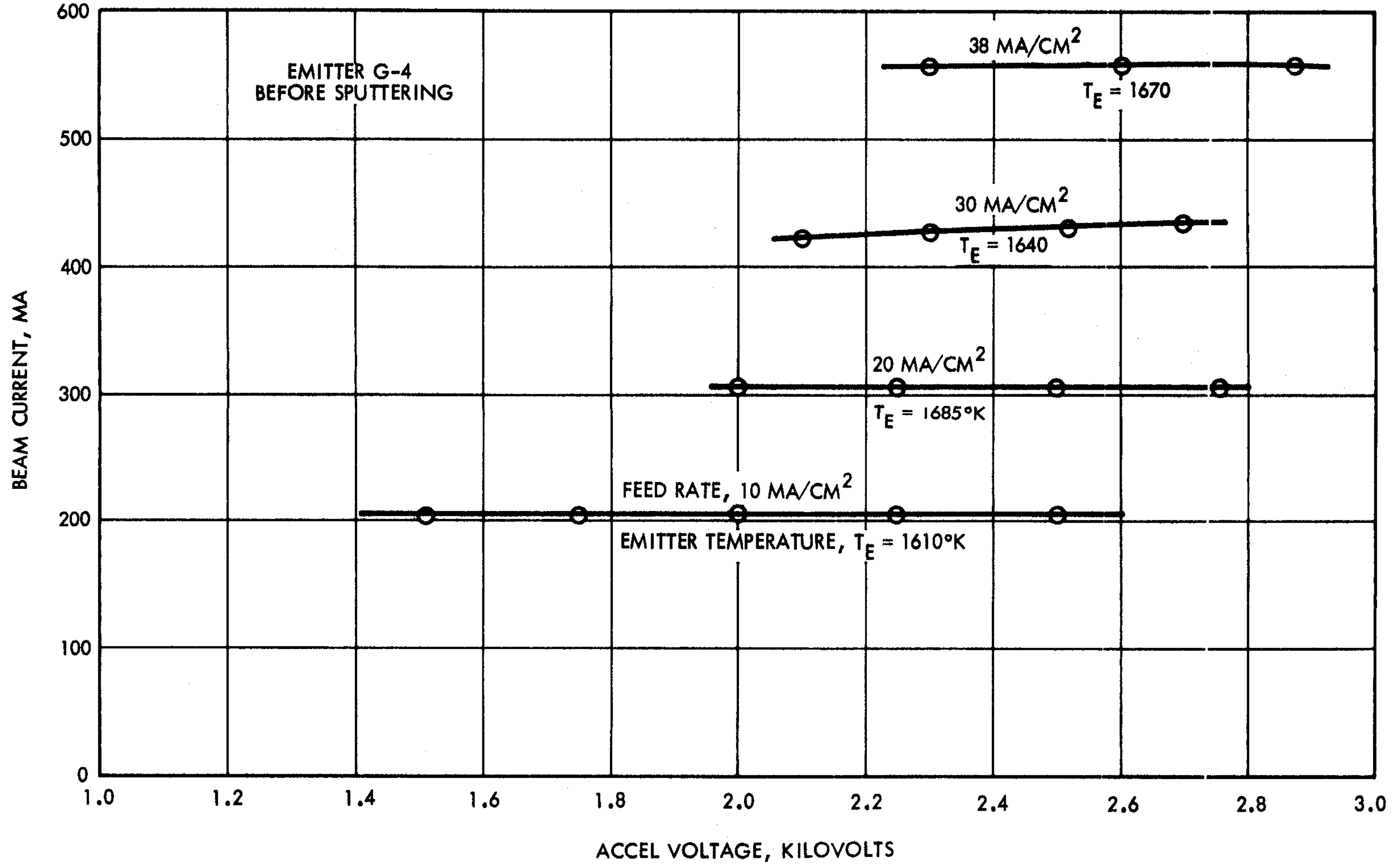

Figure 41. Beam current versus accelerating voltage (G-4).

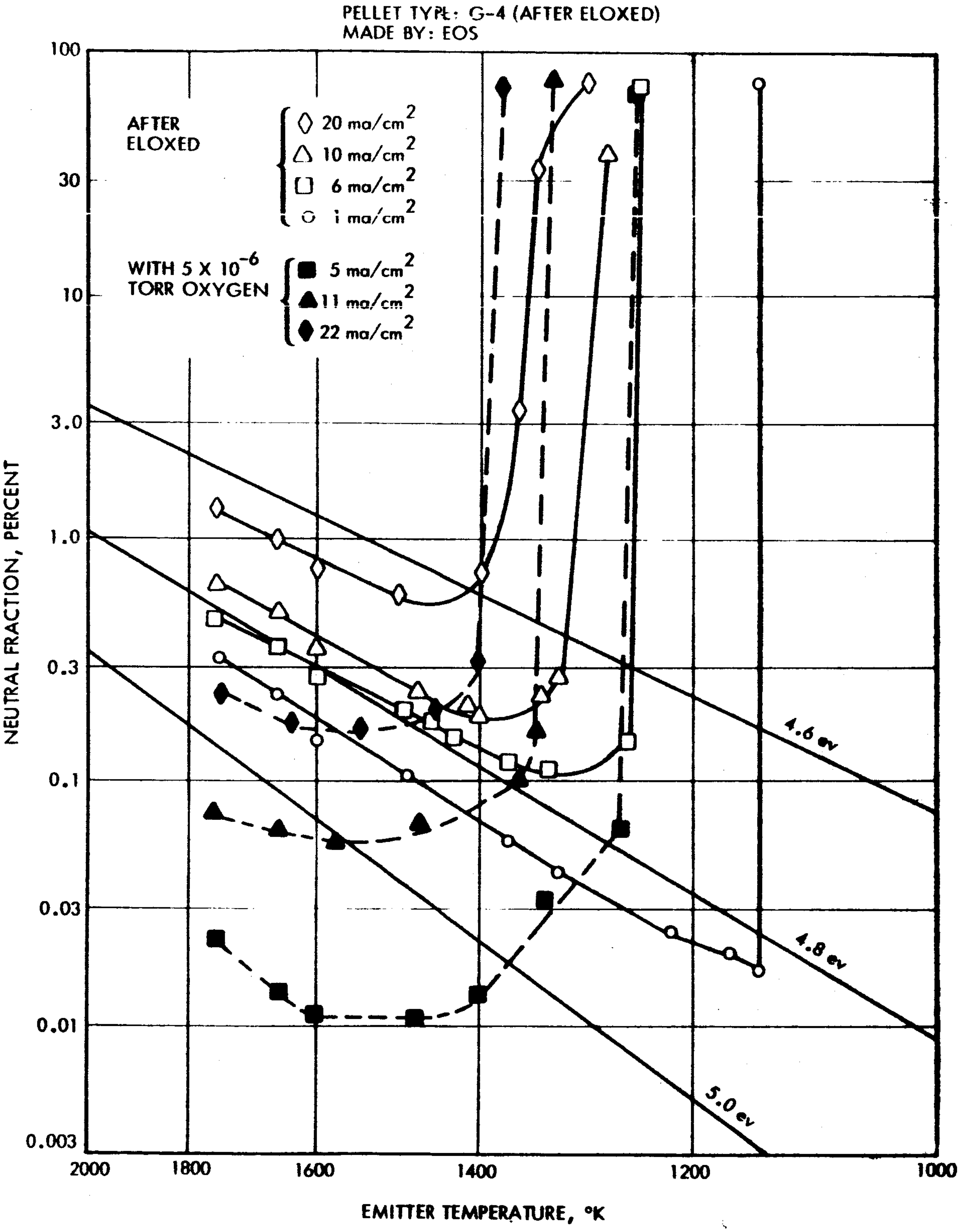

Figure 42. Cesium neutral fraction versus temperature of ion emitter after Elox machining (G-4).

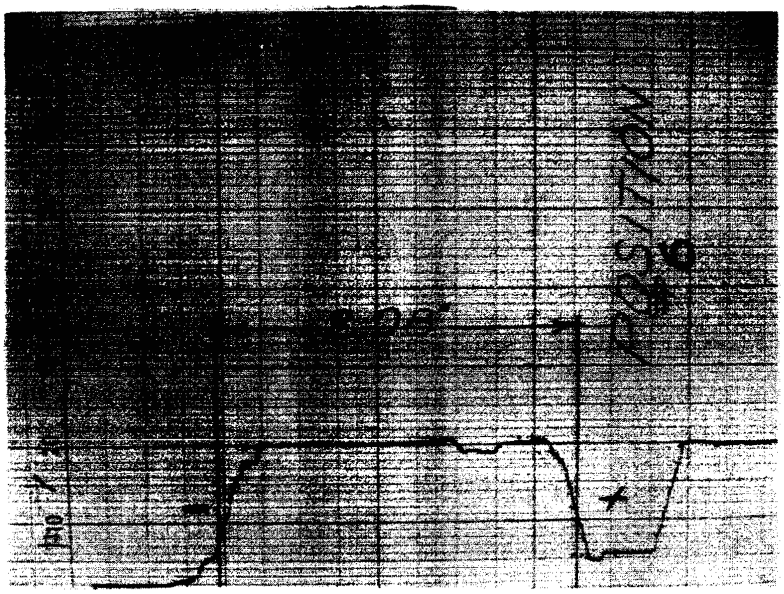

Figure 43. Beam profile of Emitter G-4.

Discussion

The performance of G-4 was disappointing, in that the neutral fraction and critical temperature results were far inferior to the values obtained with pellets of the same material (Figure 42).

It was suspected when the test data obtained with G-1 and G-3 showed large differences between the performances of large emitters and small buttons made of the same material, that the Elox process used to form the emitter grooves might be responsible. To test this hypothesis, experiments to compare the performance of buttons before and after being subjected to the Elox process were conducted by Cho.[2] The tests showed only a small difference in performance; if anything, the performance following Eloxing was slightly improved. As a further check, however, photographs were taken of the surface of emitter G-4 and of the Eloxed button made of the same material. The surfaces were strikingly different, as shown in Figures 44 and 45. Figure 46 shows Semicon emitter D-1, which was machined and electropolished, and Figure 47 shows emitter F-8, made of Eloxed and electropolished Semicon material. While neither surface is as good as that of the button made of G-4 material, the surfaces of both are noticeably less rough than that of the G-4 ionizer.

Cho's button had been sputtered and operated in oxygen for cleansing, whereas the G-4 ionizer had not. The latter was therefore oxygenated and sputtered. The surface smoothness was markedly improved to where it resembled that of the G-4 button (see Figure 48). The emitter was heated in a vacuum furnace at 1200°C to remove copper that had been sputtered onto the back and then put back into the engine.

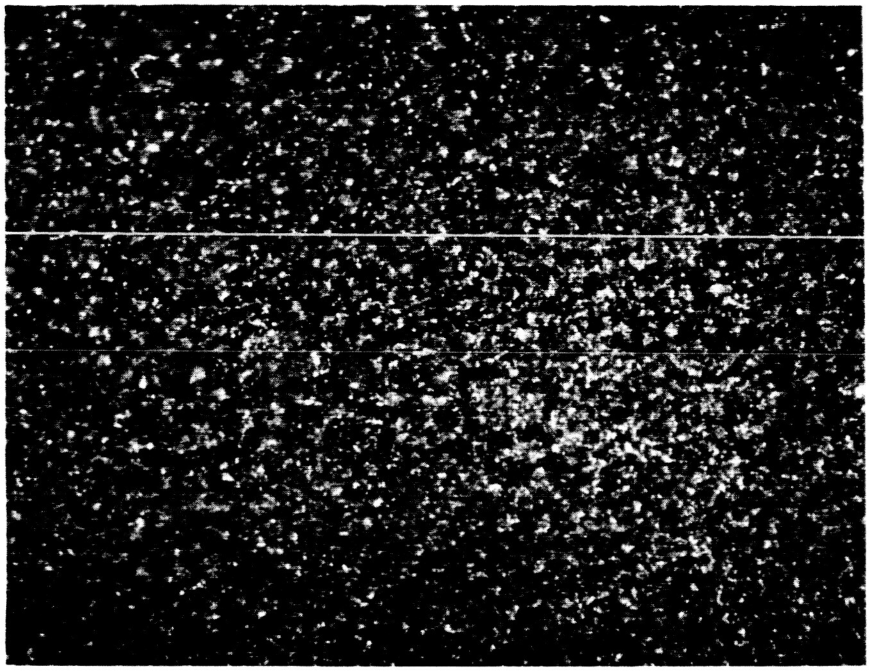

Figure 44. G-4 ionizer surface after eloxing (225X)

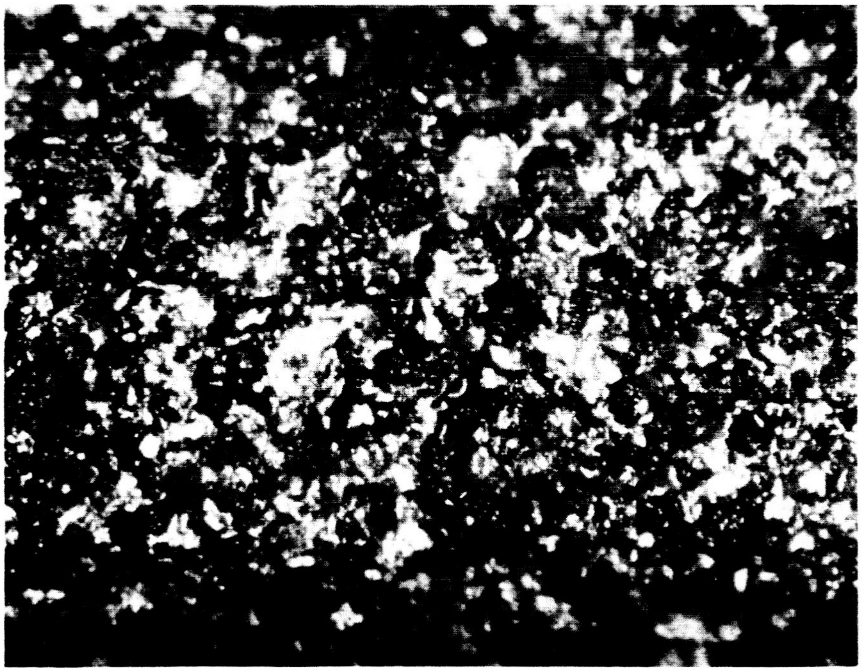

Figure 45. G-4 button surface after eloxing, oxygenation, and sputter cleaning (250X).

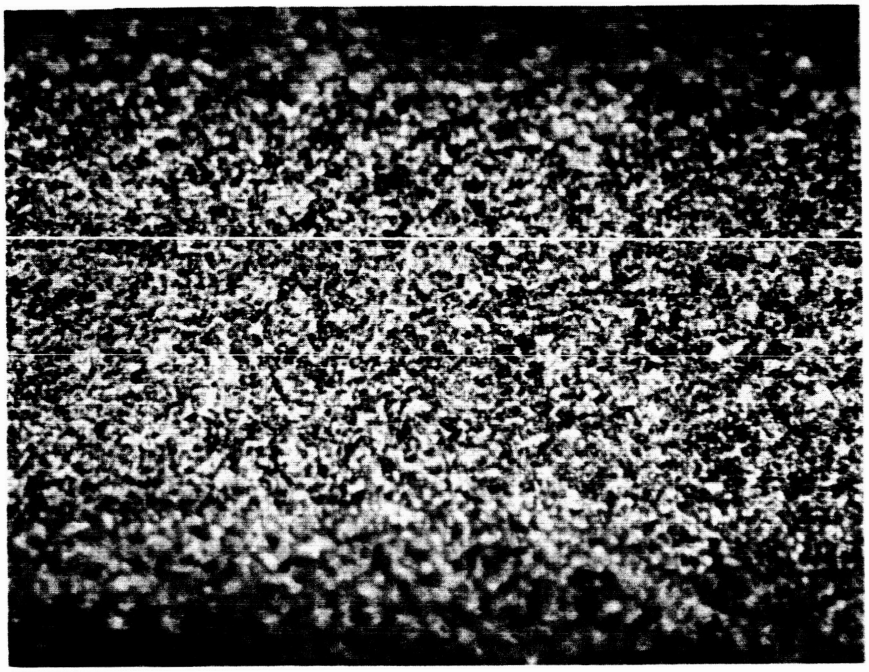

Figure 46. Emitter D-1, Semicon material machined and electropolished (225X).

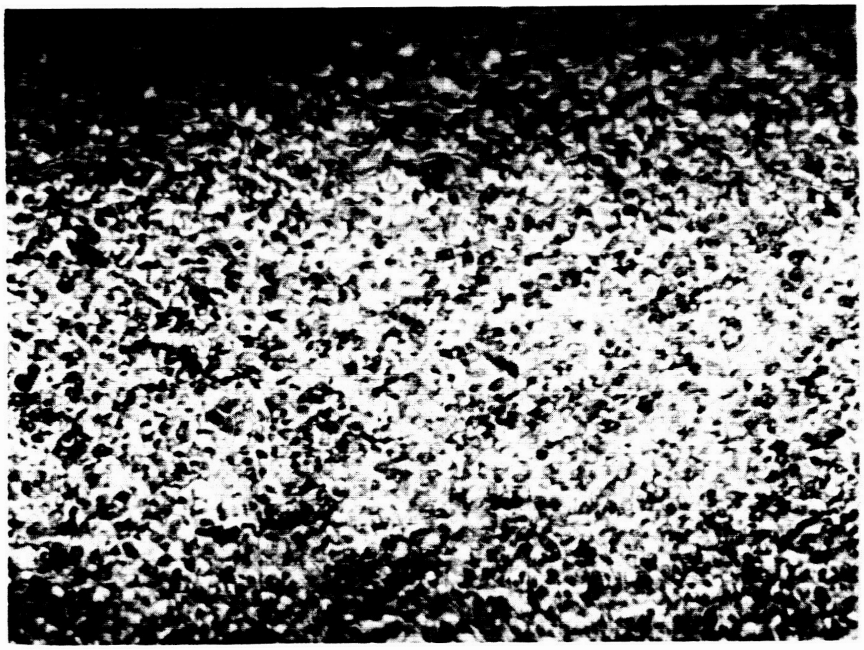

Figure 47. Emitter F-8, Semicon material eloxed and electropolished (225X).

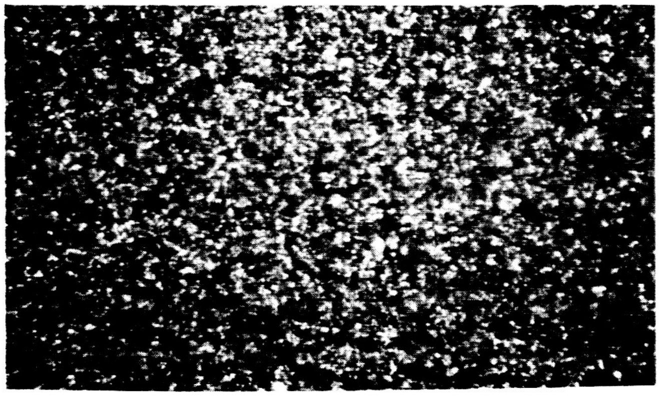

Figure 48. G-4 ionizer after sputtering

As a result of this treatment both the neutral fraction and critical temperature were reduced. Test results for 10 and 20 ma/cm^2 are shown in Figure 49. These emitter characteristics are still not ideal, but it seems clear that the sputtering treatment is beneficial.

EMITTER F-8

Emitter F-8 was prepared during the previous contract but because of a leak in the side had never been used. It proved possible to seal the leak, and it was decided to use the emitter as one of the test samples in order to provide a comparison with previous work.

The material was made by Spectra-Mat [AF33(657)-10788] from 5μ powder. Its emissivity was 0.293 at 1432°K.

Since the emitter was already fabricated it was not possible to obtain the transmissivity and make pore-size measurements.

Test results on this emitter are shown in Figures 50 through 55.* The observed characteristics are typical of an oxygenated surface, and it was concluded that the water vapor accumulated by the cesium in the vacuum tank was responsible. The beam profile of this emitter showed considerable irregularities, as shown in Figure 56. As the mass 18 peak decreased, the behavior shifted toward the higher neutral fraction. At this point in the program it was concluded that F-8 was probably not a candidate for a long life grid test, and it was decided to proceed with testing of G-5 without waiting for the surface condition to stabilize, and F-8 was removed from the system.

EMITTER G-5

Emitter G-5 was fabricated from material that was made by TRW Systems and consisted of 2-5μ spherical powder [SW-10 powder lot, Contract No. AF33(657)-11726]. It was tested over a period of 15 days, from 15 April to 29 April 1965. The engine was removed twice during this period for thermocouple repairs. Pressure was

---

* Neutral fraction data uncorrected for grid backscatter. See footnote on Page 34.

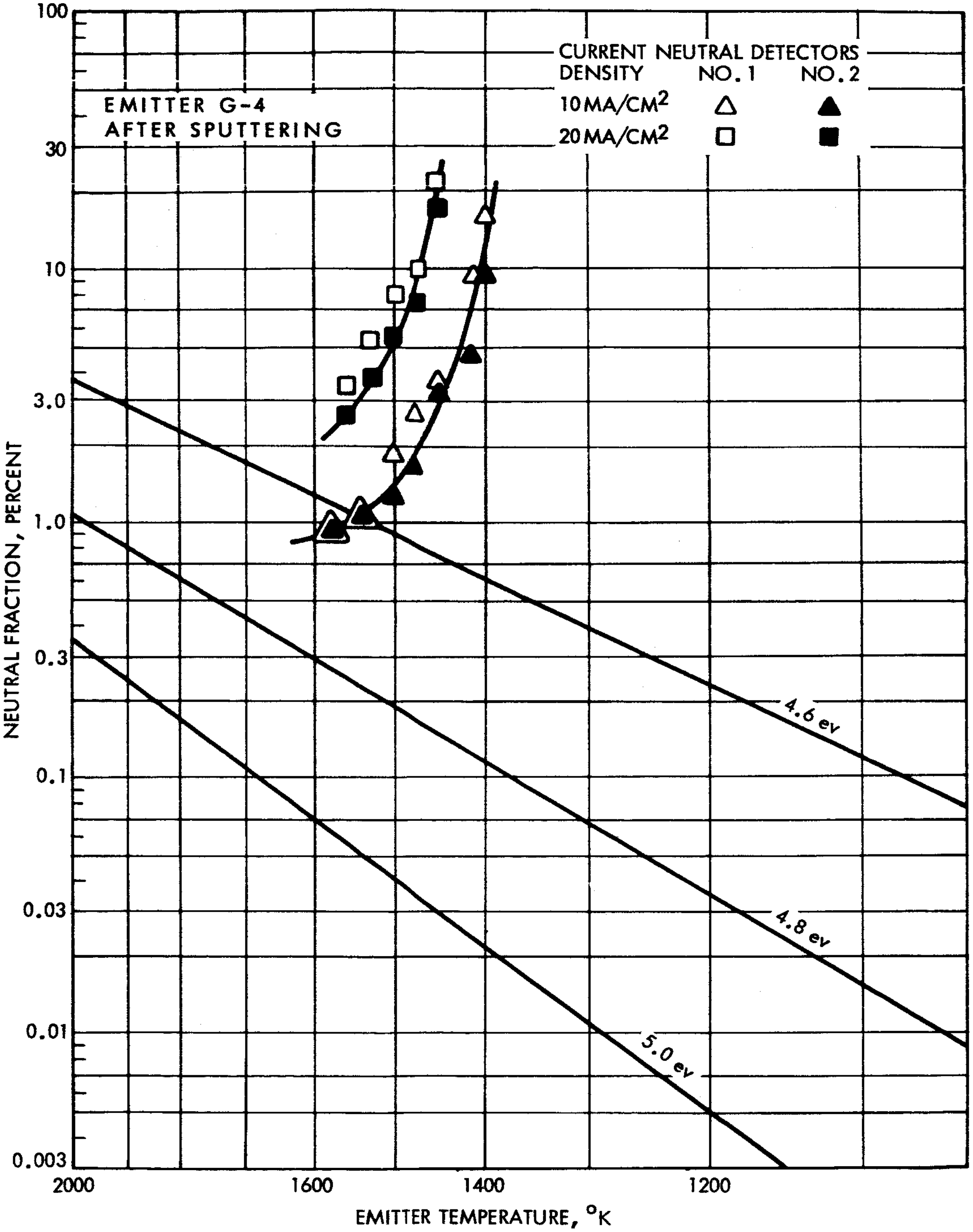

Figure 49. Neutral fraction versus temperature after sputtering (G-4).

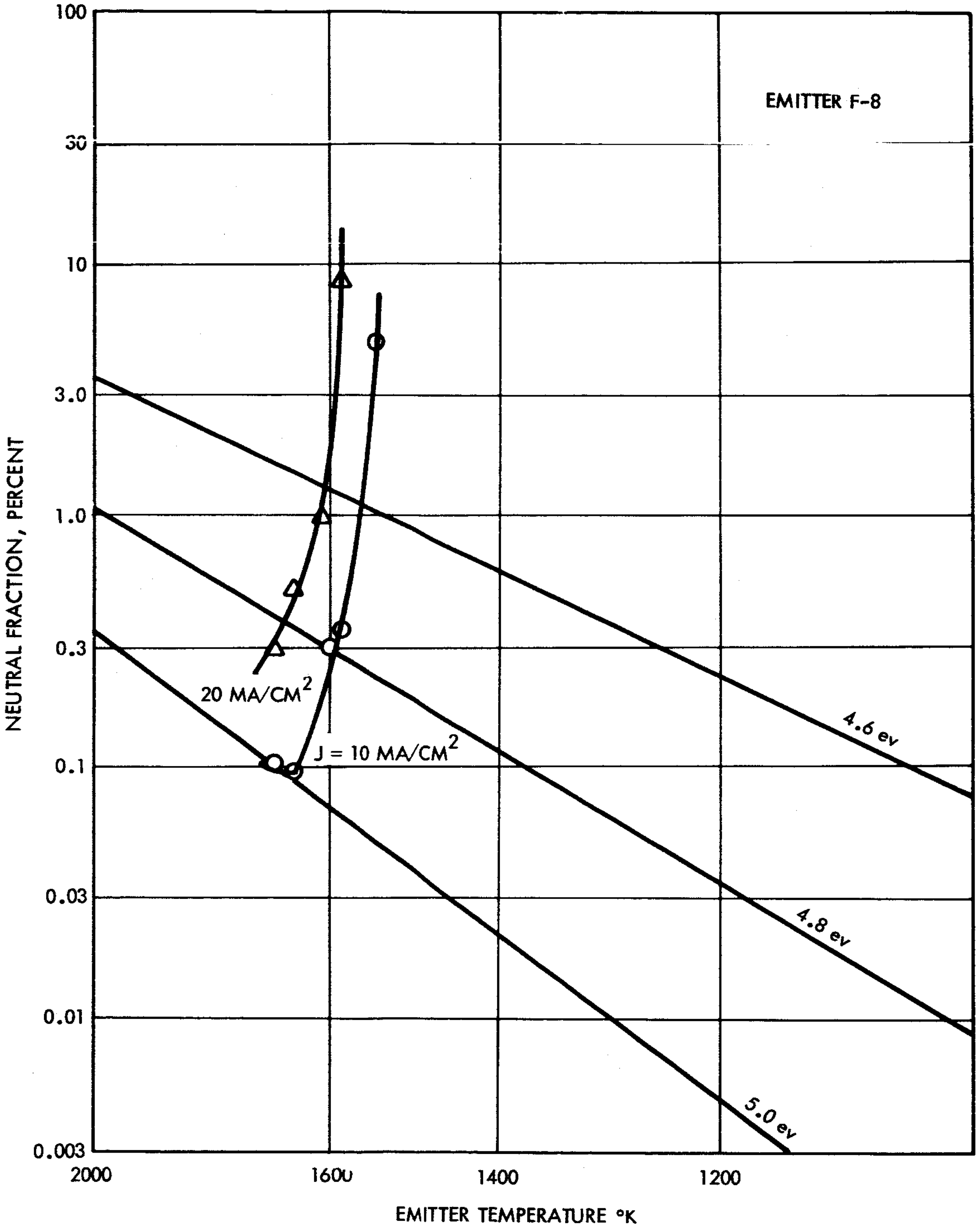

Figure 50. Neutral fraction versus temperature (F-8).

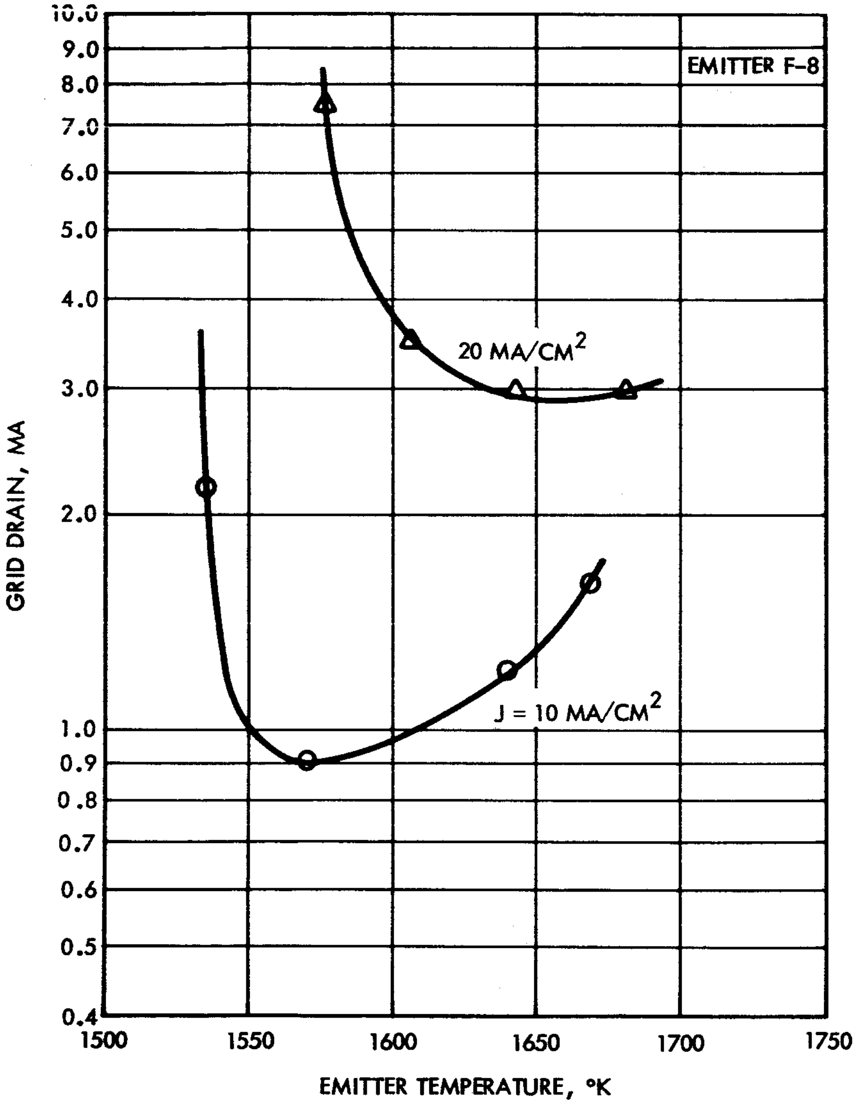

Figure 51. Grid drain versus emitter temperature (F-8).

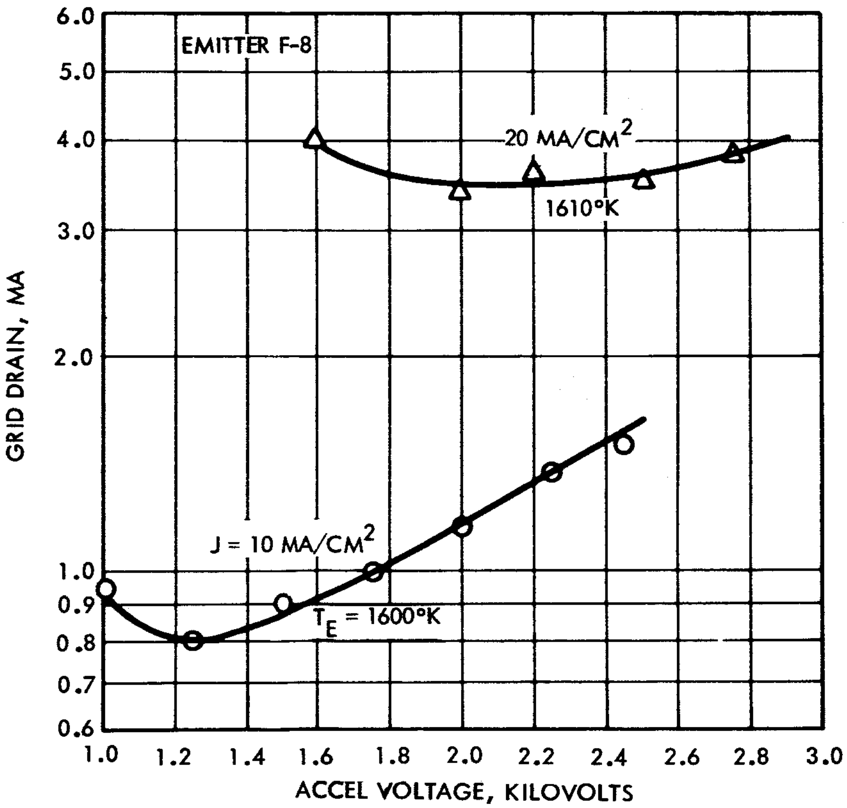

Figure 52. Grid drain versus accelerating voltage (F-8).

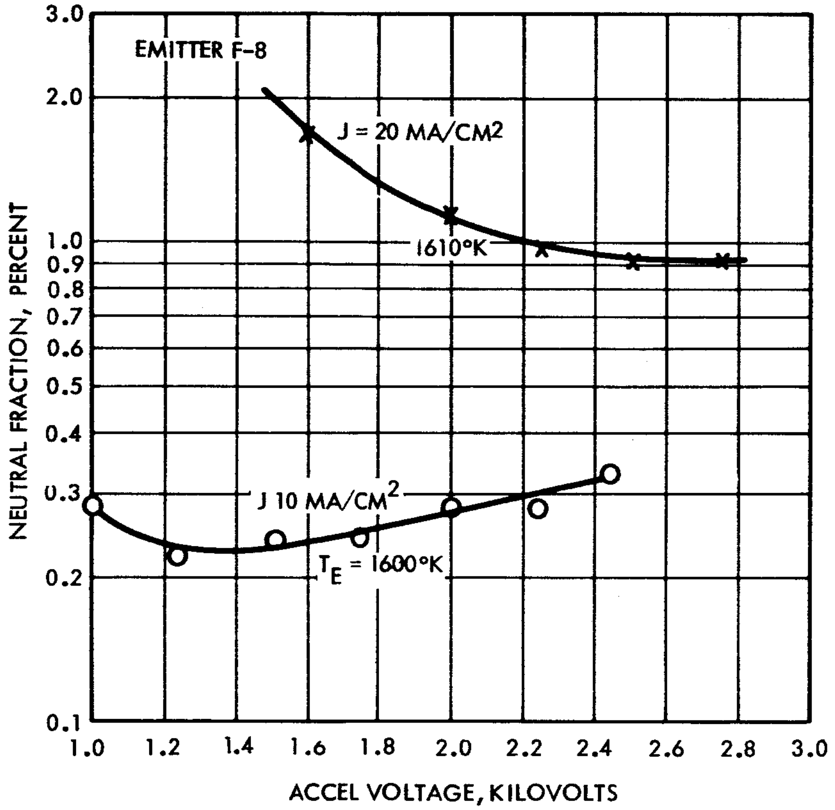

Figure 53. **Neutral fraction versus accelerating voltage (F-8).**

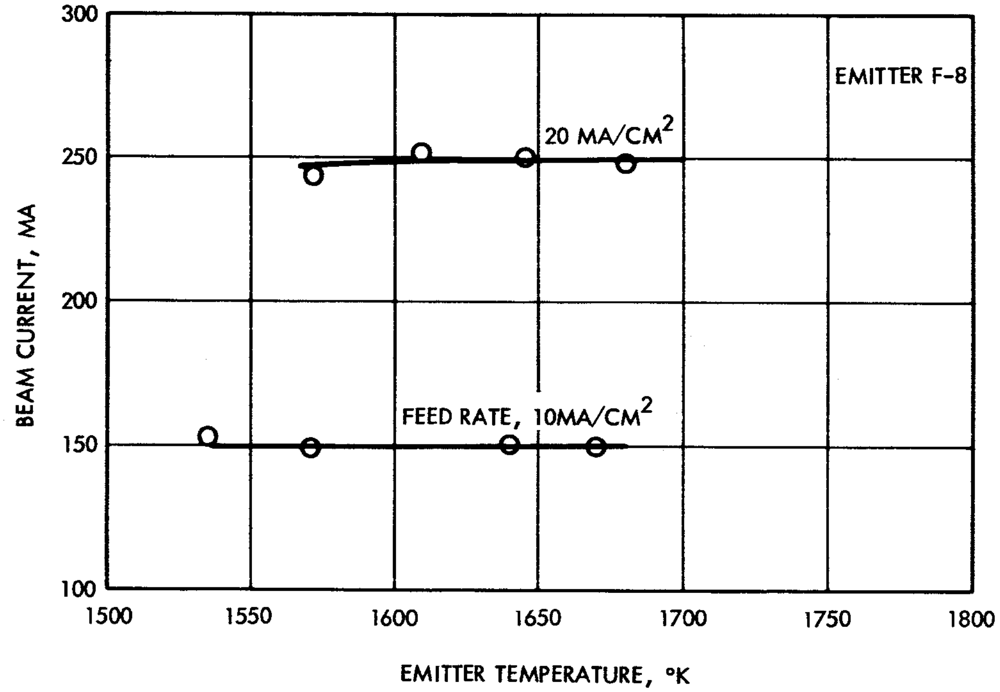

Figure 54. **Beam current versus emitter temperature (F-8).**

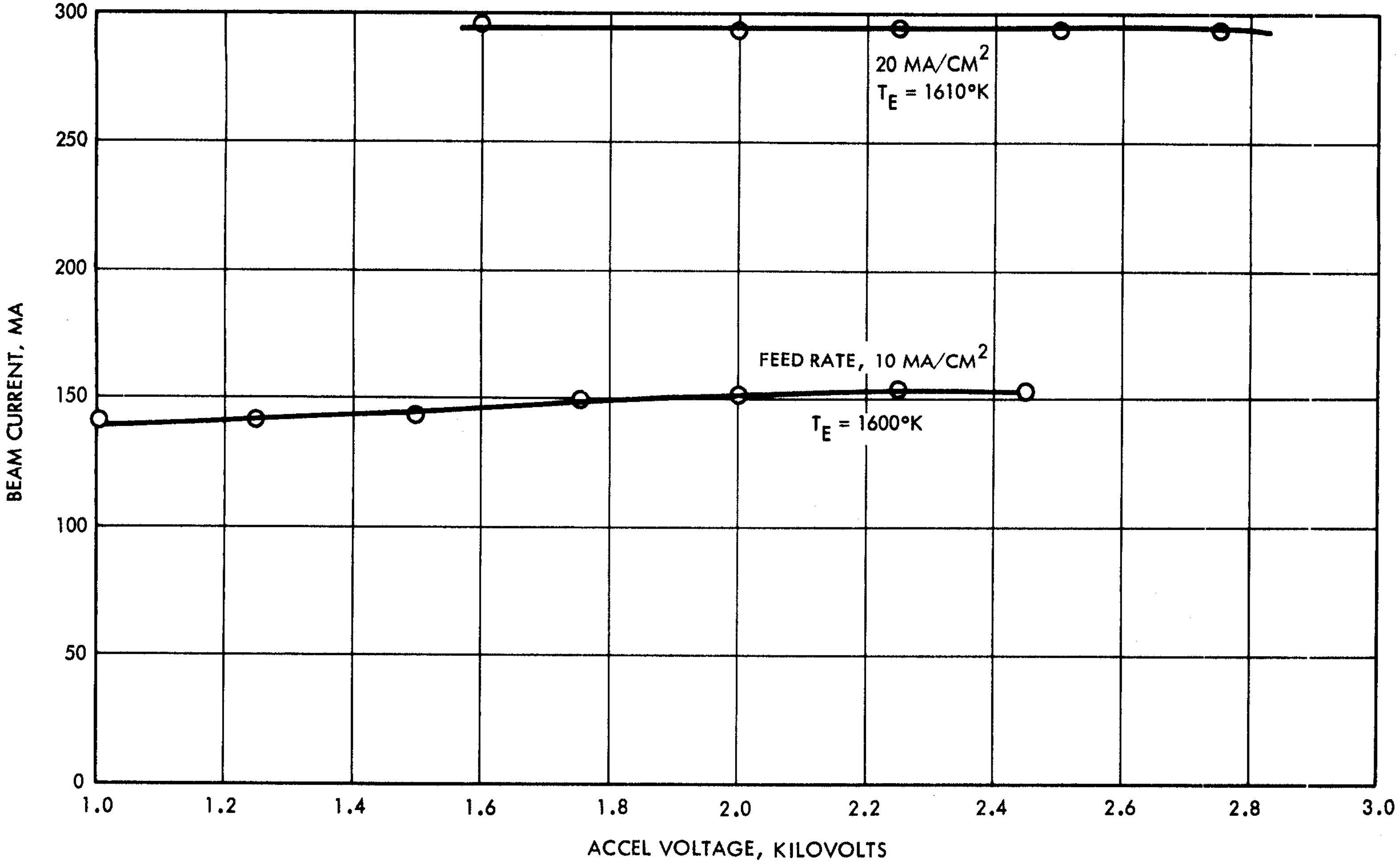

Figure 55. Beam current versus accelerating voltage (F-8).

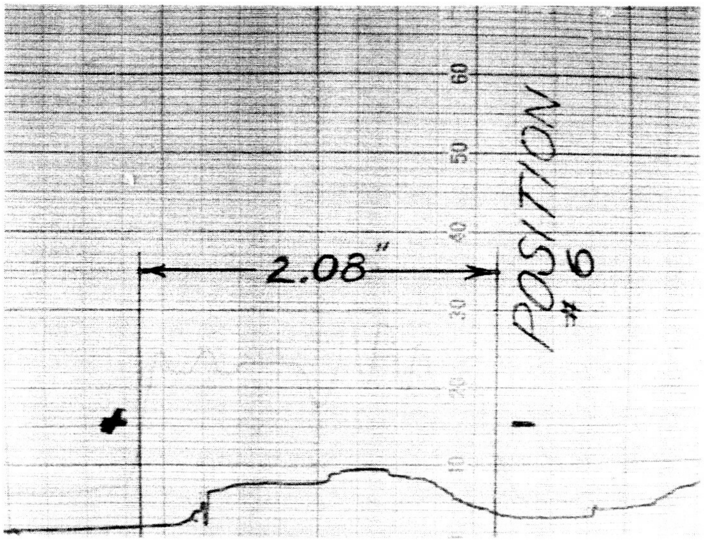

Figure 56. Beam profile of F-8. The lighter trace is the beam profile. The darker trace is the change in neutral detector current as the beam scanner is swung across the beam.

generally between 8×10^{-7} and 1×10^{-6} mm Hg. Pore count data and transmittivity data obtained on emitter G-5 are given in Figure 57.

All of the data taken with G-5 indicated poor emitter performance. Beam profile data taken at 10 ma/cm^2 for G-5 is shown in Figure 58. The profile data shows large variation in throughput across the face of the emitter. Critical temperatures were consistently high (i.e., $T_c = 1480^oK$ at 3.3 ma/cm^2 beam), and the measured neutral fraction varied from very high (2.7% at 1470^oK for a beam of 3.3 ma/cm^2) to very low (0.01% at 1600^oK for a 10 ma/cm^2 beam). Both the critical temperatures and neutral fractions varied from hour to hour. During the last three days of testing, the emitter surface opposite the feed started to crumble and disintegrate. Visual study of the emitter surface indicated this condition ranged over a circle approximately 1 inch in diameter and was centered over the feed tube. Also, there was a blister-like swelling of the porous tungsten on one side of a flute peak within this area.

The final measurements that were made, which were taken at 10 ma/cm^2, are shown in Figure 59 (measured neutral fraction vs temperature)* and Figure 60 (grid drain vs temperature). The curve in Figure 61 which shows measured neutral fraction vs accelerating voltage, was obtained during an earlier part of the test. The curves for measured neutral fraction vs temperature indicate one neutral detector saw a much higher neutral current than the other. This detector, No. 1, was measuring neutral fraction from the damaged area of the emitter. The difference ratio at 1570^oK is 50/1.

Two total emissivity measurements were made. The first, taken at the beginning of the test, gave a value of 0.307 at 1350^oK. The second measurement, made midway in the test run, gave an emissivity of 0.308 at 1408^oK.

* Uncorrected for grid backscatter. See footnote on Page 34.

FEED TUBE END

1 Pore Count 5.73 x 10^6/cm^2 Pore Size 1.70μ Transmission 1.39 x 10^{-4} Relative J	4 Pore Count 5.67 x 10^6/cm^2 Pore Size 1.62μ Transmission 2.54 x 10^{-4} Relative J	7 Pore Count 5.42 x 10^6/cm^2 Pore Size 1.67μ Transmission 1.93 x 10^{-4} Relative J
2 Pore Count 5.40 x 10^6/cm^2 Pore Size 1.63μ Transmission 1.67 x 10^{-4} Relative J	5 Pore Count 5.38 x 10^6/cm^2 Pore Size 1.64μ Transmission 2.53 x 10^{-4} Relative J	8 Pore Count 5.30 x 10^6/cm^2 Pore Size 1.56μ Transmission 1.82 x 10^{-4} Relative J
3 Pore Count 5.47 x 10^6/cm^2 Pore Size 1.63μ Transmission 1.45 x 10^{-4} Relative J	6 Pore Count 5.67 x 10^6/cm^2 Pore Size 1.63μ Transmission 2.54 x 10^{-4} Relative J	9 Pore Count 5.22 x 10^6/cm^2 Pore Size 1.61μ Transmission 1.80 x 10^{-4} Relative J

Density 79.39%

Mean Pore Count - 5.47 x 10^6 cm^2

Mean Transmission - 1.96 x 10^{-4}

Total Transmission - 1.18 x 10^{-4}

Emitter - Top View

Material STL-SW10

Lot SW10

Sample G-5

Figure 57. Pore-count and transmissivity data on Emitter G-5.

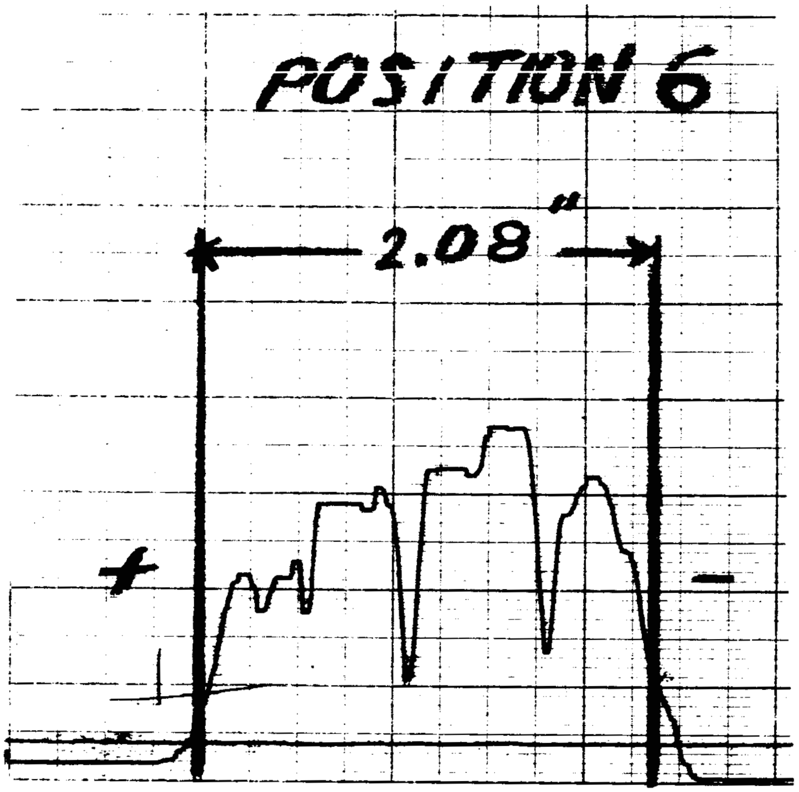

Figure 58. Beam profile of G-5.

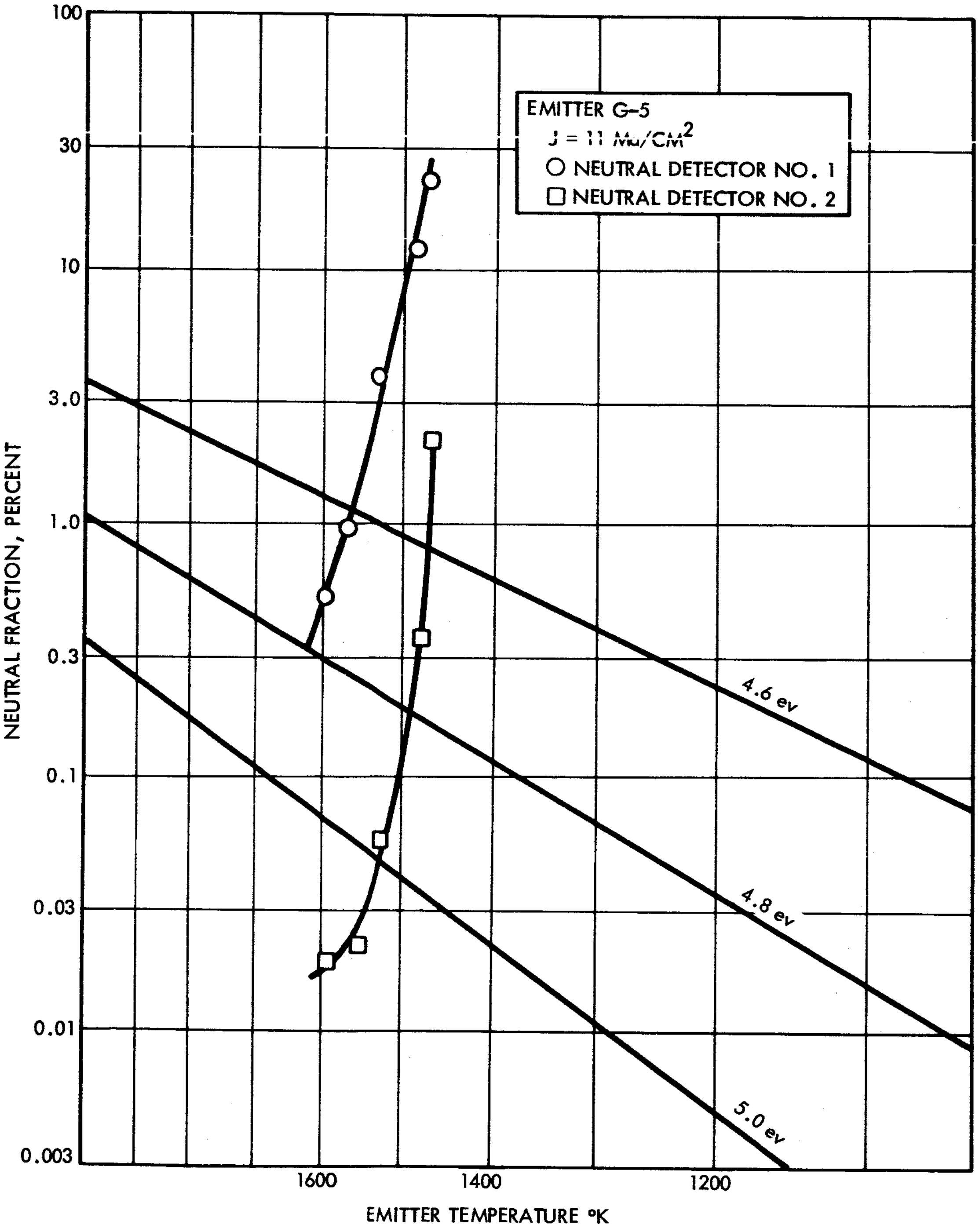

Figure 59. Neutral fraction versus temperature (G-5).

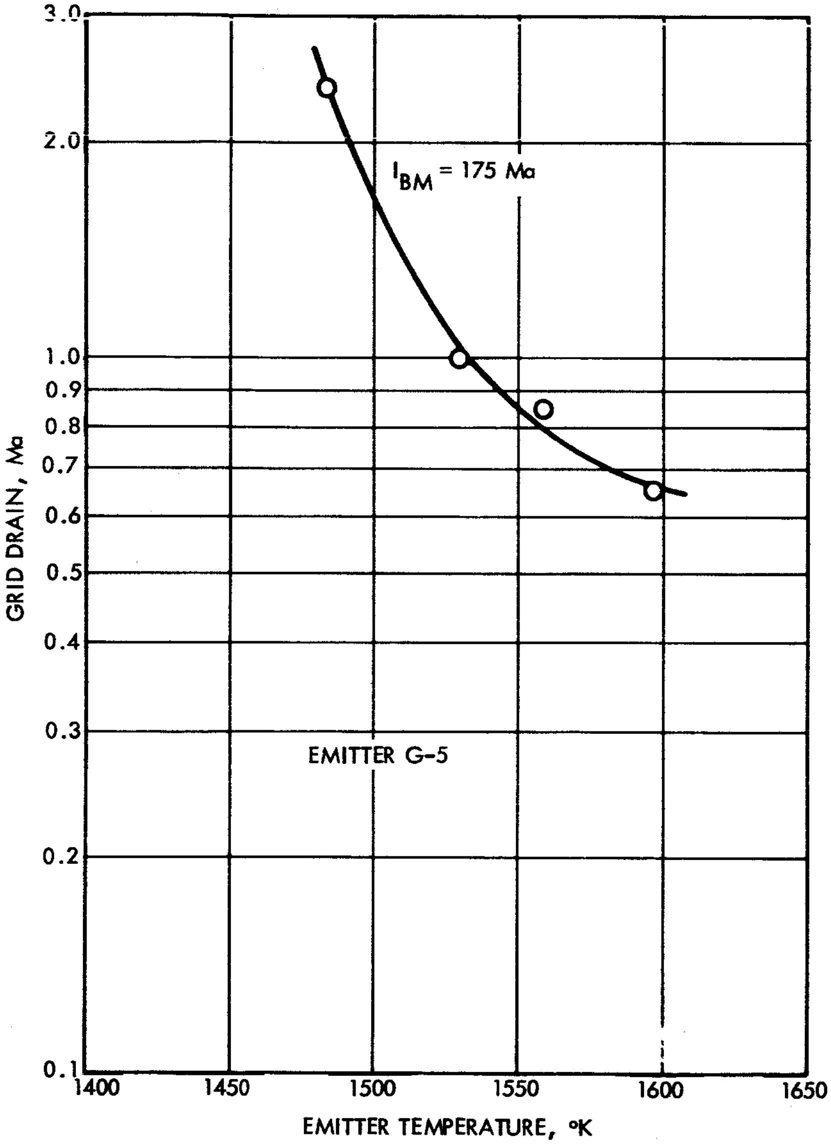

Figure 60. Grid drain versus emitter temperature (G-5).

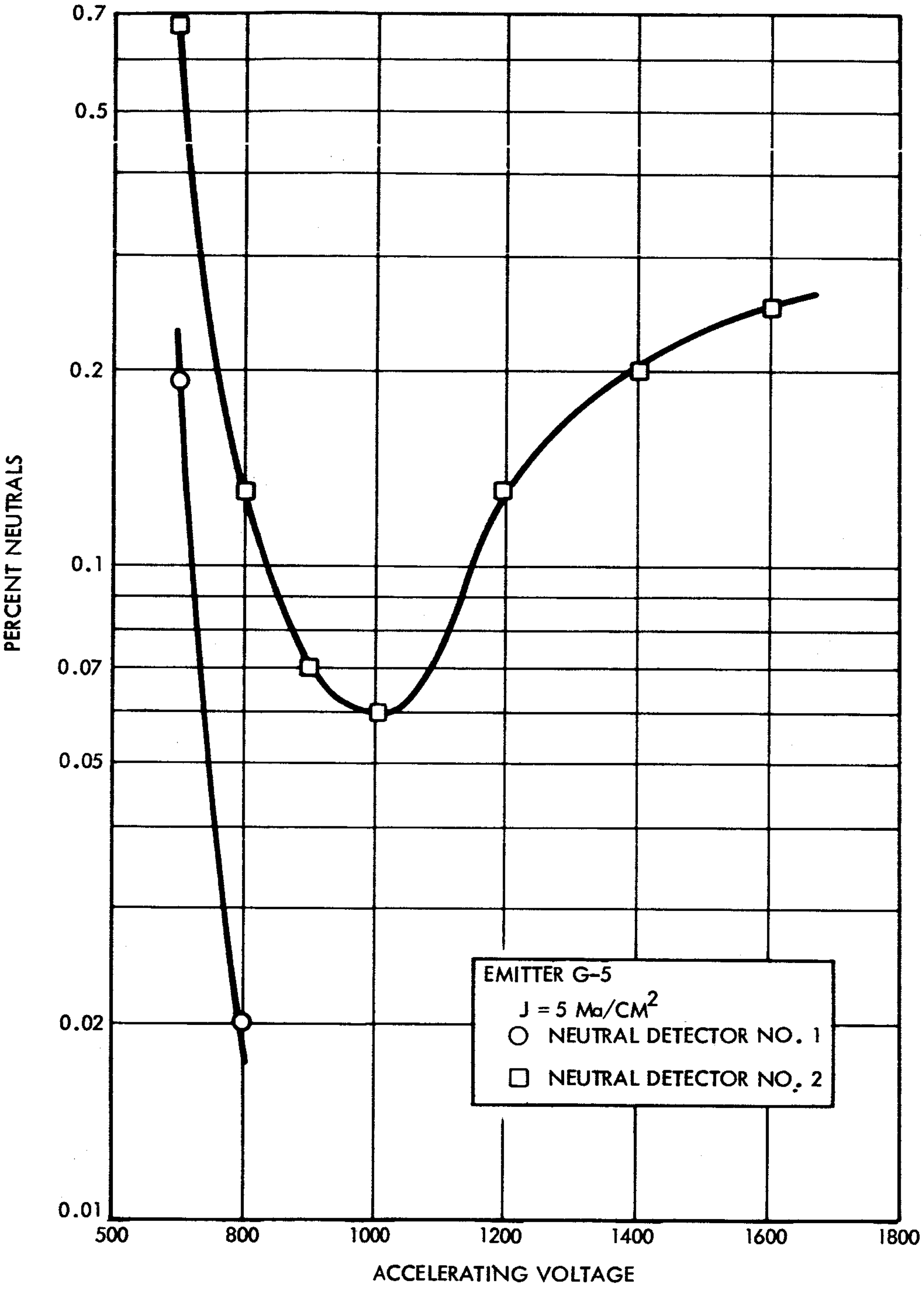

Figure 61. Neutral fraction versus accelerating voltage (G-5).

4. CONCLUSIONS AND SUMMARY

One obvious conclusion to be drawn from these investigations is that the large ionizers tested did not give results comparable with those obtained from smaller samples. In efforts to determine the reason for this difference of behavior, it was found that improvements in vacuum cleanliness produced no significant change in ionizer behavior. The emitters were not subject to gross hycrocarbon contamination, since easily recognizable and reproducible oxygenated characteristics could be produced. (The fact that these characteristics would disappear after the oxygen was removed from the system probably indicates the presence of some carbon in either the tungsten or in the system. This same behavior was exhibited in the button work of Cho and Shelton.)

Since excellent characteristics were obtained from 2.5-cm^2 samples of TRW material tested (under another contract) in this same system, it seemed probable that vacuum conditions were not solely responsible for the anomolous results. It was found that such treatments as electropolishing and sputtering, which were intended to reduce surface roughness, were beneficial to performance. This improvement may have resulted either from reduced surface irregularities or the exposure of high-work-function crystal faces.

Operation with a copper boiler instead of our stainless steel feed system at first seemed to indicate that contamination from the feed line was responsible for the poor performance characteristics of the large ionizers; however, later tests did not appear to substantiate this conclusion.

The achievement of good performance in large ionizers remains as a prime target for improved ion-engine technology. The following courses are indicated to reach this goal:

1) Improvement of ionizer surfaces through electropolishing, sputtering, or improved machining techniques

2) Careful removal of contaminants, such as carbon and oxygen, from the ionizer material.

3) Removal of suspect materials in the feed system and engine structure until the difficulty is identified

4) Additional tests to compare the performance of buttons and larger ionizers. These should include transferring buttons from the ultrahigh vacuum test chamber to the larger test facilities, comparative tests of two or more samples of the same material, and extended operation of small buttons to see if their characteristics can be maintained over long periods.

REFERENCES

1. S.G. Forbes, J.C. Beynon, D.A. Gordon, and M.E. Kirkpatrick, "Design of a Modular Source Contact Ion Engine (U)", Final Reports on Contract Nos. AF33(657)-8687 (August 1963) and AF33(657)-10788 (November 1964), ASD-TDR-63-545 and AFAPL-TR-64-126.

2. A.Y. Cho, D.F. Hall, and H. Shelton, "Program of Analytical and Experimental Study of Porous Metal Ionizers," Final Report on Contract No. NAS3-5254 (15 July 1965), NASA CR-54325.

3. S.G. Forbes and J.C. Beynon, "Design of a Modular Source Contact Ion Engine," Technical Report No. AFAPL-TR-64-126, prepared under Contract No. AF33(657)-10788 (November 1964).

4. Private communication with H. Shelton, D. Hall. The correction is required because the angular distribution of neutrals is different when accel voltage is on compared to when it is off.

DISTRIBUTION LIST FOR SUMMARY REPORT

CONTRACT NAS3-5906

NASA-Lewis Research Center (1)
Spacecraft Technology Procurement Section
21000 Brookpark Road
Cleveland, Ohio 44135
Attention: John H. DeFord

NASA-Lewis Research Center
Electromagnetic Propulsion Division
21000 Brookpark Road
Cleveland, Ohio 44135
Attention: E. A. Richley (1)
P. D. Reader (1)

NASA-Lewis Research Center
Spacecraft Technology Division
21000 Brookpark Road
Cleveland, Ohio 44135
Attention: F. E. Kavanagh (8)
T. Riley (1)
D. L. Lockwood (1)
J. H. Childs (2)
J. A. Wolters (1)
A. E. Anglin (1)

NASA-Lewis Research Center
Technology Utilization Office
21000 Brookpark Road
Cleveland, Ohio 44135
Attention: John Weber (1)

NASA-Lewis Research Center
Technical Information Division
21000 Brookpark Road
Cleveland, Ohio 44135 (1)

NASA Headquarters
FOB-10B
600 Independence Avenue, S. W.
Washington, D. C. 20546
Attention: RNT/James Lazar (2)

NASA Marshall Space Flight Center
Huntsville, Alabana 35812
Attention: M-RP-DIR/Dr. E. Stuhlinger (1)

Commander
Aeronautical Systems Division
Wright-Patterson Air Force Base, Ohio 45433
Attention: AFAPL(APIE)/Robert Supp (1)

NASA-Lewis Research Center
21000 Brookpark Road
Cleveland, Ohio 44135
Attention: Library (2)

NASA-Lewis Research Center (1)
21000 Brookpark Road
Cleveland, Ohio 44135
Attention: Reports Control Off.

AFWL (1)
Kirtland AFB, New Mexico
Attention: WLPC/Capt. C.F. Ellis

Aerospace Corporation (1)
P.O. Box 95085
Los Angeles, California 90045
Attention: Library Technical
Documents Group

Jet Propulsion Laboratory
Pasadena, California
Attention: J. J. Paulson (1)

Colorado State University
Fort Collins, Colorado
Attention: L. Baldwin (1)

Hughes Research Laboratories
3011 Malibu Canyon Road
Malibu, California 90265
Attention: Dr. G. R. Brewer (1)
Dr. H. Husmann (1)

Defense Metals Information Center
Battelle Memorial Institute
505 King Avenue
Columbus, Ohio 43201 (1)

North American Aviation, Inc.
12214 Lakewood Avenue
Downey, California
Attention: Technical Info. Cent.
Dept. 4096-314 (1)

Ion Physics Corporation
Burlington, Massachusetts
Attention: Dr. S.V. Nablo (1)

United Aircraft Corporation
Research Department
East Hartford, Connecticut
Attention: Dr. R. G. Meyerand, Jr. (1)

General Electric Company
Flight Propulsion Lab.
Cincinnati, Ohio 45215
Attention: M. L. Bromberg (1)

Westinghouse Astronuclear Labs.
Pittsburgh, Pennsylvania 15234
Attention: H.W. Szymanowski, Mgr. (1)
Elec. Propulsion Lab.

Aerojet General
San Ramon, California
Attention: Dr. J. S. Luce (1)

Electro-Optical Systems, Inc.
125 North Vinedo Avenue
Pasadena, California
Attention: Mr. R. C. Speiser (1)
Dr. Kuskevics (1)

TRW Electromechanical Division
TRW Systems
23555 Euclid Ave.
Cleveland, Ohio 44117
Attention: Mr. R. T. Craig (1)

Rocketdyne
6633 Canoga Avenue
Canoga Park, California
Attention: J. F. Hon (1)

NASA Scientific & Tech. Information Facility
Box 33
College Park, Maryland 20740
Attention: NASA Representative RQT 2448 (6)

Phillips Metalonics
888 South Columbus Avenue
Mt. Vernon, New York
Attention: Mr. Roberto Levi (1)